ADSORPTION THERMODYNAMICS AND KINETICS OF NANOMATERIALS AT INTERFACES

A Dissertation

by

I-CHENG CHEN

Submitted to the Office of Graduate and Professional Studies of
Texas A&M University
in partial fulfillment of the requirements for the degree of

DOCTOR OF PHILOSOPHY

Chair of Committee,	Mustafa Akbulut
Committee Members,	Maria Barrufet
	Charles Glover
	James Holste
Head of Department,	M. Nazmul Karim

December 2015

Major Subject: Chemical Engineering

ABSTRACT

Investigations on the adsorption dynamics or interactions of nanomaterials at interfaces have enabled applying nanotechnologies in current industrial systems effectively. In this work, enhanced oil recovery (EOR) and impacts of nanoparticles on environment are energy-related and environmental-related systems investigated respectively. Amphiphilic materials were investigated at liquid-liquid and liquid-solid interfaces in the EOR system. Dynamics of asphalt recovery using surfactant floods was studied using quartz crystal microbalance with dissipation (QCM-D) and a promising mobility control approach that could replace current methods was proposed.

The kinetic model of asphalt (heavy oil) recovery via surfactant flooding is related to a fast removal process of large microemulsions and a slow removal process of loaded micelles at interfaces of the asphalt film and the surfactant solution. Effective type of surfactant and the concentration range of surfactant flooding useful for the asphalt recovery were also found.

One novel system was developed based on the complexation and supramolecular assembly of amino-amide type amphiphiles and maleic acid to change viscosity of aqueous displacement fluids for mobility control in EOR. It was shown that the addition of only 2 wt. % of adaptable amphiphiles/maleic acid into water increased the viscosity of water by 4.5×10^5 times. This superior viscosity behavior was ascribed to the formation and entanglements of layered cylindrical supramolecular assemblies having diameters of several hundred nanometers. Furthermore, the viscosity of the amphiphile

solution could be changed in a reversible manner by changing pH with no obvious degradation. Sand column displacement experiments were carried out with different process variables for future pilot applications.

Polymeric nanomedicines were studied at liquid-solid interfaces in the environmental-related system. Deposition trends of various polymeric nanomedicines were investigated in environmental related media for wastewater control in hospitals or pharmaceutical manufacturers. Adsorption dynamics and transportation behaviors through porous media were studied considering the effect of surface chemistries of polymeric nanomedicines. The mobility of negatively charged nanoparticles is strongly dependent on the amount and types of salts in solutions. With the presence of calcium ions, even at low ionic strengths (i.e. 10mM), induced adsorption appeared on silica surfaces and strongly limited the mobility of polymeric nanomedicines.

DEDICATION

To my love, Ching-Fen, Yung-Chao and Hsiung-Hsiung.

ACKNOWLEDGEMENTS

I would like to thank my advisor Professor Mustafa Akbulut. He has been a dedicated mentor and I am grateful for many opportunities and encouragements he provided and for his patience in guiding me. Sincere thanks to my committee members Professor Maria Barrufet, Professor Charles Glover and Professor James Holste for their guidance and support throughout the course of this research.

It has been a great pleasure to be able to work with a group of great colleagues who are constantly full of drive in Professor Akbulut's group. Graduate students, past and present, have been a source of motivation to me. There have been numerous inspiring discussions. It has been a great experience to collaborate on projects with experts from different backgrounds and to lead undergraduates in Texas A&M University.

I would also like to extend my thanks to the staff of the Microscopy and Imaging Center, the staff of the Materials Characterization Facility and staff in machine shop for their support and training on state-of-the art equipment. Thanks for the funding from ASC-PRF and NSF to support my research. Many thanks to faculty and staff from chemical engineering department who make my research life here comfortable.

Lastly, I give thanks to my family for their love, support and encouragement.

NOMENCLATURE

AFM	atomic force microscopy
AS	alkaline-surfactant
ASP	alkaline-surfactant-polymer
CFT	colloidal filtration theory
CMC	critical micelle concentration
DLS	dynamic light scattering
DLVO	Derjaguin–Landau–Verwey– Overbeek
DMPDA	N,N- dimethyl-1,3-propanediamine
EO	ethoxylate
EOR	enhanced oil recovery
ICM	iodized contrast media
IFT	interfacial tension
IOR	improved oil recovery
M	mobility ratio
NOM	natural organic matter
NP	nanoparticle
OPEC	organization of the petroleum exporting countries
O/W	oil-in-water
PAA	polyacrylic acid
PAM	polyacrylamide

PCL	poly-ε-carprolectone
PEI	polyethyleneimine
PEO	polyethyleneoxide
PLA	polylactide
PNDDS	polymeric nanoparticulate drug delivery systems
PNVP	polyvinylpyrrolidone
PO	propoxylate
PS	polystyrene
PV	pore volume
QCM-D	quartz crystal microbalance with dissipation
RF	resistance factor
ROS	residual oil saturation
SD	standard deviation
SEM	Scanning electron microscopy
SFM	spectrofluorometry
SP	surfactant-polymer
TEM	transmission electron microscopy
THF	tetrahydrofuran
vdW	van der Waals
W/O	water-in-oil

TABLE OF CONTENTS

Page

LIST OF FIGURES

Page

LIST OF TABLES

Page

CHAPTER I

INTRODUCTION

1.1 Background of oil recovery

Over the past 15 years, studies of improving flooding process in petroleum industry have dramatically increased to decelerate the increasing rate of oil price. Although several events occurred related to the precipitous fall of the oil price like global economical recession, massive oil production by shale gas method in the US, oil production by organization of the petroleum exporting countries (OPEC) and development of clean energy supply to the energy market, with the growing population and energy demand, oil price will grow by 2040 predicted by US energy information administration, and several companies like Exxon mobile, Shell. Currently, international energy agency estimates that there is more than 150 years of oil supply. As the new discoveries of conventional oil fields are declining, questions arise as how to effectively, economically, environmental friendly drill out petroleum remaining in underground reservoirs.

World oil resource exists in various forms, thus development of traditional methods like primary depletion and second water flooding are not enough for the large energy demand. For primary and secondary recovery, pressure gradient is the driving force. Pressure depletion of primary recovery is from the natural reservoir energy like solution-gas drive, natural water drive, fluid and rock expansion and etc. Secondary recovery is commonly used by injecting water or gas as an effective pressure support to

the production wells; however, only 20-50% of oil can be extracted from an oil reservoir due to the poor sweep efficiency as a result of the oil property or reservoir environment[1–3]. The remaining 50-80% of oil stays underground where oil is adsorbed on rock surfaces, leading to oil entrapment within the rock pores[4–6]. To extend the lifetime of the oil reservoir before reaching economical limit by conventional method, tertiary recovery or later called enhanced oil recovery (EOR) has been actively investigated by researchers[7–10] trying to squeeze extra barrels from oil fields. There is another term called improved oil recovery (IOR), which includes EOR and other activities to increase oil recovery like reservoir characterizations or improved reservoir management[11]. Typical EOR techniques aim to achieve one of the following: (i) decrease oil viscosity, (ii) increase viscosity of water, (iii) reduce capillary force or interfacial tension between oil and oil-stratum. Various EOR techniques such as miscible gas injection, chemical injection, microbial injection, or thermal recovery have been investigated to apply to different reservoir characteristics.

Since 1960, EOR of chemical injection has been attractive since small quantities are necessary to effectively change properties of the displacing fluid, however, technical and economical problems appeared to effectively use this method. Although chemical EOR is a less common method than thermal and gas EOR, huge projects have been initiated or revisited around the world since 2000. Surfactant and polymer flooding are the two main methods in chemical EOR that have been applies in fields in China, Middle East, USA and etc. Surfactant flooding is known to reduce oil-water interfacial tension or change the wettability of the reservoir[12–15]. Polymer flooding is well-known in

improving water-oil mobility ratio by increasing the viscosity of injecting fluid. This approach enables a uniform advance of water front to sweep a larger volume of the reservoir.

Surfactants and polymers are commonly combined as surfactant-polymer flooding to enhance sweep efficiency with both chemical's properties in oil fields. There is another system applying smart materials which can respond to environment stimuli with particular changes in one or more properties to decrease pumping costs. The smart amphiphilic system has recently received great attention[16–18].With more investigations in this system, cost-effective and similar displacement efficiency will be attractive to apply in oil fields in the next decades.

1.2 Background of environmental impact from polymeric nanomedicine

Significant developments in nanomedicines have occurred over the past few decades. According to a recent study relying on literatures, clinical data and the Web, about 250 nanomedicines have been approved for use under clinical trials or on the verge of clinical study[19]. While the increasing production and consumption of nanomedicines on treatment, prevention of disease and research, concerns have arisen in the fate of nanomedicines in the environment, bioaccumulation may occur and the potential consequences to human health[20–22]. Currently, among the major types of nanomedicines like nanoemulsions, liposomes, polymeric nanoparticles, surfactant micelles, dendrimers, and semiconductor nanocrystals, the commonly used form of nanomedicines is polymeric nanoparticulate drug delivery systems (PNDDS) (Fig. 1.1)

due to their increased bioavailability, ability to solubilize hydrophobic molecules, the higher payload capacity, excellent thermodynamic solution stability in aqueous environments, and prolonged blood circulation times[23–27]. The high stability of PNDDS can be undesirable when nanomedicine is released to environment through various ways like sewer system or underground leak of storage tank and ultimately end up in aquatic system. As most of the therapeutic component of PNDDS can be ecotoxic, their improved solubility and bioavailability in PNDDS will be much danger to living organisms at lower concentrations. Moreover, therapeutics in PNDDS can travel with prolonged stability to distribute in aquatic environment. Thus, if the sustainable implementation of nanaotechnology is to occur, detail information regarding the mechanism that control retention, deposition and release of nanomedicine under relevant environmental conditions needs to be done to control the contamination in specific aquatic environments.

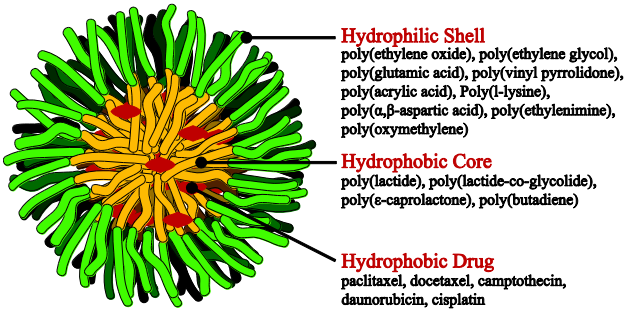

Figure 1.1 Illustration of PNDDS structure and typical building blocks used in current formulations[28].

1.3 Objectives statement

In oil recovery part, since a large part of world oil remaining underground in the form of heavy oil like in North Sea, Canada and Venezuela, it is essential to effectively apply EOR to these reservoirs. For surfactant EOR, mechanism of heavy oil recovery was unclear about choosing the suitable chemical combinations to the field. Thomas[29] stated that the insufficient understanding of the mechanisms and scale-up methods to fields are the main technical limitations. An urgent need will be to develop a suitable model for effective surfactant flooding in heavy oil resources. The goal of this dissertation is to investigate the removal process of asphalt (heavy oil) from the silica surface. Furthermore, developing the heavy oil desorption mechanism happening at interface of surfactant solution and heavy oil to help choose the suitable surfactants for oil fields.

The other goal is to develop a system using a novel type of adaptable amphiphile which can respond to environmental stimuli with changes in viscosity to increase oil recovery. Various stimuli have been considered, such as light, oxidation reactions, enzymes, pH, and temperature[30–33]. Comparing conditions between well surfaces and reservoirs, specific condition that is different from the well surface and the reservoir will be chosen as a natural existing stimulus. The concept is viscosity of the injecting amphiphile solution will be maintained at low near the wellbore region which enables injecting fluid flow with a relatively low pressure drop. This process can save a considerable amount of energy required during injection. In addition, the low viscosity injection can avoid the generation of unwanted fractures near the wellbore. Then, away

from the near wellbore region, the solution viscosity can be spontaneously increased via an external stimulus just before or upon contacting the oil (Fig. 1.2). The increased viscosity lowers the injecting fluid mobility and increases oil displacement efficiency. The goal is to develop the adaptable mechanism of the new system by evaluating rheological properties of the material such as steady-shear viscosity and viscoelastic behavior as a function of the reservoir conditions. Lab-scale column experiments with several environmental conditions from oil fields such as concentrations, salinities and temperatures need to be considered for future pilot application.

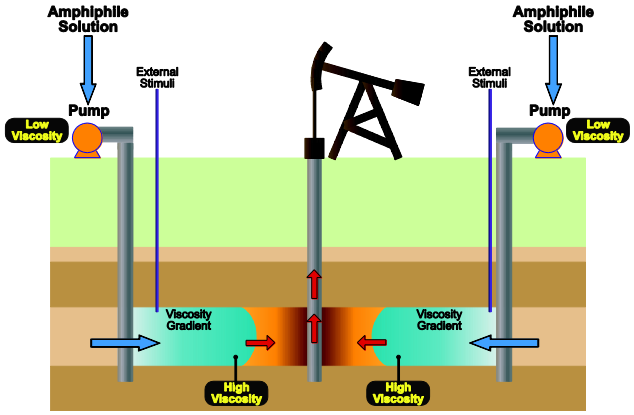

Figure 1.2 Concept of using adaptable amphiphiles for controlling viscosity of injected water in EOR[34].
Initially low viscosities will lead to easier injectivity and efficient pumping while later high viscosities will yield favorable mobility ratios and elimination of water fingering.

In environmental aspects, the transportation of engineered nanoparticles has received increased attentions as the consumption and production volumes of such nanoparticles increase. For instance, many field and laboratory investigations dealing

with the distribution, retention, and fate of nanomaterials such as TiO_2[35–37], SiO_2[38,39], CeO_2 [40–42], ZnO[43,44], Fe_2O_3[45], Ag[46,47], Au[48,49], fullerenes[50–53] and carbon nanotubes[54,55] have been conducted. A general conclusion of these studies is that hydrodynamic parameters (such as flow velocity[40,43]) as well as parameters that modulate the particle-surface and particle-particle interactions (such as surface potential of nanoparticles [36,41,46,56], the presence of organic species[55,57], particle aggregation[46,58], and concentration of NPs[38,40] (i.e. interparticle distance) play a role on the retention and transport behaviors of NPs. However, similar environmental studies on soft nanomaterials such as polymeric nanomedicines are rather limited. Efforts have been made to model PNDDS adsorption and desorption mechanism on environmental surfaces[59,60] and organisms[61]. Our goal is to model the transport behaviors of different surface types of PNDDS at various environmental conditions like solution chemistries (ionic strength or existence of natural organic material) and different salts' (such as monovalent vs divalent) impacts. PNDDS solutions will also flow through porous media which more related to the real world conditions (Fig. 1.3).

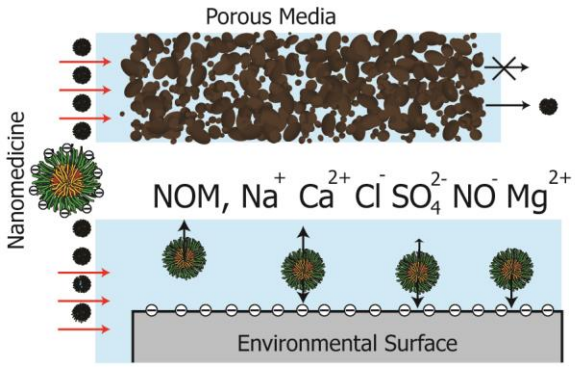

Figure 1.3 Concept of nanoparticle flow through a porous media at different conditions[28].
Ionic strength, different types of salt, natural organic material and pH may have effect during the transport in a porous media. Arrow direction is showing the possible types of competing force direction between NP and the large surface.

1.4 Outline of the dissertation

The dissertation is organized to 6 chapters, with this introduction providing a brief background served as chapter I.

Chapter II discusses more details about chemical EOR like surfactant flooding and polymer flooding with underlying theories. Commercial products are discussed to understand the advantages and limitations in oil fields. At last, discussions on how to improve the current chemical flooding processes by designing surfactants and polymers.

Chapter III provides a background of nanoparticle transportation behaviors in a porous media. Extended DLVO model and CFT model for the deposition process are discussed.

Chapter IV describes the details of surfactant flooding dynamics on surfaces coated with asphalt. The effect of surfactant concentration on recovery efficiency was investigated. For the recovery model, four complementary techniques were conducted to evaluate.

The results also provided experimental evidence to support current model from simulation.

Chapter V describes the synthesis of a pH-responsive supramolecular material and its application in EOR. Extensive rheological measurements were conducted in terms of pH, concentrations, temperatures and salinities. Sand column flooding experiments were conducted to simulate reservoir conditions.

Chapter VI presents the transport behaviors of PNDDS in the proximity of silica and sand. The effects of ionic strength, electrolyte types and natural organic species were investigated and discussed. The effects on adsorption of different surface functional groups of PNDDS were evaluated.

Chapter VII is devoted to conclusions and recommendations for future research work based on these studies.

CHAPTER II

CHEMICAL ENHANCED OIL RECOVERY

2.1 Introduction

Among numerous techniques to improve oil recovery, EOR strived to improve microscopic displacement efficiency by removing hydrocarbon stuck to the rock surface. Started in 1960's, chemical methods including polymers, surfactants, foams, alkalines and etc. are important and attractive methods because small quantities effectively change the injecting fluid property. Several technical issues appeared to lessen the usage until recently. In chemical flooding, the effective recovery of unswept remaining oil is dependent mainly on two conditions: one is the relative mobilities of the displacing and displaced fluids during the flood from one well to another (polymer flooding), the other is the maintenance of low interfacial tension during the flood (surfactant flooding). Other effect like wettability alteration (surfactant method) plays an important role in some oil-wet reservoir. Combinations of surfactant and polymer as alkaline-surfactant-polymer (ASP), surfactant-polymer (SP) or alkaline-surfactant (AS) processes are also considered as potential methods[62,63].

Mobility of the resident oil or water is the ratio of the permeability of the porous rock and the viscosity of the solution. Permeability is governed by Darcy's law which measures the capacity of the medium to transmit fluids. To obtain an effective process, the mobility of the displacing fluid must be equal or less than the mobility of the mobilized oil to prevent the injected fluid from bypassing the oil-water bank. Since the

mobility of the mobilized oil is low due to relative permeability effects in the rock, the viscosity of the displacing fluid usually must be higher than the resident oil in order to achieve the same or lower mobility. Polymers are usually applied to increase the viscosity of displacing fluid to reach higher oil displacement efficiency.

Interfacial tension (IFT) between the oil and injecting fluid plays an influential role at the pore regions in reservoir. Considering the curvature and wettability around the two phases, capillary pressure which is the pressure difference existing across the interface of two immiscible fluids can be obtained. In the same pore size, strong IFT will trap oil and cause relatively high residual oil saturation. Reduction in IFT by adding chemicals like surfactants to remobilized oil is regarded as an important method to attain higher oil displacement efficiency. For non-fractured and fractured reservoirs, strong capillary forces make different influences. In non-fractured reservoir, strong capillary forces during water flooding will trap oil and cause relatively high residual oil saturation[64]. In fractured reservoirs, higher displacement efficiency can be achieved by spontaneous imbibition of water due to strong capillary forces[65]. Capillary forces are often the strongest forces in a multiphase flow and the combination of all the active surface forces determines the capillary pressures in the porous rock

In chemical EOR, viscous forces and capillary forces are determining the flow of oil and water in porous media. Capillary number is a dimensionless value in oil field to evaluate whether the injection of fluid is effective. A large capillary number means less residual oil. In an oil reservoir, capillary fingering regime is for very slow displacement where is controlled by the capillary pressure of the interface. Viscous fingering regime is

fast displacement where viscous forces overcome capillary effect. Extensive studies have been done on two regimes to apply the appropriate fluid during the flooding process.

On the other hand, wettability of a reservoir can also have a significant impact on flow during oil recovery and upon the volume and distribution of the residual oil[64,66]. Fluid distribution in porous media depends on solid-liquid and liquid –liquid IFT. Thus, wettability of the rock affects flooding behavior and capillary pressure. Wettability depends on the mineral ingredients of the rock and the composition of the oil and water and temperature. This dissertation does not focus on changing the wettability of rocks in the reservoir to increase the displacement efficiency. However, this is a useful parameter in some fractured reservoirs where flooding is not effective.

Since 1980's, significant amount of pilot tests have increased. Several field performances of chemical EOR have been demonstrated in the United States by Shell[67], Exxon[68], Bill Barret Corp.[69], in China by Surtek[70] or by administration bureau, PRC[71], in Canada by Pengrowth[72], in Oman by Shell[73,74] and etc. The chemical EOR which often applies in mature reservoirs takes a long time like about 20 years to evaluate the additional yield of the oil production. Due to the good feedback from around 20 years ago, the number of projects has increased lately[74].

2.1.1 Mobility ratio

Mobility of fluid is a measure of how easy the fluid flow through a porous media as in equation 2.1. Mobility ratio is defined in equation 2.3 as the ratio between mobility (λ) of displacing fluid and displaced fluid. Lake[7] defined as the ratio of mobility behind

and ahead of a displacing front. When measuring a fluid's flow rate in porous media, mobility term and pressure drop term are combined in equation 2.3 known as Darcy's law.

$$\lambda = \frac{\kappa}{\mu} \quad [2.1]$$

$$M = \frac{\lambda_{displacing\ fluid}}{\lambda_{displaced\ fluid}} = \frac{\mu_{displaced}\kappa_{displacing}}{\mu_{displacing}\kappa_{displaced}} \quad [2.2]$$

$$\frac{q}{A} = v = \frac{k}{\mu}\frac{\Delta P}{L} \quad [2.3]$$

where λ is mobility of a fluid, μ is the viscosity of the fluid, κ is the effective permeability to the fluid, M is the mobility ratio, $\mu_{displaced}$ is the viscosity of the displaced fluid, $\mu_{displacing}$ is the viscosity of the displacing fluid, $\kappa_{displaced}$ is the effective permeability to displaced fluid, $\kappa_{displacing}$ is the effective permeability to displacing fluid. q is the volumetric rate, A is the cross section area, v is Darcy's velocity, ΔP pressure gradient in a distance L.

A favorable mobility ratio is maintained to avoid fingering of injected fluids as in Fig. 2.1(b). For an inefficient displacement where injecting fluids tend to bypass the oil, M is larger than 1 as in Fig. 2.1(a).

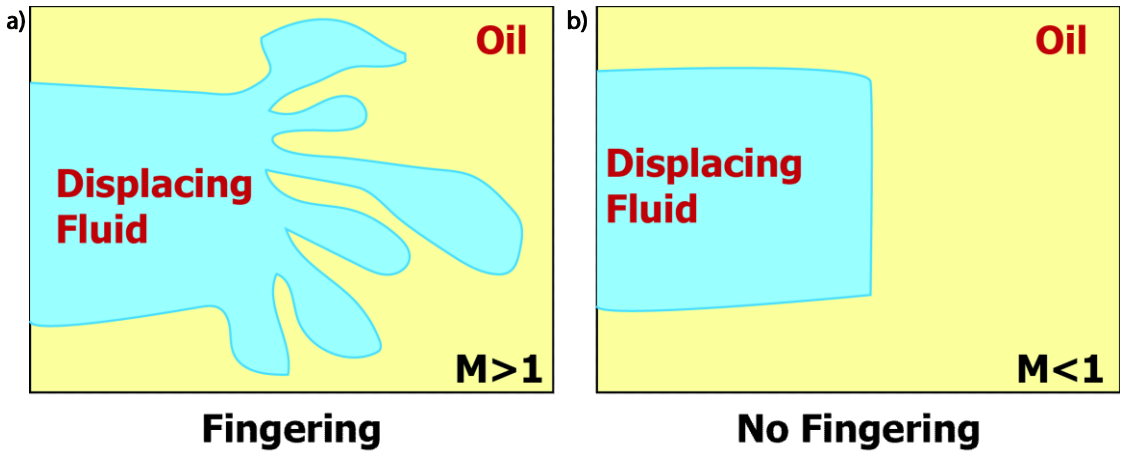

Figure 2.1 Flow path of displacing fluid with different mobility ratio in oil bank.
a) Mobility ratio higher than unity where fingering effect is obvious. b) Mobility ratio lower than 1 to prevent fingering effect.

2.1.2 Capillary pressure

Capillary pressure has a great influence on oil recovery efficiency, because it controls the fluid distribution in the reservoir rock. Capillary pressure is usually measured as a function of saturation of wetting phase due to the complex structure of the porous media. In oil reservoir, it is defined as the pressure of the non-wetting fluid minus the pressure of the wetting fluid. It can also be described using Laplace equation with known interface parameters as in equation 2.4. For a water-wet reservoir saturated by water and oil as in Fig. 2.2(a), water tends to fill inside pores by capillary force because rock surfaces prefer this liquid and oil is trapped in larger pores. Any oil in small pores will be displaced to larger places by water imbibition to lower the energy in the system. At production well, recovery at water breakthrough will be high, with little additional production afterwards. Residual oil is trapped as small globules or completely

surrounded by water. In an oil-wet reservoir as in Fig. 2.2(b), on the other hand, oil occupies small pores and water is staying in large pore areas due to hard penetration. In this case, water breakthrough happens earlier with simultaneously oil and water production during a long period of time afterwards. Over 60% of reservoirs in the world are oil-wet, the injecting liquid pressure equal to the capillary pressure must be applied to push the oil out of pores. More energy is required to displace wetting fluids (oil) by non-wetting fluids[75,76].

$$P_c = P_{NW} - P_w = \sigma_{ow}\left(\frac{1}{R_1} + \frac{1}{R_2}\right) \quad [2.4]$$

where P_c is the capillary pressure, P_w is the pressure of wetting phase at interface, P_{NW} is the pressure of non-wetting phase at interface, R_1 , R_2 are the orthogonal radii of curvature at any point of the curved surface respectively (curved surface is formed between wetting and non-wetting phase), σ_{ow} is the interfacial tension of the two immiscible phases (non-wetting & wetting phases).

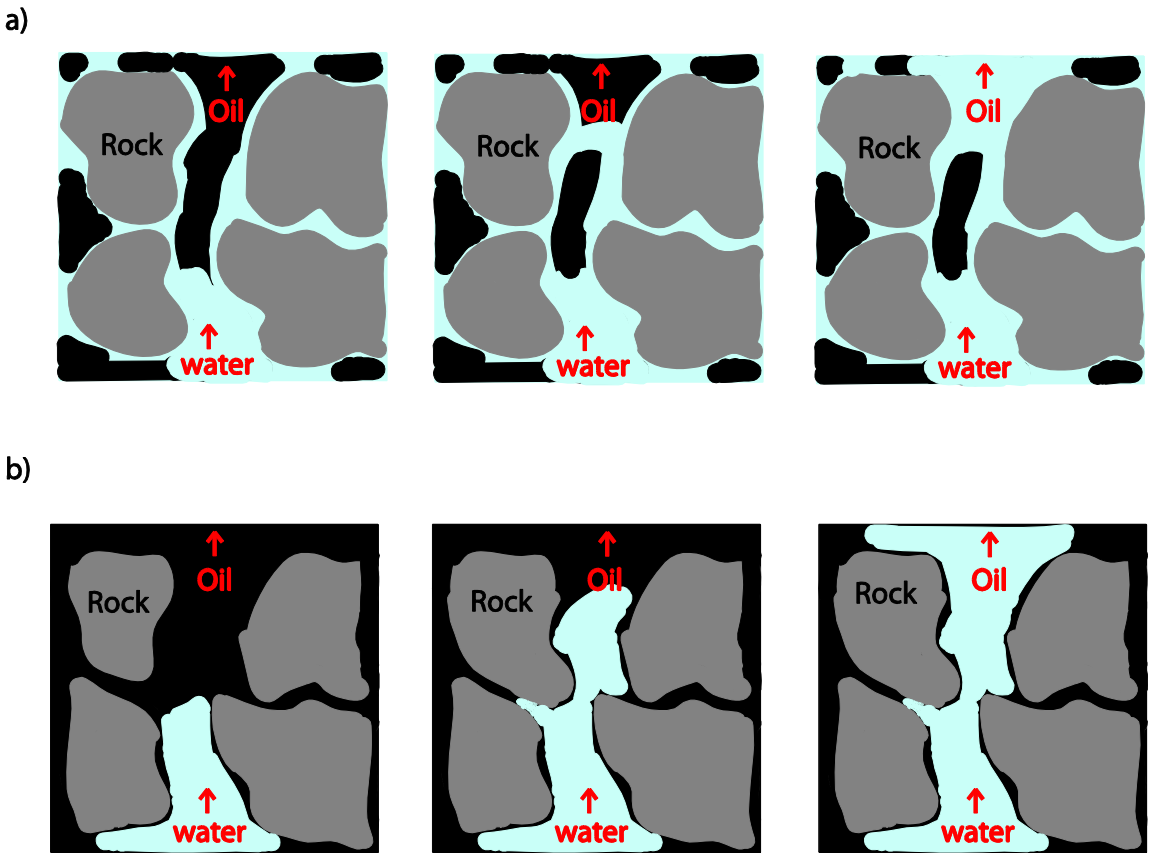

Figure 2.2 Displacement of oil by water in reservoir of different wettability. a) Water-wet reservoir where oil globules trapped in the large pores during flooding. b) Oil-wet reservoir where oil is trapped in small pores.

Capillary number is a dimensionless ratio between the viscous force and the capillary force as in equation 2.5. By reducing the interfacial tension between the displacing and displaced fluids in oil-wet reservoirs, the effect of capillary force is lowered, yielding a lower residual oil saturation and higher oil recovery. Increase the viscosity of injection fluids in water-wet reservoirs, oil trapped by fingering effect in Fig. 2.2 (a) will decrease. In operation of secondary oil recovery, typical capillary

number (N_c) is < 10^{-6} and values on the order of 10^{-7} are probably most common in reservoir pores.

$$N_c = \frac{Viscous\ force}{Interfacial\ force} = \frac{v\mu}{\sigma} \quad [2.5]$$

where v is the Darcy's velocity, μ is viscosity of the displacing fluid, σ is IFT between the displaced and displacing fluid.

2.1.3 Oil recovery efficiency

The overall oil recovery efficiency can be defined as

$$E_{or} = \frac{N_r}{N} \quad [2.6]$$

where N_r is the amount of oil recovered, N is the original amount of oil in reservoir.

Overall efficiency consists of volumetric sweep efficiency (E_v) and displacement efficiency (E_d) as below.

$$E_{or} = E_v * E_d \quad [2.7]$$

E_v is the fraction of volume swept by the displacing fluid to the total volume in the reservoir[7]. E_d is the ratio of amount of oil recovered to the oil in the swept volume. E_v depends on several parameters like the fracture of reservoir, mobility ratio, flow rate and etc. Thus, it consists of vertical and areal sweep efficiency in the reservoir. Poor E_v will increase the costs to inject fluids and this can be improved by mobility control such as polymer flooding. E_d is a function of time, IFT, wettability, viscosity and etc. In oil or water wet reservoirs, there are residual oil remaining due to those parameters. Proper

processes like surfactant or polymer flooding can be applied after systematic characterizing petroleum reservoirs.

2.2 Surfactant flooding

Surfactant flooding or so called detergent flooding, miscible type floods, microemulsion flooding represents the important method to inject surface active chemicals and recover trapped oil by changing the IFT between displacing and displaced fluid or by changing wettability of the rock after water flooding. When contacting with oil and water interfaces, many surfactant dispersions can spontaneously take up water or oil forming water-in-oil (W/O) or oil-in-water (O/W) microemulsions, respectively. With this concept, it was first described as an improved oil recovery method in late 1920's[77]. Since then, there are two common strategies has widely been used in 1960's: one is using large pore volumes of low concentration surfactant slugs where less than 2% of surfactant was used. The other is small pore volumes of high concentration slugs where surfactant concentration is usually larger than 5% (3-20%). Meanwhile, electrolytes, co-surfactants (usually alcohol) or polymers are often considered adding in the surfactant displacing flood to improve the process.

Technical feasibility of oil recovery via surfactant flooding were demonstrated in early field tests by Surkalo et al.[78,79], Hill et al.[80,81], Pursley et al.[82,83], and Lake and Pope[84]. Besides, numerous studies focusing on the bulk oil recovery properties of surfactant floods have been conducted. Majority of these studies have investigated the effects of phase behavior[85], wettability[86], interfacial tension[87–91], water mobility[89], and

foaming performance[92] on the behaviors of oil recovery using surfactant floods. While there are many studies on enhanced oil recovery via surfactant floods at the bulk scale[93–96], studies on the nanoscale dynamics of oil recovery via surfactant floods are very limited.

Overall, in surfactant flooding process, several factors need to be considered to increase displacement efficiency like recovery mechanisms in various fluids' and reservoirs' conditions, loss of surfactants due to adsorption, scaling methods from laboratory results to the fields. Cost of surfactants, the current oil price and tax load are also major limiting factors running the process.

2.2.1 Types of surfactant

A surfactant is an amphiphilic molecule with at least one hydrophobic part called tail and at least one hydrophilic part called head. The hydrophilicity of a surfactant is determined by the structure of tail and head. According to the head group, surfactants are categorized into four types: anionic, cationic, nonionic and zwitterionic surfactants. Anionic surfactants are negatively charged amphiphiles with small cations like sodium ions, potassium ions or ammonium ions. They are the most used surfactants in oil fields because of their relatively cheap prices, low adsorption on sand reservoirs. Sulfonates, sulfates, carboxylates and phosphates are common-used anionic surfactants. However, in carbonate reservoirs, anionic surfactants would have high adsorption because of positive charged reservoir surfaces. Salts like sodium carbonate are sometimes added to change the surface potential to less positive and reduce adsorption amount[97]. Cationic

surfactants are positively charged molecules like ammonium organics, pyridinums, imidazoliniums. They are not popular in sandstone reservoirs because of loss in adsorption. Cationic surfactant flooding is mainly used to change the rock surfaces to water-wet[98,99]. Nonionic surfactants use hydrogen bonding, not ionic bonds, with water to exhibit surfactant properties. Oxygen-rich functional groups like ethylene oxide or propylene oxide are usually found in heads to make molecules locally polar to interact with aqueous phase. In chapter IV, one commercial nonionic surfactant was found to be the good candidate for heavy oil recovery. The benzyl ring at the polar region interacted with benzyl-rich compound like asphaltenes in heavy oil, thus forming emulsions during flooding process. Anionic and Cationic surfactants were tested useless in this system. Zwitterionic surfactants have both positive and negative charges in the head group. Dipole moment formed at head region makes the head polar and soluble in water. Since they have more resistance than ionic and nonionic surfactants on salt concentration and temperature, recent studies have worked to improve main challenge in surfactant loss by adsorption[100].

2.2.2 Mechanism

Lowering IFT is the main mechanism in surfactant flooding. Salinity and brine hardness are two most important factors that affect the surfactant's ability to lower IFT. In solution, surfactants will have different phases like monomers, micelles, microemulsions depending on the surfactant concentration. At low concentration, monomers stay in the solution or at interface. With increasing surfactant concentration,

amount of monomers increases and at concentration where monomers start to aggregate to form micelles, the concentration is called critical micelle concentration (CMC). IFT is decreasing during the increase of surfactant concentration until CMC is reached. Two immiscible fluids can form a continuous phase above this critical surfactant concentration. At higher surfactant concentration, the amount of monomers and IFT of the solution will not change much, but the number of micelles increases. Micelles, which structures have various forms, are formed to stabilize two phases into one continuous phase by dispersing one phase inside and one phase outside. For example, W/O micelles are water dispersed inside the structures with oil as solvent staying outside of the micelles. Micellar solutions with thermodynamically stable dispersion of oil, water and surfactant are frequently called microemulsions. Microemulsions' sizes are usually lower than 100nm. The phase behavior of microemulsions is important in EOR because it is related to IFT. Salinity, temperature, concentration of surfactants and etc. form a combination of phase behaviors in oil and water solution. There are mainly four types of phase system in surfactant, oil and water solution: Winsor type I, II, III, VI in Figure 2.3. Type 1: surfactants prefer to stay in aqueous phase and O/W microemulsions formed near the excess oil interface. IFT will not reach ultra-low value at this condition. In type II system, surfactants form W/O emulsion in oil phase near water excess interface. This leads surfactant retention in oil which is unfavorable in recovery process. For type III, a three phase system where surfactant microemulsion phase formed in the middle of water and oil excess phase. This type will reach ultralow IFT which is applicable in EOR. Type 4 is a single phase of solution. This type although reach low

IFT, large amount of surfactants is needed which is not favorable in field application. Increasing the salinity, for example, in ionic surfactant solutions will change the phase behavior from type I to type III to type II. Find the optimum condition of salinity with type III phase is essential for surfactant flooding. As investigations in heavy oil recovery are limited, surfactant flooding has been commonly used for light and middle oil reservoir. However, type II and III conditions are hardly seen for many commercial surfactants. For the optimum condition in surfactant recovery, different mechanism is presented in chapter IV for detail discussion.

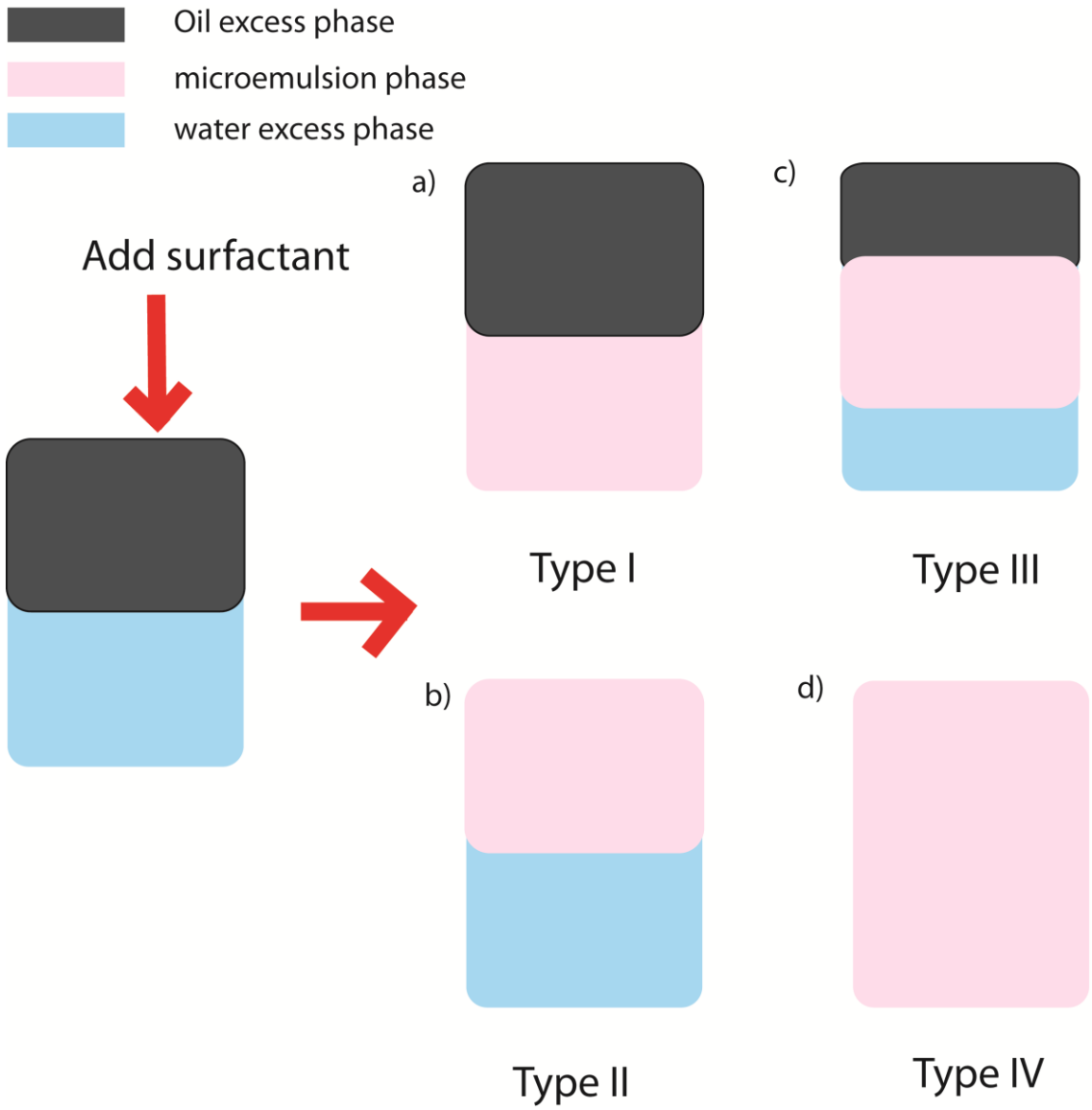

Figure 2.3 Phase equilibrium of water, oil and microemulsion solution.(Winsor type)
a) Type 1, b) Type II, c) Type III, d) Type IV

2.2.3 Design of surfactants and flooding process

To have a commercial application of surfactant process, several factors needs to be considered in designing surfactants and the process for specific conditions. Co-

surfactants, surfactant retention effect, length of hydrophobic tail, types of hydrophilic head are four main variables considered in designing effective surfactant flooding. For co-surfactants, alcohols are commonly used to help inhibit formation of high viscosity phases that traps surfactants in reservoir[101] or to adjust the desired solution condition to reach optimum IFT. However, alcohols will raise the minimum IFT and need extra costs in flooding prices.

Surfactant retention by adsorption on reservoirs, precipitation or phase trapping would be mostly unfavorable in EOR. In oil-wet reservoirs, adsorption may sometimes be desired to change wettability. Most of the time, like mentioned in chapter II 2.2.1, surfactant adsorption by head characteristics (anionic or cationic) and rock properties (sand or carbonate) increase the consumption. In addition to reservoir surfaces, fluid properties like salinity, pH, temperature, or ion types affect surfactant retention as well. Precipitation caused by reduction in electric potential at high ionic strength, reaction of divalent ions with head groups, phase trapping effect mentioned in chapter II 2.2.2 as Winsor type II where surfactants lost in oil phase during flooding are undesirable. A common observation[102] in designing surfactants is branching the tail or mixing two different anionic surfactants that often reduce adsorption amount. Also, the ethoxylate (EO) and propoxylate (PO) groups help surfactant to have tolerance to divalent ions. In chapter IV, head region with benzyl group was found to be helpful in heavy oil recovery. In the surfactant flooding process, even preflush which often used to form the best conditions for reduction of IFT is not effective, thus designing surfactant and the process is important[103] to recover residual oil.

2.3 Polymer flooding

Polymer flooding is the simplest and important method to thicken the displacing fluids with a small amount mainly for increasing the volumetric displacement efficiency as in equation 2.7[104]. The primary function is to reduce the mobility of water thus forcing water to flow through more channels in reservoirs. There is another system called conformance control using polymer gels to block the high permeability regions and then diverting remaining floods to low permeability regions. The less amount of the displacing fluid used in polymer process can also reduce the operational costs in handling disposal of produced water. In 1960's, polymer flooding was first introduced in mobility control[105]. Conformance control was first done by Phillips till 1970's[106]. The typical concentration of polymer process is 0.025 to 0.4 wt. %. Performance of polymer process is commonly evaluated by resistance factor (*RF*), which compares the polymer solution resistance to flow through a porous media to the water solution flow resistance. It can be defined as the ratio of water mobility to polymer solution mobility in Eqn. 2.8. Higher *RF* means lower mobility in the porous media.

$$RF = \frac{\lambda_{water}}{\lambda_{polymer\ soltuion}} \qquad [2.8]$$

Economic and technical successes are reported for polymer floods in sandstone and carbonate reservoirs. It has been shown that production costs of polymer flooding were comparable to water flooding[107]. The polymer injection has successfully been implemented in Marmul (Oman)[74], Oerrel (Germany)[108], Courtenay (France)[109], and Daqing (China) fields[110]. In addition, there are several promising field trials and pilot studies undergoing in Argentina, Brazil, Canada, India, the USA, and Venezuela[63,111–113].

However, there are several critical factors limit the use of polymer process such as low values of polymer-injectivity and pumping-efficiencies, the loss of polymers due to degradation or retention. Similar to surfactant process, the costs from polymer consumption is a very important factor. Thus, designing an adaptable system that maintains low mobility at injection well, and then increases via an external stimulus just before or contact the oil as in Fig. 1.2 is desirable. Besides, to decrease the amount of polymer degradation during flooding is important in the design. Chapter V discusses a novel amphiphilie system for flooding purpose which had the adjustable property to overcome injectivity limitation and the potential to resolve degradation effect.

2.3.1 Types of polymer

In the context of oil recovery, most commonly investigated viscosity modifiers are water soluble polymers such as polyacrylamide (PAM)[114–116], polysaccharide[117], polyvinyl alcohol[118,119], poly(vinylpyrrolidone)[120]. PAM is a synthetic polymer that performance depends on molecular weight and degree of hydrolysis. The polymer's monomeric unit is an acrylamide molecule. When hydrolyzed, acrylamide group is converted to negatively-charged acrylic acid. Partially hydrolyzed PAM has been selected for better solubility in water or viscous behavior. If the hydrolysis is too small, polymers will not be soluble[121]. Typical degree of hydrolysis is 30-35%. In EOR process, partially hydrolyzed PAM is commonly used in fields[7]. Due to the anionic groups in hydrolyzed PAM, PAM polymers lose the high viscous property through ionic shielding. When flowing in porous media, PAM polymers may lose its performance

caused by shear degradation through high shear rates in small pore regions. Polysaccharide bio-polymers known as xanthan gum or seleroglucan are other candidates used for EOR. They are pseudoplastics with viscosifying effect and with excellent tolerance in high salinity conditions because polysaccharide molecules are relatively non-ionic and, therefore, free of the ionic shielding effects. Moreover, compared to PAM polymers, they have higher resistance to shear degradation and less retention in the reservoirs due to more rigid and branched structures. However, they are very susceptible to bacteria attack, no tolerance to extreme pH and more expensive than PAM polymers. Other polymers are not as commonly used as these two types in fields.

2.3.2 Design of polymers and flooding process

To have a commercial application of polymer flooding process, there are several challenges to overcome like the cost of pumping due to high injection pressure, creation of unwanted injection well fractures, polymer retention in pore structures and mechanical degradation of polymers due to high shear rates in porous media. Moreover, the focus on environmental friendly chemicals in the industry continues to grow. For example, EOR of bio-surfactant flooding is taking place in Norway. Researchers have aimed to find new effective chemicals to build a white system meaning having biodegradable environmental friendly ingredients in EOR[122]. Although biopolymers have been developed that mentioned in chapter II 2.3.1, only promising but not profitable materials created at that time. There is still need in designing new environmental-friendly materials for mobility control process.

In conformance control, besides materials' properties, there are two issues in the process of injecting polymer-gel system through the narrow pore. First, different adsorption rates and amount of polymers and cross linkers may change the desired gelling time. Second is polymers may block the wrong sites due to the trigger time of gelation. Polymers and cross linkers are later designed to inject separately to ensure the polymer-gel system is transported to the desired positions. One commercial product, Bright water[123,124], has been developed for conformance control in fields with easy injection at begins and then gel formation in pores by stimuli at specific sites.

In chapter V, utilizing the acrylamide groups in PAM, a novel type of adaptable amphiphile system based on the complexation of a long chain amino-amide and maleic acid had a property to reversibly adjust viscosities. This can enable us to overcome the injectivity limitation in flooding process. The choice of hydrophobic tail can come from environmental friendly materials. Mechanical degradation properties of polymers can be resolved by the reversible structure of the designed supramolecular assembly.

CHAPTER III

TRANSPORT OF POLYMERIC NANOPARTICLES IN POROUS MEDIA

3.1 Introduction

In general, the fate and transport of both natural and engineered nanoparticles (NPs) in porous media depend on their aggregation and deposition behaviors[125] which involve the interaction between NPs or NPs with a mobile surface during transport. They were first developed in 1970's to improve packed bed filter performance in water treatment[126,127]. During transport, the mechanisms of attachment between two NPs are dependent on Brownian diffusion, fluid velocity gradient and differential settling. For deposition of NPs on surfaces, Yao et al[126] first classified Brownian diffusion (BD), interception, and sedimentation as three mechanisms. Normally, for a polymeric NP flowing in a low velocity region, BD is the dominant mechanism in deposition and aggregation. Under favorable conditions, the most common model[126] to describe the deposition behavior of NPs in porous media is known as colloidal filtration theory (CFT).

After knowing the possible mechanisms of deposition and aggregation during the flow, the interaction energy between the surfaces needs to be considered to explain the models. Classic Derjaguin–Landau–Verwey–Overbeek (DLVO) theory has been universally employed to explain the aggregation and deposition behaviors of charged particles in the presence of simple electrolytes[128,129]. DLVO theory and CFT model are often compared to check consistency of the deposition behaviors. In some conditions

like deposition at secondary minimum of energy curve or surface charge heterogeneity, observed results deviated from the CFT predictions[130,131]. For deposition behavior of polymeric nanomedicines, there have been some studies on the adsorption and desorption behaviors in pure water over large plate[59,60], very little is known about kinetics in saturated porous media with environmental related conditions. Secondary minimum effects may appear with higher salinity or with natural organic materials (NOM). It is important to plot the DLVO energy curves before applying CFT model to the deposition process.

3.2 Interaction between polymeric nanoparticles and surface

In a given medium, most important nanoparticle characteristics that determine the nature of interactions between a nanoparticle and an immobile surface are chemical composition, size, shape, surface area, porosity, crystallinity, and heterogeneity of the nanoparticle[132,133]. Suspending medium determines other important properties of nanoparticles, such as the effective surface charge (zeta potential), particle aggregation, stability/biodegradability, dissolution characteristics, and hydration and valence properties of the surface layers[23,134,135]. Chemical or physical interactions are used to classify deposition behaviors between NPs and surfaces. Usually physical interactions (adsorption) are weak and reversible, while chemisorptions are much stronger and irreversible. Formation of strong covalent bonds only happens to the adsorbed particles during their rearrangement or deformation on surfaces. In physical interactions, several types of interaction such as van der Waals (vdW) interaction, Born interaction, electrical

double-layer interaction and etc., play the important roles in the adsorption process. Consider physical interactions in a simple system (Fig. 3.1a) of a spherical rigid nanoparticle with a flat surface where radius of the particle is R and the closest distance between the particle and the surface is h.

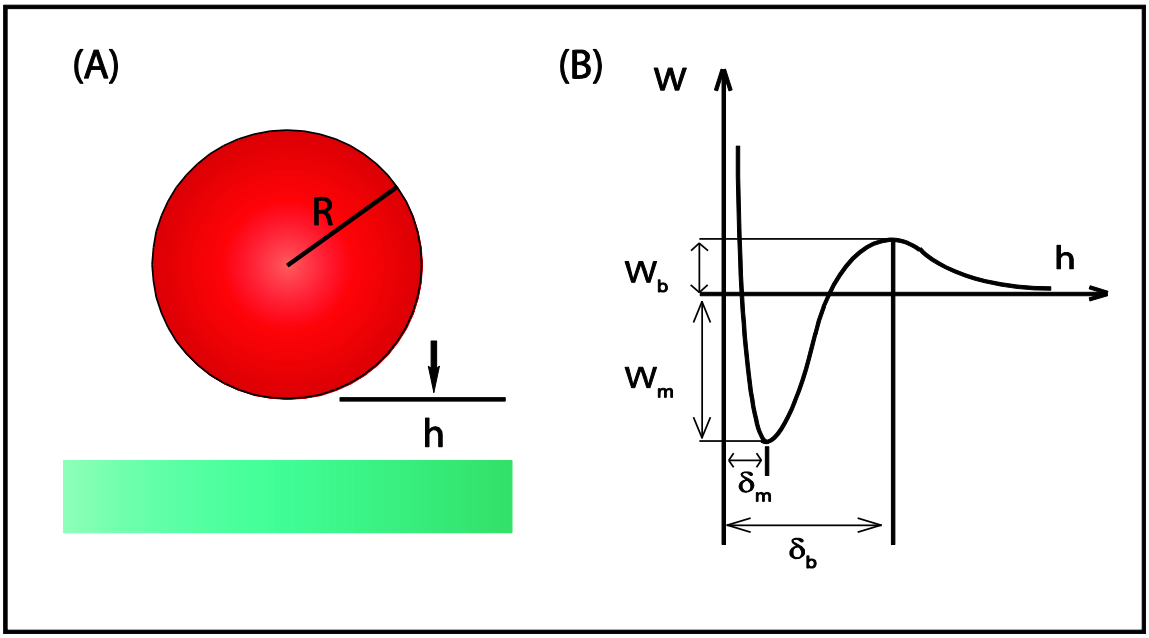

Figure 3.1 Interaction of rigid nanoparticle to the surface[136]**.**
a)Illustration of a simple system. b) Total interaction energy versus distance, x axis is the distance, y axis is the interaction energy. W_m is the primary attractive minimum energy, δ_m is the distance between particle and surface at primary minimum. W_b is the primary repulsive maximum energy at a larger disctance δ_b.

First, the van der Waals interaction energy between a sphere and a semi-infinite plate can be expressed as [137]:

$$W_{vdw}(h) = -\frac{A}{6}\left[\frac{R}{h} + \frac{R}{h+2R} + ln\frac{h}{h+2R}\right] \quad [3.1]$$

where *A* is the Hamaker constant.

Second, Born repulsion is a short-range molecular interaction, resulting from the overlap of electron orbitals. It is the twelfth-order term of the empirical Lennard-Jones 6-12 potential. The born repulsion between a sphere and a plate can be estimated by assuming that these molecular interactions are linearly superimposed [138]:

$$W_{Born}(h) = \frac{A\sigma^6}{7560}\left[\frac{h+8R}{(h+2R)^7} + \frac{6R-h}{h^7}\right] \quad [3.2]$$

where σ is the collision diameter. (typically 0.3-0.5 nm).

Third, the double-layer interaction between a sphere and a plate can be expressed as [139]:

$$W_{DL}(h) = 16\epsilon(\frac{kT}{e})^2 R \times tanh(\frac{e\varphi_{s1}}{4kT}) \times tanh(\frac{e\varphi_{s1}}{4kT})e^{-\kappa h} \quad [3.3]$$

where ε is fluid dielectric constant of the medium, φ_{s1} and φ_{s2} are surface potential of the polymer nanoparticle and flat surface, κ^{-1} is Debye length. This expression is appropriate for monovalent electrolyte solutions when $\kappa h > 2$ and $\kappa R >> 1$. For low surface potentials (φ_{s1}, φ_{s2} <50 mV), the follow equation may also be used [139].

$$W_{DL}(h) = 16\epsilon R \times \varphi_{s1} \times \varphi_{s2} \times e^{-\kappa h} \quad [3.4]$$

Summing the contributions from each effect (equation 3.1, 3.2, 3.3 or 3.4) gives the total energy of interaction between a particle and a plate:

$$W(h) = W_{vdw}(h) + W_{Born}(h) + W_{DL}(h) \quad [3.5]$$

Figure 3.1(b) shows the total interaction curve with the activation energy or energy barrier to adsorption W_b. The corresponding rate constants of adsorption can be estimated using Kramers' rate theory[138,140]:

$$k_a = D(x^*)\sqrt{\frac{\frac{d^2E(x)}{dx^2}\Big|_{x=x^*}}{2\pi kT}}e^{-E_a/kT} \approx \frac{D(x^*)}{R}\sqrt{\frac{E_a}{2\pi kT}}e^{-E_a/kT} \quad [3.6]$$

where *E(x)* is the interaction potential between PNDDS and silica surface, E_a is the activation energy, *x** is the distance at which the potential energy has a maximum, *D(x*)* is the diffusivity of a NP at the distance leading to the maximum in the potential energy profile. For NPs, large activation energies will lead to infinitesimally small adsorption rates due to the exponential dependence. Once total interaction curve shows secondary minimum at longer distance, the activation energy is the difference between repulsive maximum and secondary minimum.

3.2.1 Adsorption isotherms

For polymeric NPs in the solution condition where particle-particle aggregations were not observed due to repulsion interaction, multi-layer adsorption will not exist. Then, the polymeric nanoparticle adsorption equilibrium isotherm is commonly seen as a Langmuir-type or Freundlich-type shape. The Langmuir-type model is described by

$$\Gamma = \frac{\Gamma_{max} K_L C_{eq}}{1 + K_L C_{eq}} \quad [3.7]$$

where C_{eq} is the equilibrium concentration, Γ is the absorbed mass of the polymeric nanoparticle, Γ_{max} is the plateau value and K_L is the Langmuir coefficient.

Langmuir-type model is based on the assumption that the adsorption enthalpy does not vary with coverage. The isotherm shows a steep initial slope followed by attainment of a plateau at high concentration. Freundlich model is described by

$$\Gamma = K_F (C_{eq})^m \quad [3.8]$$

where K_F is the Freundlich coefficient is the Freundlich constant, $1/m$ is is heterogeniety index or adsorption intensity, Γ is the absorb mass of the polymeric nanoparticle, C_{eq} is

the equilibrium concentration. Freundich model is based on the assumption that the adsorption enthalpy decrease linearly with surface coverage. Freundlich-type isotherm shows a monitonic increase for all range of concentrations.

Due to the complicated interaction between polymeric NPs, Langmiur-Freundlich model might be used as in equation 3.9. This isotherm is the composite of Langmuir and Freundlich isotherm and can reduce to Freundlich-type at low concentration and to Langmuir-type at high concentration. Langmuir-type isotherm is more widely used and it is valid for most of adsorption cases.

$$\Gamma = \frac{\Gamma_{max} K (C_{eq})^m}{1 + K (C_{eq})^m} \qquad [3.9]$$

3.3 Deposition behaviors in porous media

Elimelech and co-workers has investigated the transportation behaviors of various nanoparticles in different solution conditions through saturated porous media, studies on transport of polymeric nanomedicines are rather limited. CFT model mentioned in chapter III 3.1 has been commonly used in modeling transportation of nanoparticles in saturated porous media without energy barriers utilizing a pore-space geometry called Happer's sphere-in-cell model[141]. One of the earliest and most widely used equation was proposed by Rajagopalan and Tien called R-T equation[127]:

$$\eta = 4A_s^{\frac{1}{3}} N_{pe}^{-\frac{2}{3}} + A_s N_{Lo}^{\frac{1}{8}} N_R^{\frac{15}{8}} + 0.0038 A_s N_G^{\frac{6}{5}} N_r^{-\frac{2}{5}} \qquad [3.10]$$

$$A_s = \frac{2(1-\gamma^5)}{2-3\gamma+3\gamma^5-2\gamma^6} \; ; \; \gamma = (1-\theta)^{\frac{1}{3}} \qquad [3.11]$$

where η is the contact efficiency of particle to porous media, A_s is the Happer's coefficient, N_{pe} is the Peclet number, N_{Lo} is the London number, N_r is the aspect ratio of nanoparticle to the grain or called interception number, N_G is the gravity number. θ is the porosity of the porous media.

$$N_{pe} = \frac{nanoparticle\ advection\ rate}{nanoparticle\ diffustion\ rate} = \frac{vd_g}{D} \quad [3.12]$$

$$N_{Lo} = \frac{4A}{9\pi d_p^2 v} \quad [3.13]$$

$$N_G = \frac{(\rho_p - \rho_f) g d_p^2}{18\mu v} \quad [3.14]$$

$$N_r = \frac{d_p}{d_g} \quad [3.15]$$

where v is the Darcy's velocity, d_g is the diameter of grain, D is the diffusion coefficient of the nanoparticle, A is the Hamaker constant calculated based on nanoparticle-grain – solution system. d_p is the diameter of the nanoparticle, ρ_p is the density of nanoparticle, ρ_f is the density of the solution, μ is the viscosity of the solution.

Therefore, it is clear that diffusion, interception and gravitational sedimentation are three mechanisms used in R-T equation for the CFT model. New modified terms considering hydrodynamic interactions and vdW interactions[142] have later improved the prediction of the column efficiency in equation 3.10. Although knowing the contact efficiency between nanoparticles and grains, attachment efficiency (α) shall be considered to know the amount of nanoparticles adsorbed on the grains. This can be calculated by fitting an empirical equation to the early-stage breakthrough curve of a nanoparticle solution flowing through a column with porous media:

$$ln\frac{C_{out}}{C_{in}} = \frac{3(1-\theta)\alpha\eta L}{2d_g} \quad [3.16]$$

where C_{out} and C_{in} is the concentration of nanoparticles at outlet and inlet, respectively. θ is the porosity of the column, α is the attachment efficiency, η is the contact efficiency, L is the column length or transport distance of the solution, d_g is averaged diameter of grains. Based on the fitting value α and calculated value η from experiment, deposition rate constant can be known. For first order kinetics, the deposition rate constant is as:

$$k_{dep} = \frac{3(1-\theta)\alpha\eta v}{2d_c} \quad [3.17]$$

At unfavorable conditions, theoretical attachment efficiency calculated by DLVO theory will be less from equation 3.16, because it neglects the secondary minimum effect from surface heterogeneity and straining effect happened when flowing in porous media.

CHAPTER IV

NANOSCALE DYNAMICS OF HEAVY OIL RECOVERY USING SURFACTANT FLOODS*

4.1 Introduction

Using primary and secondary recovery, only 20-50% of oil can be extracted from an oil reservoir[1–3]. The remaining 50-80% of oil stays underground where oil is adsorbed on rock surfaces, leading to oil entrapment within the rock pores[4,6,66]. At a time of surging global energy demand, researchers are now actively investigating ways[7–10] to squeeze extra barrels from oil fields via various enhanced oil recovery (EOR) techniques such as gas injection, chemical injection, microbial injection, or thermal recovery.

Surfactant flooding, which is one type of EOR, involves the addition of surfactants to water floods to reduce oil-water interfacial tension (IFT) to ultra-low values so that mobility of oil droplets is increased[12–15]. Such a low IFT typically leads to a three-phase behavior in which a bicontinuous microemulsion is in equilibrium with excess oil and water phases[12–15]. The technical feasibility of oil recovery via surfactant flooding were demonstrated in early field tests by Surkalo et al.[78,79], Hill et al.[80,81], Pursley et al.[82,83], and Lake and Pope[84].

*Reprinted with permission from "Nanoscale dynamics of heavy oil recovery using surfactant floods" by I-Cheng Chen and Mustafa Akbulut, 2012. *Energy & Fuels*, 26(12), pp.7176-7182. Copyright 2012 American Chemical Society.

Since then, numerous studies focusing on the bulk oil recovery properties of surfactant floods have been conducted: Majority of these studies have investigated the effects of phase behavior[88], wettability[86], interfacial tension[87–91], water mobility[89], and foaming performance[92] on the behavior of oil recovery using surfactant floods. However, while there are a numerous studies on enhanced oil recovery via surfactant floods at the bulk scale[93–96], studies on the nanoscale dynamics of oil recovery via surfactant floods are very limited.

In this work, we have investigated the kinetics and mechanism of asphalt removal using a model non-ionic surfactant solution, 4-nonylphenyl-polyethylene glycol at nanoscale. We focused on asphalt because asphalt, which is found in the heavy ends of crude oil[143], has been shown to have a great impact on the EOR process[144,145]. 4-nonylphenyl-polyethylene glycol is used mainly due to its ability of heavy oil recovery[146]. This study was conducted using four complementary techniques: quartz crystal microbalance with dissipation (QCM-D), atomic force microscopy (AFM), ellipsometry, and dynamics light scattering (DLS).

4.2 Materials and methods

4.2.1 Materials

Asphalt (Cheyenne Oilfield, CO) was received from Valero Energy Corporation (TX, USA) and used as received. 4-nonylphenyl-polyethylene glycol (polyoxyethylene (n=9) nonylphenylether, average M_n=617) and tetrahydrofuran (THF, >99.9%) were purchased from Sigma-Aldrich.

4.2.2 Preparation of asphalt film

Asphalt was rigorously mixed with THF to form a homogenous solution without any sediment. A few drops of asphalt-THF mixture were casted on a SiO_2 QCM sensor. Then, the sample was thoroughly dried in a vacuum chamber (using an Edwards XDS-5c scroll pump) at 0.1 torr over at least 24 hrs to ensure the comprehensive removal of THF. The mass of the dried asphalt film on the sensor was measured using QCM-D. The surface topography of the dried asphalt layer was characterized by atomic force microcopy.

4.2.3 Quartz crystal microbalance with dissipation (QCM-D)

The removal dynamics of asphalt from SiO_2 surface was studied using a QCM-D (E1, Q-sense) and a SiO_2 QCM sensor (QSX 303, Q-sense). The QCM consists of a thin quartz disc sandwiched between a pair of electrodes[147,148]. Due to the piezoelectric properties of quartz, it is possible to excite the crystal, resulting in oscillation, by applying an AC voltage across its electrodes. The resonance frequency (f) of the crystal depends on the total oscillating mass, including water coupled to the oscillation[147,148]. When a thin film is attached to the sensor crystal, a decrease in the oscillation frequency occurs while an increase in the oscillation frequency takes places upon the removal of mass from the sensor crystal surface. The time sensitivity of QCM-D (E1, Q-sense) is 200 points per second, and its mass sensitivity is 1.8 ng/cm^2 in liquids (hydrocarbons). In

this work, QCM was utilized as a very sensitive balance with nano-gram resolution and time resolution of 0.1 s.

Figure 4.1 shows typical steps involved in a QCM experiment. First, a baseline for a dry sensor was acquired. Then, the mass of asphalt film deposited was calculated from the oscillation frequency shift that was induced by the presence of asphalt film. Then, a new baseline was obtained using Milli-Q water (18.2 MΩ cm^{-1} @ 25 °C). Next, Milli-Q water was replaced by surfactant solutions to initiate and measure the removal (desorption) process of asphalt film from the SiO_2 surface. The flow rates of both Milli-Q water and surfactant solutions were 0.2 g/min. Measurement data for frequencies (f) was acquired at several harmonics (15, 25, 35, 45, 55, and 65 MHz) simultaneously. All measurements in the flow chamber were performed at a temperature of 25°C, to within 0.1°C to avoid drifts in f. The asphalt film was exposed to the surfactant solution for about 10 hour during which frequency and dissipation data were simultaneously recorded via QCM-D.

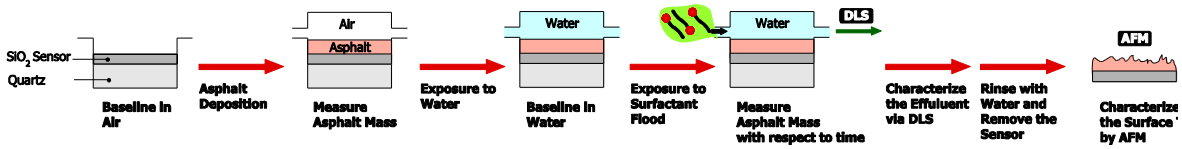

Figure 4.1 Different stages of experiments used for investigating the removal dynamics of asphalt from the SiO_2 surface.
First step involves obtaining a baseline for the dry sensor. The second step is the deposition of asphalt film on the SiO_2 surface and determination of the asphalt mass. The third step involves the exposure of the loaded sensor to water and obtaining a new baseline for the wet system. The fourth step consists of the exposure of the sensor to surfactant solution, the measurement of the asphalt mass on the sensor as a function of time, and the analysis of effluent with DLS. The final step is the characterization of the asphalt film with AFM at pre-defined intervals.

In addition, the effluent coming out of the QCM chamber was collected at pre-defined times and analyzed using dynamic light scattering (DLS) (Zetasizer Nano ZS90, Malvern) to determine the particle size distribution of potential micelles and emulsions.

4.2.4 Atomic force microscopy (AFM)

The surface topography of asphalt deposited and the change in the surface topography was measured via AFM in tapping mode (Nanoscope IIIa, Veeco Instruments, CA, USA) as a function of time of exposure to surfactant solution. The AFM measurements were conducted using a tip radius of less than 10 nm. AFM measurements were performed at a 0˚ scan angle on a 50-µm ×50-µm area at a speed of 0.2 µm/s.

4.2.5 Ellipsometry

Film thicknesses were measured using image nulling ellipsometry (EP3 Ellipsometer-Nanofilm, Germany). The xenon lamp was used as light source, which was polarized from 400 to 800 nm, and had an angle of incidence at 50°. Measurements were performed on at least five different spots on each sample for each different flooding time.

4.3 Results

4.3.1 The formation of asphalt film on QCM-D SiO_2 sensor surface

We found that the evaporation of asphalt/tetrahydrofuran mixture under vacuum condition led to fairly smooth and robust asphalt film (Fig. 4.2). The interplay among hydrogen bonding and donor/acceptor interactions and dispersion forces determines the wetting behavior of thin films[149,150]. Asphalt is a mixture of acids (e.g. phenol and benzoic acid), bases (e.g. quinoline and hydroxyquinolone), and polar and non-polar neutrals[151–153]. Considering that SiO_2 is typically negatively charged[154,155] and also can act as Bronsted acid[154–156], it is no surprise that SiO_2 and the basic components of asphalt can form strong acid-base electrostatic attraction, leading to the complete wetting of the asphalt film on the SiO_2 substrate. Furthermore, interaction between polar components of asphalt such as aromatic groups and silica surface can also contribute to the observed wetting behavior[154,155,157–163].

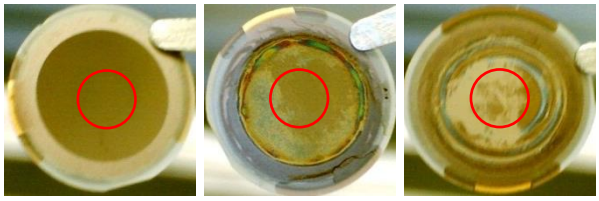

Figure 4.2 Photographs of SiO_2 quartz sensor during the surfactant flooding.
(a) clean SiO_2 quartz sensor, (b) asphalt film on the sensor, and (c) asphalt film that is treated with 60 hour flow of surfactant solution at a concentration of 0.7 g/L. In addition, the effects of surfactant concentration and exposure durations on the removal of asphalt are also investigated and described in the proceeding section.

4.3.2 Removal dynamics of asphalt from SiO_2 surface

Figure 4.3 shows the mass of asphalt film remaining on the SiO_2 surface as a function of time of surfactant exposure at various surfactant concentrations. The analysis of this figure revealed the following results: First, the rate of asphalt removal increased with increasing concentration of surfactant solution. Second, when the surfactant concentration is below critical micelle concentration (CMC, 0.07 g/L), the removal dynamics of asphalt followed a different trend compared to the dynamics obtained at concentrations above CMC. Third, for all surfactant concentrations, desorption data could be well described by two term exponential decay fits, Eqn.1, (dashed lines in Fig. 4.3), suggesting that two different first-order processes are responsible for the overall removal of asphalt.

$$m(t) = m_0 + m_1 e^{-k_1 t} + m_2 e^{-k_2 t} \qquad [4.1]$$

The corresponding rate constants for the asphalt removal process at various surfactant concentrations are listed in Table 4.1.

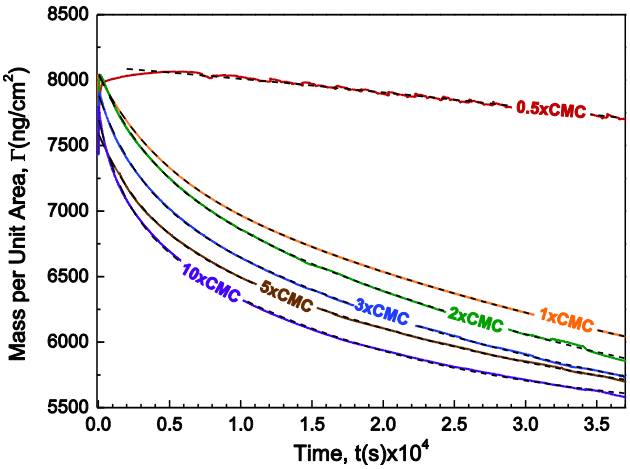

Figure 4.3 Mass desorption trend from QCM-D via surfactant flooding.
The mass of asphalt film remaining on the SiO_2 surface as a function of time of surfactant exposure at various concentrations and two-term exponential fits for the mass vs. time data (shown with dashed lines).

Table 4.1 Desorption rate constants of asphalt film.
The summary of rate constants ± 1 standard deviation (SD) obtained through fitting mass vs. time data with Eqn. 1 and the removal efficiency calculated at 10 hrs of surfactant flooding. Note: Experiment in each surfactant concentration was repeated 4 times. The data fitting was carried out using Originlab Pro 8.0.

Surfactant concentration in terms of CMC	**Rate constant k_1, $\times 10^{-4}$ s^{-1}**	**Rate constant k_2, $\times 10^{-5}$ s^{-1}**
0.5	—	1.46±0.14
1	2.32±0.13	1.95±0.04
2	2.35±0.15	2.02±0.08
3	2.69±0.12	2.16±0.06
5	2.97±0.14	2.85±0.13
10	3.35±0.24	3.80±0.50

In equation 4.1, one rate constant, k_1, was larger (faster process) and in the order of 10^{-4} s^{-1} while the other one, k_2, was smaller (slower process) and in the order of 10^{-5} s^{-1}. Both rate constants increase with increasing surfactant concentrations above the CMC.

At 10 hrs of surfactant exposure, the asphalt removal efficiency, $(m_{in}-m_{10hr})/m_{in}$, ranged from 21% to 29% depending on the concentration of the surfactant flood (Fig. 4.4). Below CMC, the fast process disappeared, leading to an inefficient removal.

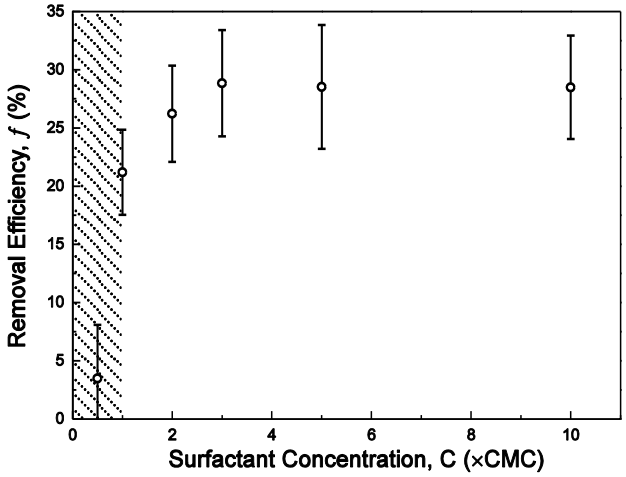

Figure 4.4 Removal efficiency relation with surfactant concentration.
Asphalt removal efficiency ± 1 SD as a function of surfactant concentration upon 10 hrs of surfactant flooding. Note: Experiment in each surfactant concentration was repeated 4 times.

4.3.3 Characterization of the effluent containing asphalt emulsions

To determine the size characteristics of colloids in the effluent, we used the dynamic light scattering technique. Figure 4.5 displays the particles size analysis of the effluent that is formed by flowing a 5×CMC concentration of surfactant over the asphalt film as function of time. For all times, the effluent contained micelles that are several nanometers and microemulsions that are a few to several hundred nanometers. The empty (unloaded) micelles were 2-4 nm in size, suggesting that the micelles shown in

figure 4.5 are loaded with a trace amount of oil. In addition, the relative ratios of loaded micelles to microemulsions increased with increasing time of flow. Furthermore, while the mean sizes of both microemulsions and micelles mostly decreased with increasing time of flow, the decrease was more pronounced for the microemulsions (i.e. 63% decrease for microemulsions and 20% decrease for micelles). Considering that the overall removal process has one fast and one slow component (Fig. 4.3 and Eq. 4.1), these trends suggest that the fast process (effective at early times) is related to the formation of larger microemulsions while the slow process is related to the formation of micelles. Alternatively, these trends may be formed because the inlet is continuously supplied with a fixed concentration of surfactant above CMC while there is a limited amount of asphalt film on the substrate. However, even at longer times, since 55-65% of asphalt remained on the surface, it is unlikely that the latter effect —the finite mass effect— is responsible for these trends.

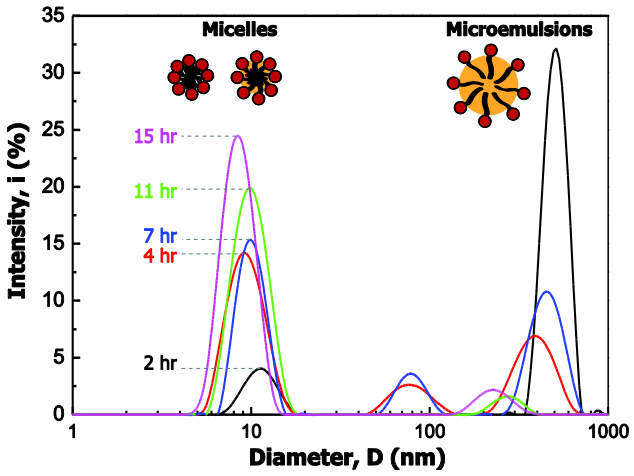

Figure 4.5 Size distribution from dynamic light scattering measurements. The particle size distribution of the effluent stream, which formed upon exposing asphalt films to a flow of surfactant solution, as a function of time. At CMC, empty (unloaded) micelles had a mean size ranging from 2-4 nm in the absence of oil.

4.3.4 Topography of asphalt film on SiO_2 surface before and after surfactant rinsing

We relied on atomic force microscopy (AFM) to determine the structural changes on the asphalt surface due to the exposure of surfactant solution. The neat asphalt film on SiO_2 was mostly smooth while the surface also had some randomly distributed, small asperities (Fig. 4.6a). Upon the flow of surfactant solution, these asperities mostly disappeared (Fig. 4.6b-e). The comparison of the topographical maps obtained at different times of exposure reveals that there is a gradual formation of holes on the asphalt film as the surfactant solution passes over it (Fig. 4.6b-e)

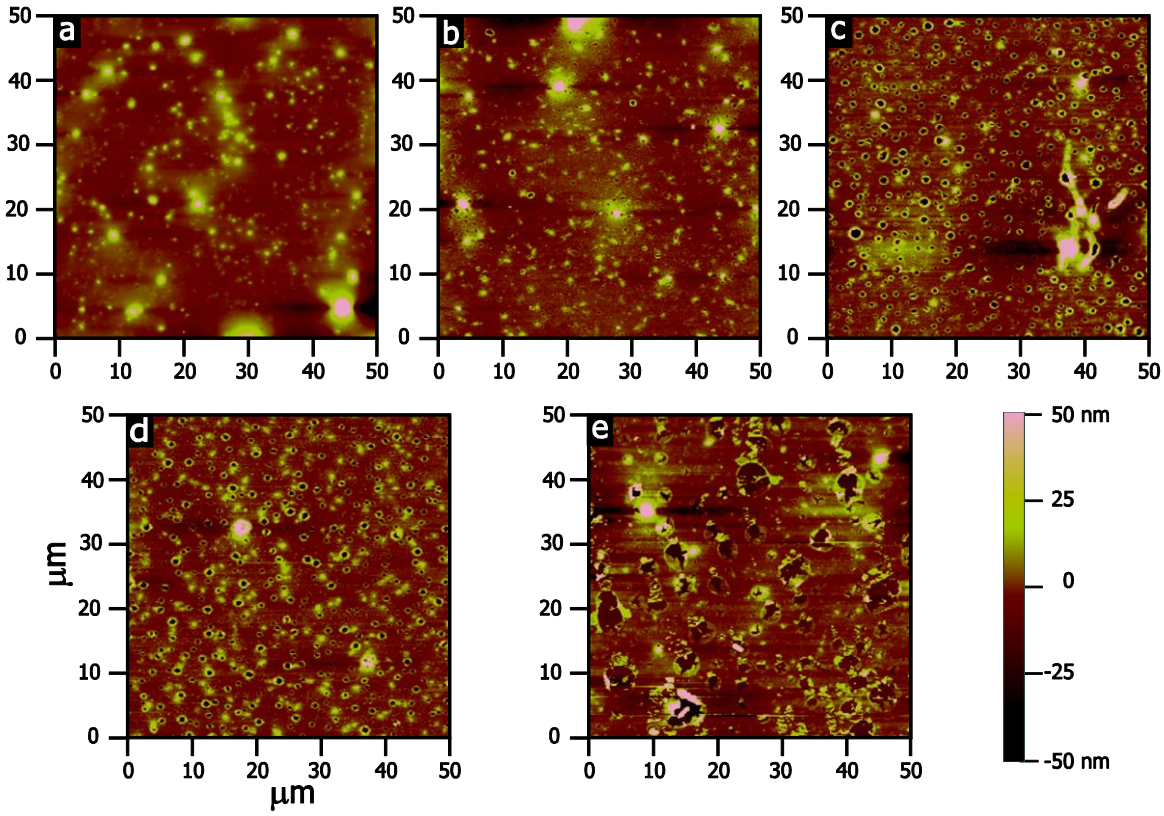

Figure 4.6 AFM micrographs of the asphalt-film on SiO_2 surfaces.
(a) before surfactant flood, after (b) 2 hr, (c) 6 hr, (d) 10 hr, and (e) 18 hr surfactant flood exposure. Surfactant concentration 0.35g/L in 200 mg/min flow rate at 25°C.

It is important to note that AFM measures only the relative displacement of structures on a surface. Therefore, to determine whether there is a continuous, uniform (throughout) removal of asphalt film in addition to the local removal of asphalt forming holes on the surfaces, we have compared the removed mass measured by the QCM with that estimated by analyzing total volumes of holes using the AFM data. Such comparison revealed that the removal of asphalt from the holes could not solely account for the total mass removal, suggesting that there is also a continuous uniform removal of

asphalt for this process (Fig. 4.7). The presence of uniform (throughout) removal has also been confirmed by independent, time-resolved ellipsometry studies (Fig. 4.7).

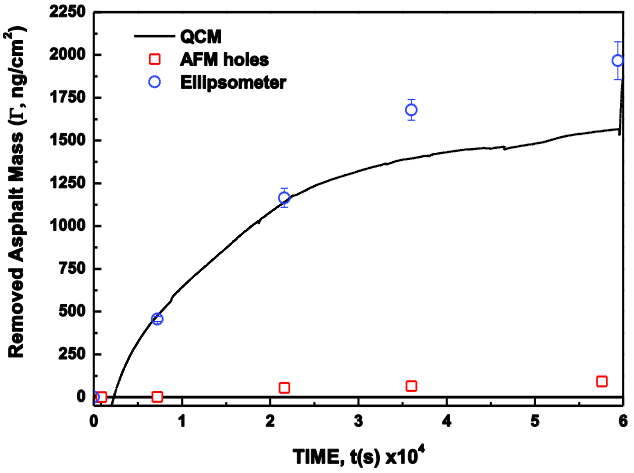

Figure 4.7 Removal of asphalt masses by QCM-D, AFM and ellipsometer. Removal of asphalt mass ± 1 SD as a function of time due to the exposure of surfactant solution (5×CMC) to a thin film of asphalt on SiO_2 surfaces measured by QCM-D, AFM, and ellipsometry. Note: Removed asphalt masses at specified time intervals measured by ellipsometer were repeated 3 times.

4.4 Discussion

4.4.1 Further details of QCM-D studies

In each QCM-D experiment, two types of data were recorded simultaneously: variations in resonance frequency and energy dissipation response. While the former provides information on the mass of adsorbate on the surface, the latter provides information about the elastic property of the adsorbed film[164–167]. In all experiments, the dissipation traces were very small, indicating that the asphalt film was relatively rigid.

Therefore, the use of Sauerbrey equation is appropriate for calculating the adsorbed mass on the sensor[167].

It is important to underline that even without soft layer dissipation effect, the frequency changes can be related to more than simple mass loading factors[154,155,166,168,169]. Liquid loading effect due to the change of viscosity/density[168] and liquid trapping effect due to the surface roughness (interfacial cavities and pores)[166,169] can also partially contribute to the frequency drift/shifts during the measurement.

To understand the influence of viscosity/density change, we monitored the frequency change upon alternating exposure of pure water and surfactant solutions several times. These control experiments revealed that viscosity/density effect is noticeable within the first 5 seconds only. Considering that all experiments had time scales in the order of several hours, the influence of the viscosity-density effect on this study is insignificant.

Regarding the surface roughness effect on the QCM studies, AFM micrographs revealed that the depths of cavities and holes formed on the asphalt surface due to surfactant flows were in the order of 10 to 50 nm depending on the time of surfactant exposure (Fig. 4.6). Martin et al.[169] showed that surface features can be considered hydrodynamically smooth in a steady flow if they are smaller than 30% boundary layer thickness. For water oscillating at 5 MHz above a quartz sensor, the boundary layer is about 38 nm.[169] Namely, at early times, the depths of cavities are much smaller than the boundary layer for almost all the surface, suggesting that the influence of surface roughness is insignificant on the QCM measurements. However, the roughness effect becomes noticeable at longer times of surfactant exposure. This finding is also consistent with

independent ellipsometry studies relying on an optical means rather than a mechanical means to detect the adsorbed mass (Fig. 4.7): The difference between QCM-D and ellipsometry results is very small before 7-8 hrs of surfactant exposure while the difference is noticeable after 7-8 hr.

4.4.2 The presence of two exponential terms in the removal rate equation

Influences such as surface inhomogenities and interplay between diffusion and adsorption can lead to the presence of two different rate constants. First, surfaces are usually not perfectly homogeneous as are the asphalt surfaces used in this study. On heterogeneous surfaces, the binding energy of an adsorbate will generally not be a fixed value, but there is a distribution of binding energies[170–172]. In other words, some regions of the surface can have higher affinity for surfactants, leading to a faster adsorption while other regions can have lower affinity, giving rise to a slower adsorption. Considering that the removal of the asphalt is ultimately related to the amount of surfactant adsorbed on the asphalt surface[94,173], the surface heterogeneity can explain the presence of fast and slow removal processes.

4.4.3 Comparison of the results with previous bulk and computational studies

Previous bulk scale studies suggest that the removal of an oil droplet from a solid using surfactant solution involves two stages. First, the roll-up of the oil into the shape of a droplet takes place due to the imbalance of forces at the contact line arising from the presence of surfactant in the aqueous phase[174,175]. Second, the emulsification of the oil

droplet in the aqueous solution occurs after detachment from the solid surface[176–178]. Two major mechanisms have been proposed for mobilizing oil: (i) lowering oil-water interfacial tension (IFT) while buoyancy is the driving force for oil recovery[15,179,180], and (ii) altering formation wettability from oil-wet to intermediate or water-wet[181–183]. Qiao et al.[184] have recently shown that upon increasing surfactant concentration, IFT of crude oil rapidly decreases first and then reaches a steady-state value (stabilizes). This finding is very similar to the trend in Figure 4.3, indicating that IFT is directly related to the oil removal efficiency.

Past studies on adsorption kinetics of non-ionic surfactants on surfaces have displayed the following common trends: (i) a linear increase in adsorption with time; (ii) a transition regime where the rate of adsorption decreases; and (iii) a plateau regime[185–187]. The range over which each region extends varies as a function of the bulk concentration, nature of the surfactant, nature of the surface, presence of salt, etc. In this study, adsorption of surfactants on asphalt surface is much more complex than a typical adsorption process because surfactant adsorption and consequent removal of asphalt simultaneously take place. Studies on polymer adsorption and desorption have shown that desorption is usually non-exponential in time when it is rate-limited by diffusion away from the surface rather than by energetics of surface detachment[188,189]. When desorption is rate-limited by the energetics of surface detachment, desorption is exponential and extensions of classical Langmuir kinetics are appropriate[188,189]. Therefore, due to the existence of the exponential kinetics, we believe that the detachment of microemulsions and loaded micelles is the rate-limiting step (as opposed

to diffusion) in the oil recovery experiments. This may be reasonable considering the relatively high viscosity and rigidity of asphalt film.

However, it is important to note that the detachment of microemulsions is still faster than the detachment of loaded micelles (Fig. 4.5). If we only consider the thermodynamical aspects of this process, the energy change in the overall system due to the formation of micelles and microemulsion is equal to the sum of the energy required to create surface area (surface area between the oil and aqueous phases, ΔA, multiplied by the interfacial tension, γ) and the decrease in the configurational entropy ($-T\Delta S$)[170]. The change in the interfacial area is always positive and configuration entropy is always negative. Configurational entropy dominates over the interfacial term as the size of emulsions decrease or number of emulsions increases[170]. Therefore, according to the Arrhenius equation, ($k \propto \exp(-E_{binding}/kT)$[190], the micelles are expected to form faster than the microemulsions. However, we observed an opposite trend, suggesting that the mechanism of micelle formation is different from that of microemulsion formation. The formation of water channels that predominantly assist the formation of microemulsions is presumably responsible for this discrepancy.

Liu et al.[175] has recently studied the mechanism of oil detachment from a silica surface using surfactant floods via molecular dynamics simulations. Their study has shown that formation of water channel within the oil is a critical element of oil detachment process[175]. In addition, the diffusion penetration of water molecules into oil-water interface and subsequent gel layer formation in the vicinity of the contact line was found to accelerate the removal of the oil molecules from the silica surface[175]. In light of

this study, we suspect that the pores and nanochannels within the asphalt film could guide the formation of water channels and may facilitate the removal of asphalt using surfactant floods.

Chanda and Bandyopadhyay[191] have shown that the surfactant molecules exhibit more extended conformations with increasing the thickness of the monolayer in the presence of the oil medium. They also observed that the hydrocarbon tails of the surfactants are more vertically oriented at the oil/water interface[191]. In addition, the reorientation of both the head and the tail parts of the surfactant molecules is slower in the presence of the oil medium and that the rigidity of the surfactant monolayer increases in the presence of oil due to penetration of the oil molecules into the hydrocarbon tail region of the monolayer[191]. These effects may also be responsible for the retardation of asphalt removal that was observed at late exposure stages (i.e. when more oil is dispersed into water).

4.4.4 Overall mechanism of oil removal via surfactant floods

When we put everything together, the picture emerges that the removal mechanism involves several phenomena: diffusion, adsorption, Marangoni Effect, and the formation of water channels (Fig. 4.8). First, the surfactants that are dispersed in water at either molecular or micellar form reaches oil-water interface through diffusion and convection (Fig. 4.8a). Next, the hydrophobic part of the surfactant gradually penetrates into the asphalt phase. The local variations in surfactant concentrations that, for instance, can be induced by asphalt heterogeneity create a gradient in surface tension

(Fig. 4.8b). Such a gradient causes a liquid to flow away from regions of low surface tension because the liquid with a high surface tension pulls more strongly on the surrounding liquid than one with a low surface tension[192,193].

In addition, asphalts generally form porous structures. Water prefers to be in contact with silica rather than asphalt due to the hydrophobic interactions[194]. In the presence of surfactants, such porous structures can be filled with water/surfactant mixture to minimize the free energy of the overall system (Fig. 4.8c). Considering high viscosity and rigidity of asphalt, we believe that the surfactant encapsulated asphalt granules within water channels are likely to form the microemulsions identified in Figure 4.5 while the deformations induced by Marangoni effects are associated with the formation of micelles.

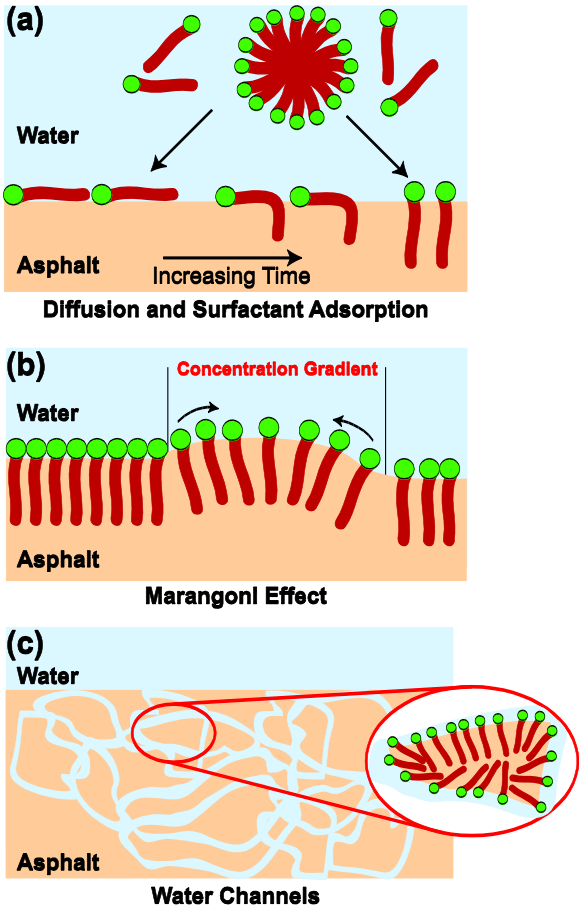

Figure 4.8 The possible processes taking place during the removal of asphalt via surfactant floods.
(a) Diffusion and adsorption of surfactant on asphalt are prerequisites for the efficient removal of asphalt. (b) Marangoni effect helps to roll asphalt film through surface tension gradients. (c) Because the asphalt is more hydrophobic than silica (the substrates), thermodynamics favors a direct contact between silica and water rather a contact between asphalt and water. Therefore, water channels are likely to form in the asphalt film with time.

4.5 Conclusion

We have investigated the removal of asphalt from silica surfaces using surfactant floods as a function of surfactant concentration and time of surfactant exposure at nanoscale. This study shows that the removal rate increased with increasing surfactant

concentration until concentration of 2-3×CMC. The removal dynamics could be well described by two-term exponential decay models, indicating that two different first-order processes are responsible for this behavior. The characterization of the effluent upon exposure to the surfactant solution as a function of time suggested that the fast process is associated with the formation of larger microemulsions while the slow process is related to the formation of loaded micelles. Overall, this work relying upon various advanced experimental techniques leads to new insights into the dynamics of heavy oil recovery via surfactant floods.

CHAPTER V

USE OF PH-RESPONSIVE AMPHIPHILIC SYSTEMS AS DISPLACEMENT FLUIDS IN ENHANCED OIL RECOVERY*

5.1 Introduction

When oil is displaced by plain water flooding, the injected water fingers through the reservoirs due to the high oil-water mobility ratios. Water fingers leave most of the oil behind, leading to inefficient oil recovery[195,196]. One approach in enhanced oil recovery (EOR) is to increase the viscosity of water by adding viscosity modifiers to better match the viscosity of reservoir oil. Such an approach enables a uniform advance of the water front to sweep a larger volume of the reservoir and helps displacing oil in micropores and crevices that cannot be otherwise displaced by water flooding[197,198].

In the context of oil recovery, most commonly investigated viscosity modifiers are water soluble polymers such as poly(acrylamide)[114–116], polysaccharides[199,200], poly(vinyl alcohol)[118,119], and poly(vinylpyrrolidone)[120]. The polymer injection in EOR has successfully been implemented in Marmul (Oman)[74,201], Oerrel (Germany)[108], Courtenay (France)[109], and Daqing (China) fields[110]. In addition, there are several promising field trials and pilot studies undergoing in Argentina, Brazil, Canada, India, the USA, and Venezuela[63,111,112,202].

*Reprinted with permission from " Use of pH-responsive amphiphilic systems as displacement fluids in enhanced oil recovery" by I-Cheng Chen, Cengiz Yegin, Ming Zhang and Mustafa Akbulut, 2014. *Society of Petroleum Engineers*, 19(06), pp.1035-1046.

Aside from water soluble polymers, wormlike micelle solutions have recently received increased attention because of their unique rheological properties as potential viscosity modifiers in EOR[203,204]. Cationic, anionic, nonionic, and zwitterionic surfactants and their mixtures have been shown to produce wormlike micelles having viscoelastic properties[205–209].

The current heuristics suggest that polymer flooding should be applied in reservoirs with oil viscosities between 10 and 150 mPa.s[210,211]. The key factor limiting the recommended range is that for oil viscosities greater than 150 mPa.s, the injected water viscosity values required for a favorable mobility ratio ($M=k_w\mu_o/k_o\mu_w\leq1$) give rise to prohibitively low values of polymer-injectivity and pumping-efficiencies. In this work, we describe a novel type of adaptable amphiphile system based on the complexation of a long chain amino-amide and maleic acid having reversibly adjustable viscosities that can enable us to overcome the injectivity limitation. The concept is that the viscosity of injected amphiphile solution will be maintained at initially low values for easy injection and pumping, and then increased via an external pH-stimuli just before or upon contacting oil (Fig. 5.1). To demonstrate the proof-of-concept, rheometry and sand column displacement experiments at various temperatures, pH, and salt concentrations were used. The mechanism of viscosity adjustment was investigated by use of cryogenic transmission electron microscope (cryo-TEM).

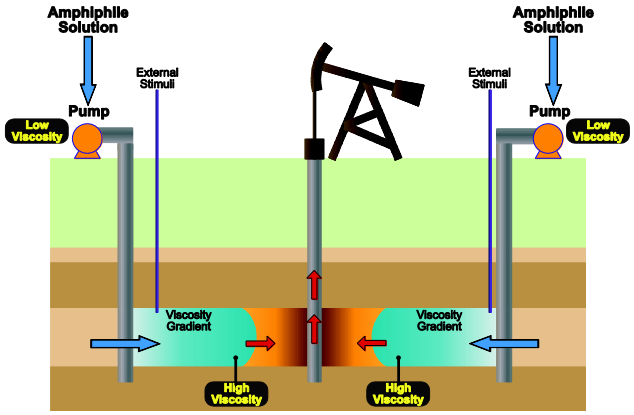

Figure 5.1 Concept of using adaptable amphiphiles for controlling viscosity of injected water in EOR.
Initially low viscosities will lead to easier injectivity and efficient pumping while later high viscosities and efficient pumping, whereas later high viscosity will yield favorable mobility ratios and elimination of water fingering. For the developed adaptable amphiphile, when the oil field has naturally basic pH such as carbonate reservoir[212], high viscosity can be spontaneously obtained and, hense, the external stimuli may not be needed in this case.

5.2 Materials and methods

5.2.1 Materials

Aluminum oxide, Al_2O_3, (activated, neutral, 150 mesh), paraffin oil, hydrochloric acid (37%), Stearic acid (95%), polyacrylamide (5-6×10^6 g/mol, non-ionic water soluble), and sodium hydroxide (≥97.0%) were purchased from Sigma Aldrich (St. Louis, MO). Maleic acid (>98%), N,N- dimethyl-1,3-propanediamine, DMPDA, (>99%), and sodium fluoride, NaF, (99%) were purchased from Alpha Aesar (Ward Hill, MA). Sand (pure, 40-100 mesh) was purchased from Acros Organics (Geel, Belgium). All chemicals were used as received.

5.2.2 Synthesis of adaptable amphiphile

Figure 5.2 describes the synthesis of the adaptable amphiphile system with pH-sensitive viscosity. N-(3-(dimethylamino)propyl)stearamide (marked in Fig. 5.2 as A) was prepared by condensation of stearic acid directly with DMPDA in the absence of any solvent using reflux at 160°C in oil bath for 10 hours by Chu and Feng[213]. The reaction was carried out under argon atmosphere to eliminate undesired oxidation byproducts. While NaF was used as catalyst to accelerate the reaction, Al_2O_3 was utilized to absorb water forming during condensation reaction. After the reaction was completed, the excess DMPDA was removed by washing with cold acetone. Then, the product was dried under vacuum at 40°C for 24 h. Next, the complexation of A with maleic acid and/or formation of 2-(dimethyl(3-stearamidopropyl)ammonio)acetate (marked in Fig. 5.2 as C) was induced by the addition of maleic acid. The chemical characterization of synthesized materials are described in chapter V 5.7.

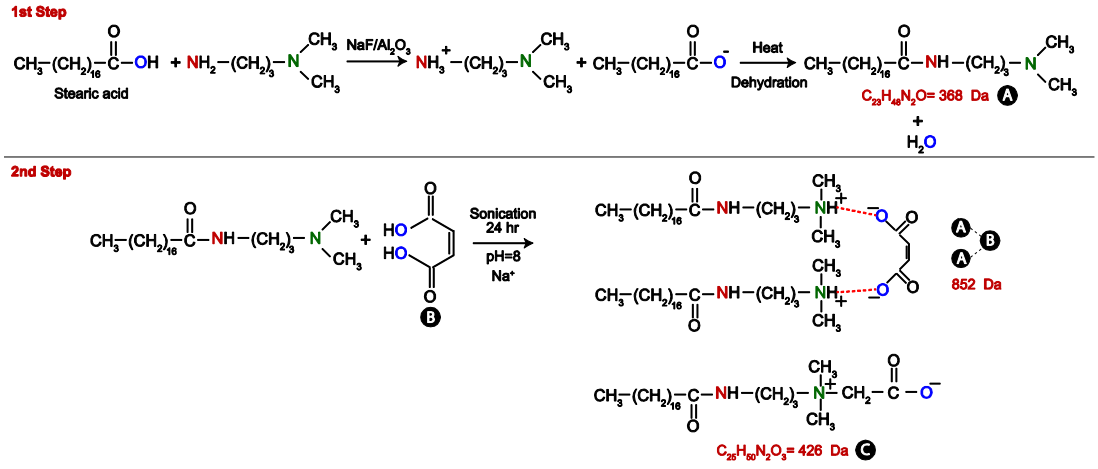

Figure 5.2 The two-step synthesis protocol for the formation of the pH-sensitive amphiphile.

5.2.3 Rheology measurements

Steady and dynamic rheological experiments were performed using a modulator compact rheometer (MCR301, Anton Paar GmbH, Graz, Austria) with a cone-and-plate geometry (50 mm diameter, 0.987 ° cone angle). The gap was set at 0.05 mm and temperature was controlled at 22 °C, within ± 0.1 °C, throughout the measurements. Samples were equilibrated at the temperature of interest for at least 30 min prior to the experimentation. Dynamic shear measurements were taken over the frequency range of 10^{-3} to 10^{3} Hz. The extrapolation of viscosity/shear-rate curve to zero frequency was used to determine the zero-shear viscosity of the amphiphile solutions. The amphiphile and polyacrylamide concentrations (10, 20, 30, 40, and 50 mM), the pH of the solution (pH 4, 5, 6, 7, 8, and 9), temperature (22, 50, and 75 °C), and salt concentrations (0.5, 1, 3 and 5 wt% in amphiphilic solution, and 1 and 5 wt% in polyacrylamide solution) were four main parameters of interest in rheological studies. Each experiment was repeated at least three times for the statistical reliability.

5.2.4 Oil displacement experiments

Oil displacement experiments were carried out in a vertical cylindrical glass column with an internal diameter of 8.2 mm and a total length of 70 mm (i.e. V=3.70 cm^3). In all sand column experiments, a fixed weight (5.81±0.03 g) of air-dried SiO_2 sand (40-100 mesh) was placed in the column using gentle shaking and tapping to ensure uniform packing of sand and to ensure that the sand is homogenously extending from the bottom to the top. Also, a stainless steel net with 250 mesh was places at the bottom and

top of the column to mechanically keep sand in place. The porosity of the sand pack was estimated to be 40.8±0.5%, and the corresponding pore volume (PV) was 1.51±0.01 cm^3. As shown in Fig. 5.3, after preparing sand column, first, it was saturated with water using a high pressure syringe pump with a flow rate of 1.96 cm^3/min. The corresponding initial water saturation was 0.97±0.01. Then, paraffin oil was pumped through the water saturated column to replace the water until irreducible water saturation was reached. The oil flow rate used to establish initial oil saturation was 0.33 cm^3/min, which leads to the initial oil saturation of 0.99±0.01. Afterwards, a predetermined volume (4.9 cm^3, 3.3 PV) of water, adaptable amphiphile solution, or polyacrylamide (PAM) solution was flooded into the sand column to displace the oil. During all flooding tests, the Darcy velocity was 0.34 mm/s. The residual oil saturation (ROS) attained and recovery fraction were calculating by separating the displaced oil-water (or amphiphile or polyacrylamide solution) mixture and volumetrically measuring each phase. These experiments were carried out at three different pH values, three different temperatures, and four different salt concentrations with at least triplicate repeats.

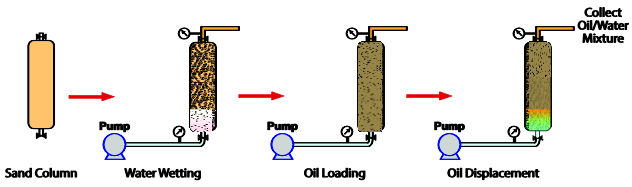

Figure 5.3 The experimental set-up used in the oil displacement experiments.

5.2.5 Pendant drop experiments

The interfacial tension (IFT) for the oil–water (or adaptable amphiphile, polyacrylamide, or brine) system was characterized using pendant drop method as described by Kim and Kovscek[214]. In essence, the method relies on capturing digital images of oil drop and the analysis of drop shape to calculate the interfacial tensions[215,216].

5.2.6 Cryogenic transmission electron microscopy (cryo-TEM)

Cryo-TEM is used to better understand the mechanism by which the developed adaptable amphiphile system modify viscosity. The sample preparation was carried out inside an automated vitrification device (FEI Vitrobot, Hillsboro, OR) as described by Regev et al.[217]. The vitrified samples were transferred to the cryo-TEM transfer stage, which inserted into the microscope (FEI, Tecnai G2 F20 FETEM, Hillsboro, Oregon) for direct observation. The experiments were maintained below -170°C throughout the specimen observation. The adaptable amphiphile solutions were characterized by cryo-TEM at pH 4 and 8 and each experiment was repeated twice.

5.3 Results and discussion

5.3.1 Rheological properties

Rheological measurements were performed to determine how viscosity of the adaptable amphiphile solution is influenced by varying pH values, amphiphile concentrations, temperatures, and salt concentrations, and to compare the rheological

properties of the developed amphiphile system with PAM solutions, which are commonly used as displacement fluids[218,219].

5.3.2 Influence of pH on viscosity

Figure 5.4a depicts the measured viscosity as a function of shear rate at 22°C and 50 mM (approximately 2 wt%). For a given pH, the amphiphile system displayed a shear-thinning behavior (i.e. a decreasing viscosity with increasing shear rate). For a given concentration (approximately 2 wt%), the viscosity of the solution increased with increasing pH, reached a maximum at pH of 8, and started going down after this value. This trend can be better seen from zero-shear viscosity, μ_0, *versus* pH plot that have been obtained by extrapolating the viscosity curves (Fig. 5.4b) as described by the Cross viscosity model[220]. At a pH of 8, the amphiphile solution was about 4.5×10^5 times more viscous than water (1 mPa·s). On the other hand, when the pH of solution was lowered to 4, the viscosity became approximately 3.7×10^4 mPa·s. Furthermore, when the solution pH was increased back to 8, the viscosity went back to 4.5×10^5 mPa·s again, indicating the reversibility of pH-induced viscosity changes. At this point, the rheological data suggest that the structure of networks that is responsible for the viscoelastic behavior changes with respect to pH. We will further discuss the mechanism of pH responsive viscosity after presenting cryo-TEM data.

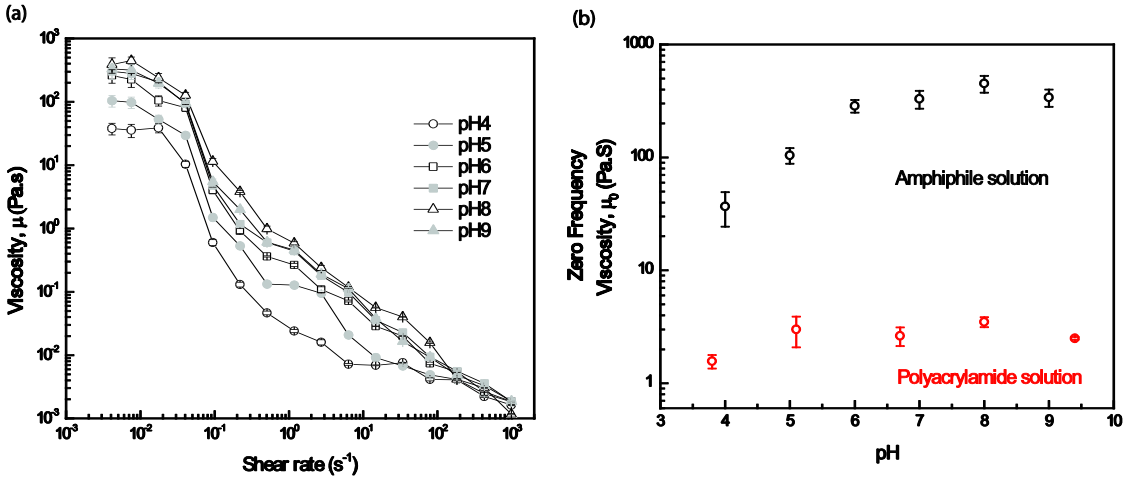

Figure 5.4 Rheology results of amphiphile and PAM solution at different pH values.
(a) Effect of solution pH on the viscosity of amphiphile solution (2% wt.) and **(b)** Zero frequency viscosity of adaptable amphiphile and polyacrylamide solution as a function of pH at 2% wt. concentration and room temperature (22 °C). Note: Rheology results and zero frequency viscosities at different pH were averaged with 3 repeats (error bar is 1 SD).

The comparison of zero frequency viscosity of the developed amphiphile and polyacrylamide solutions indicated that for a given concentration (2 wt%) and temperature (22°C), amphiphile solution had much higher viscosity than polyacrylamide solution (Fig. 5.4b). Polyacrylamide solution had mostly constant viscosity in the range of pH 5 to 9, and slight decrease in viscosity at fairly acidic conditions. The latter observation is consistent with the previous studies focusing on the rheological properties of polyacrylamide solutions[221]. Although there was a 12 fold decrease in viscosity due to acidity for amphiphile solution, there was only about 2 fold decrease in viscosity due to acidity for polyacrylamide solution. This finding indicates that amphiphile solution is much more responsive against a pH stimulus and will be more beneficial when a large

range of adjustable viscosity is desired in oil recovery applications. The reversible viscosity of adaptable amphiphiles is attributed to their ability to reversibly break and recombine. Conversely, polymers tend to irreversibly shear-degrade[222], which is another limitation of polymer-based viscosity modifiers.

5.3.3 Influence of concentration on viscosity

Systematic studies as a function of amphiphile concentrations were carried out at pH 8 since this pH gave rise to the maximum viscosity. Figure 5.5a displays the viscosity of the solution as a function of shear rate at concentrations of 10 mM (0.4 wt%), 20, 30, 40, and 50 mM (2 wt%). At low shear rates, the viscosity increased nearly two orders of magnitude as the concentration of solution was increased from 10 mM to 50 mM. At very high shear rates, the difference between the viscosities for each amphiphile concentration became negligible (Fig. 5.5a). This finding indicates that the network structure of the amphiphile solution is disrupted at extremely high shear rates[223].

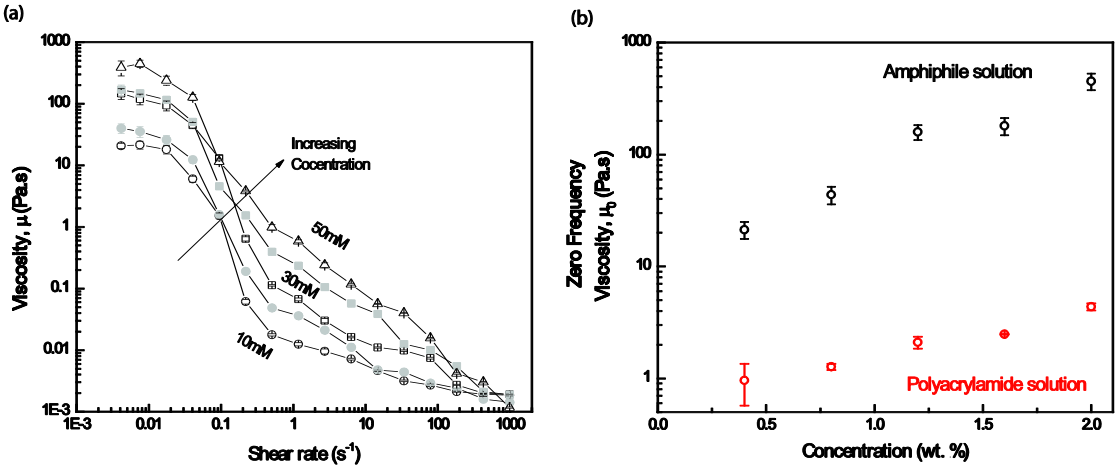

Figure 5.5 Rheology results of amphiphile and PAM solution at different concentrations.
(a) Effect of the amphiphile concentration on the viscosity at pH 8 and 22 °C. **(b)** Zero frequency viscosity of adaptable amphiphile and PAM solutions as a function of concentration at 22 °C. The concentrations used in these studies were 10 mM (approximately 0.4 wt.%), 20, 30, 40, and 50 mM (approximately 2 wt%). Note: Rheology results and zero frequency viscosities at different concentrations were averaged with 3 repeats (error bar is 1 SD).

The comparison of zero frequency viscosity behavior of the developed amphiphile and polyacrylamide solutions with respect to the solution concentration is shown in Figure 5.5b. Both viscosity curves could be fitted with a power-law function where the exponents for the amphiphile and PAM solutions were 1.9 (r^2=0.83) and 1.0 (r^2=0.91), respectively. In other words, the viscosity was much more sensitive against the amount of amphiphile solution present than the amount of PAM solution present. The concentration dependence of the viscosity can be explained as follows: Surfactant micelles self-assemble and form a network structure as a consequence of entanglements[224]. An increase in the concentration leads to an increase in micellar contour length and the degree of entanglement. The entangled structure leads to a

resistance to the flow of the solution (i.e. an increase in solution viscosity[225]). It is also important to note that the power-law dependence of viscosity on the concentration for polyacrylamide solution is in agreement with previous research concentrated polymer solutions[226,227].

5.3.4 Influence of temperature on viscosity

In oil reservoirs, the temperature increases with depth due to the geothermal gradient. Thus, it is significant to examine the rheological behavior of the amphiphile solution at elevated temperatures to better evaluate the feasibility of amphiphile solution in enhanced oil recovery. Figure 5.6a shows the temperature dependence of the viscosity of the amphiphile solution. As expected, the viscosity of the solution decreased with increasing temperature.

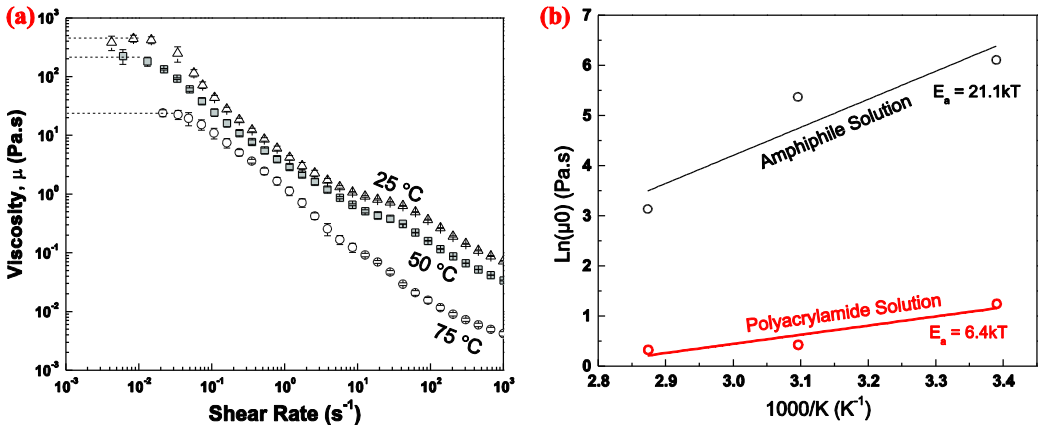

Figure 5.6 Rheology results of amphiphile solution at different temperatures. Arrhenius type plot of amphiphile and PAM solutions. **(a)** Effect of temperature on the viscosity of amphiphile solution (2 wt%). Operating temperatures are 22, 50, and 75 °C **(b)** Natural logarithm of the corresponding zero frequency viscosities (μ_0) of amphiphile and PAM solutions is plotted against 1/T in an Arrhenius type plot[228]. In both figures, the solution pH and concentration are 8 and 50 mM, respectively. Note: Rheology results at different temperatures were averaged with 3 repeats (error bar is 1 SD).

As shown in Fig. 5.6b, temperature dependence of the viscosity can be described by Arrhenius relation, $\mu(T)=\mu_0 \exp(E_a/RT)$, where viscosity is related to the inverse of the temperature[228]. By fitting a linear line on Log (μ) vs. 1/T curve plot, the activation energy, E_a, was calculated as 21.1 kT (or 52.3 kJ/mol). The typical activation energy of wormlike micelles ranges from 30 kT to 240 kT[229–231]. Given that the activation energy of the adaptable amphiphile described here is about 20 kT, it is reasonable to claim that the amphiphile system described here can form structures different from wormlike micelles. Ideally, it is desirable to have high activation energy for viscosity modifiers to have smaller viscosity reductions at elevated temperatures. In this respect, wormlike micelles may be slightly advantageous over the adaptable amphiphiles described here. However, it is known that wormlike micelles loses their assembled nanostructures and

viscous behavior in the presence of salt[232], which hinders their feasibility in oilfields. The comparison of activation energy values for adaptable amphiphile and polyacrylamide solutions indicate that the activation energy for PAM solution is about 3 times smaller than that for amphiphile solution. In other words, viscosity of amphiphile solution is less sensitive to temperature fluctuations than that of PAM solution, which is one of the most commonly used viscosity modifiers in oil fields.

5.3.5 Influence of salt on viscosity

Many oil reservoirs contain connate water with high concentrations of sodium chloride and divalent ions[233]. Therefore, it is essential to determine the influence of salt on the viscosity of the developed amphiphile system. Figure 5.7a displays the viscosity versus shear rate plots for adaptable amphiphile solutions at varying salt concentrations. There was a twofold reduction in zero frequency viscosity when 5 wt% salt was introduced into amphiphile solution containing no salt. Fig. 5.7b displays a similar plot for PAM solution. It is interesting to note that PAM solution also had a roughly twofold reduction in zero frequency viscosity when 5 wt% salt is added into the PAM solution. At high shear rates, the influence of salt was negligible for both cases. This is presumably because entanglements responsible for viscosity is reduced or disrupted at high shear rates and salt cannot further disturb and influence the viscosity.In essence, the presence of salt demonstrated a similar effect on adaptable amphiphile and PAM solutions, suggesting that both solutions will have similar resilience against oilfield brine. Overall, it is significant to emphasize that adaptable amphiphile solution has a

significantly enhanced adjustable viscosity behavior and much less sensitivity towards temperature in comparison to PAM solution and reversible viscous behavior even after experiencing prolonged high shear rates. Therefore, rheological data strongly suggest that supramolecular assembly of amino-amide based amphiphiles have a strong potential as a viscosity modifying fluid in EOR.

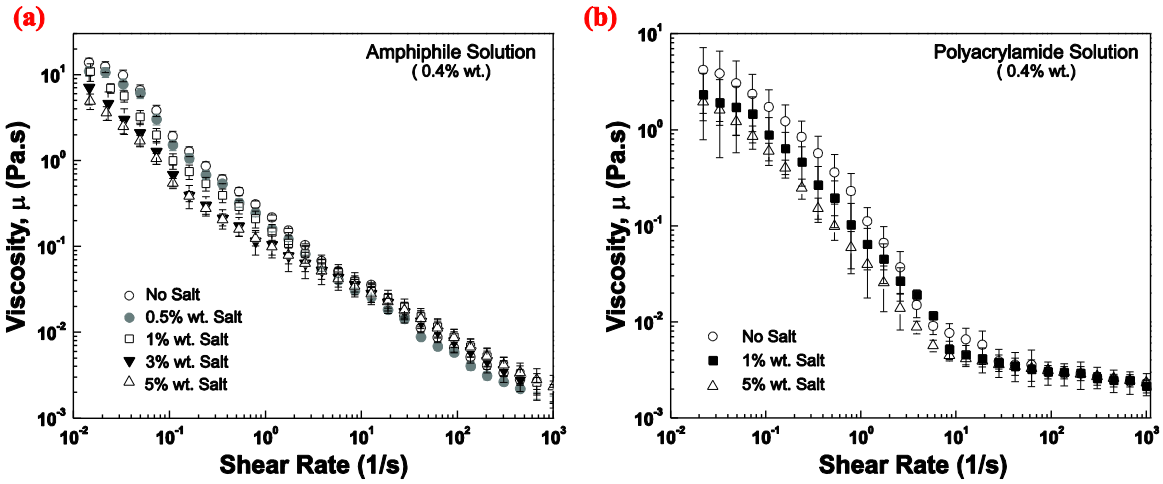

Figure 5.7 Rheology results of amphiphile and PAM solutions at different salt concentrations.
Influence of salt on the viscosity of **(a)** amphiphile solution (0.4% wt.) and **(b)** polyacrylamide solution (0.4% wt.). All experiments were conducted at pH 8 and 22 °C. Note: Rheology results at different NaCl concentrations were averaged with 3 repeats (error bar is 1 SD).

5.4 Oil displacement behavior

To go one step further than rheological measurements and to better evaluate feasibility of adaptable amphiphile solutions in EOR, we carried out oil displacement experiment involving sand columns. Figure 5.8 compares the oil recovery efficiencies of water, adaptable amphiphile and PAM solutions with a concentration of 0.4 wt. % as a

function of pH. Overall, the amphiphile solution clearly showed much higher displacement efficiency compared to water and polyacrylamide solution at basic pHs. Under basic conditions, for an injection volume of 5 cm^3, the ROS attained was 0.29-0.30 for amphiphile solution (0.4 wt. %) and 0.45-0.50 for polyacrylamide solution (0.4 wt. %) while it was 0.55-0.60 for water. In other words, there was 50-67% increase in displacement efficiency when switched from polyacrylamide to adaptable amphiphile solutions. There was 83-100% increase in displacement efficiency when switched from plain water to adaptable amphiphile solution. At acidic conditions, the ROSs attained for PAM to adaptable amphiphile solutions were similar but still higher than plain water. However, it is important to note that adaptable amphiphile solution described here is envisioned to be used solely in basic oilfields as displacement fluid while it was planned to be pumped down at initial acidic condition until reaching the reservoir to facilitate the pumping and injectivity.

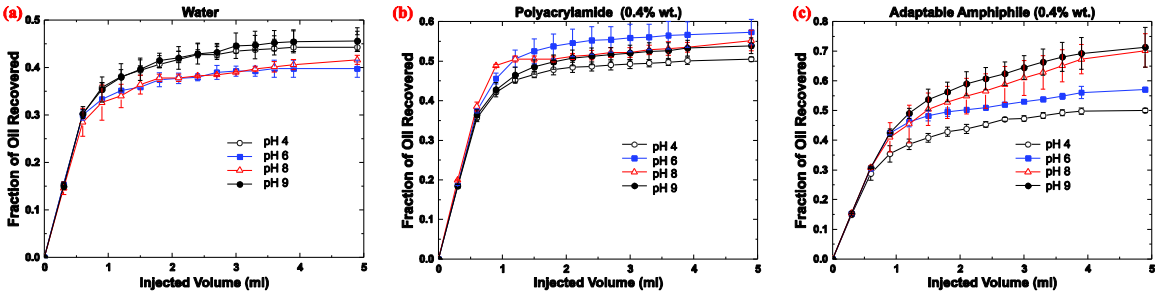

Figure 5.8 Fraction of displaced oil as a function of injected fluid volume at various pH values and 25 ˚C.
(a)water, **(b)** 0.4 wt% adaptable amphiphile solution, and **(c)** 0.4 wt% PAM solution. Injected volume corresponds to 3.3 times PV. Note: For each pH of three solutions, fraction of oil recovered from sand column was averaged with 4 repeats (error bar is 1 SD).

To explain the observed trends, we rely on the Capillary number (Ca). The ROS decreases when C_a increases beyond 10^{-3} to 10^{-4}.[234] This is found to be particularly found true for sands and sandstones. For experimental conditions used in this study, PAM and adaptable amphiphile solutions had the C_a in the order of 10^{-1} to 10^{-2} due to their viscous natures while plain water solution had the Capillary numbers in the order of 10^{-6} (Table 5.1 through 5.3). Therefore, for plain water, the displacement is controlled by the capillary pressures along the interface while for PAM and adaptable amphiphile solutions, viscous forces overcome capillary effects and control the displacement. For water, the deviation from pH 7 indicates a larger amount of H^+ or OH^- ions in the solution. The presence of such ions can disrupt the structuring of water molecules, thereby decreasing the interfacial tension. Therefore, for water, the capillary number at pH 4 was slightly larger than that at pH 6 and 8. As such, the ROS was slightly lower at pH 4 for water. For PAM, the interfacial tension decreases with increasing pH while the viscosity is mostly constant above pH of 5 and decreases changing from pH 5 to 4. Overall, the Capillary number increased with increasing pH for PAM solution. Although the ROS values for pH 6 and 8 were similar for an injection volume of 5-cm^3 PAM solution, the steady-state was reached for pH 6 but not fully reached for pH 8. In other words, PAM solution is expected to reach a smaller remaining oil saturation value as expected from C_a. For adaptable amphiphile solution, viscosity increased with increasing pH (Fig. 5.4). In this case, the decreased ROS was attributed to the increased viscous forces overcoming capillary effect.

Table 5.1 IFT of three different fluids at oil interface as a function of pH and the corresponding capillary numbers calculated by Darcy velocity, the measured viscosity, and interfacial tension.
The Darcy velocity was 0.34 mm/s for PAM and amphiphile and 0.48 mm/s for the water flooding Darcy velocity. PAM and adaptable amphiphile solutions were 0.4 wt%. All of the experiments were conducted at 22 °C. Interfacial tension between each solution at different pH with paraffin oil was averaged with 4 repeats (1 SD).

pH	Amphiphile σ (mJ/m^2)	PAM σ (mJ/m^2)	Water σ (mJ/m^2)	Ca ($\times 10^{-2}$) (Amphiphile)	Ca ($\times 10^{-2}$) (PAM)	Ca ($\times 10^{-6}$) (Water)
4	8.4±0.9	43.2±0.6	48.7±2.2	4.8±1.7	1.5±0.2	9.9±0.4
6	12.0±0.5	45.7±0.2	53.0±0.4	26.2±3.5	1.6±0.5	9.1±0.1
8	30.1±1.6	54.7+1.1	53.1+0.6	16.4±2.3	2.6±1.8	9.0+0.1

Figure 5.9 compares the oil recovery efficiencies of water, adaptable amphiphile and PAM solutions with a concentration of 0.4 wt% at pH 8 as a function of temperature. For all temperatures tested, the ROS attained was the smallest for adaptable amphiphile solution. For all cases, the ROS increased with increasing temperature. For water and PAM solution, 5 ml injection volume (3.3 times PV) was mostly enough to reach steady-state ROS while for adaptable amphiphile solution, 5 cm^3 injection volume did not lead to a steady-state ROS value. This finding indicates that if a larger volume of amphiphile solution is injected, the residual oil saturation value can decrease for adaptable amphiphile solution but not for water and PAM solution. For all three cases, the observed trends can be explained in terms of the C_a: with increasing temperature, the

C_a decreased (Table 5.2). Therefore, the increase in the ROS with increasing temperature can be attributed to the fact that oil recovery increases with increasing C_a.

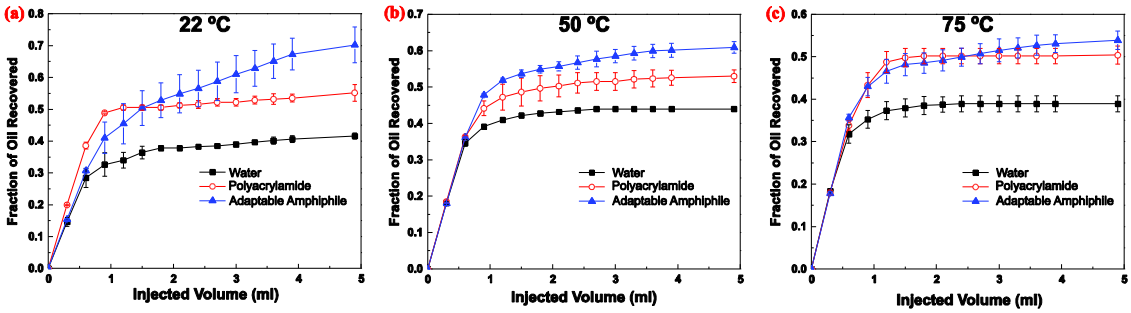

Figure 5.9 Fraction of displaced oil as a function of injected fluid volume for water, 0.4 wt% PAM solution, and 0.4 wt% adaptable amphiphile solution at various temperatures.
(a) 22 °C, **(b)** 50 °C, and **(c)** 75 °C. For all cases, pH was 8. Injected volume corresponds to 3.3 times PV. Note: For each temperature of three solutions, fraction of oil recovered from sand column was averaged with 4 repeats (error bar is 1 SD).

Table 5.2 IFT of three different fluids at oil interface as a function of temperature and the corresponding capillary numbers calculated by Darcy velocity, the measured viscosity, and interfacial tension.
The Darcy velocity was 0.34 mm/s for PAM and amphiphile and 0.48 mm/s for the water flooding Darcy velocity. PAM and adaptable amphiphile solutions were 0.4 wt%, and pH was 8. Interfacial tension between each solution at different temperature with paraffin oil was averaged with 4 repeats (1 SD).

T (°C)	Amphiphile σ (mJ/m^2)	PAM σ (mJ/m^2)	Water σ (mJ/m^2)	Ca (×10^{-2}) (Amphiphile)	Ca (×10^{-2}) (PAM)	Ca (×10^{-6}) (Water)
22	30.1±1.6	54.7±1.1	53.1±0.6	16.4±2.3	2.6±1.8	9.0±0.1
50	24.6±0.6	31.8±1.4	45.4±0.4	9.6±3.0	0.9±0.3	5.8±0.1
75	21.9±2.1	35.1±0.2	40.3±1.1	1.2±0.2	0.2±0.0	4.5±0.1

Figure 5.10 compares oil displacement efficiencies of water and adaptable amphiphile and PAM solutions with a concentration of 0.4 wt% and pH of 8 with different brine conditions (0, 0.5, 1 and 3 wt% sodium chloride (NaCl)). For water, the recovered oil increased with increasing salt concentration. When 3 wt% salt is added into water, the fraction of displaced oil increased about 14%. For PAM, the presence of NaCl did not significantly alter fraction of oil recovered. For adaptable amphiphile, there was about 20% reduction in fraction of oil recovered going from no salt to 3 wt% NaCl condition. However, the fraction of oil recovery was still the largest for adaptable amphiphile even at 3 wt% NaCl concentrations (i.e. 0.48 for water, 0.56 for PAM, and 0.57 for adaptable amphiphile). The IFT of salt water and oil decreases with increasing salt concentration and the C_a increases (Table 5.3). Hence, the slightly increased displacement efficiency of water at higher salt concentrations is attributed to this phenomenon. For PAM, both the IFT and the viscosity decrease with increasing salt concentration (Table 5.3 and Figure 5.7). Therefore, viscous and interfacial effects have opposing trends and the interplay between these two effects keep the capillary number mostly constant as a function of salt concentration. Therefore, the ROS did not significantly depend on the salt concentration for PAM solution. For the adaptable amphiphile solution, the decrease in viscosity with increasing salt concentration was ascribed to the increasing ROS. Here, it is worth noting that since the adaptable amphiphile system involve surface active components, aside from the displacement effect, the formation of emulsions may also take place, especially at relatively low interfacial values[96,235,236].

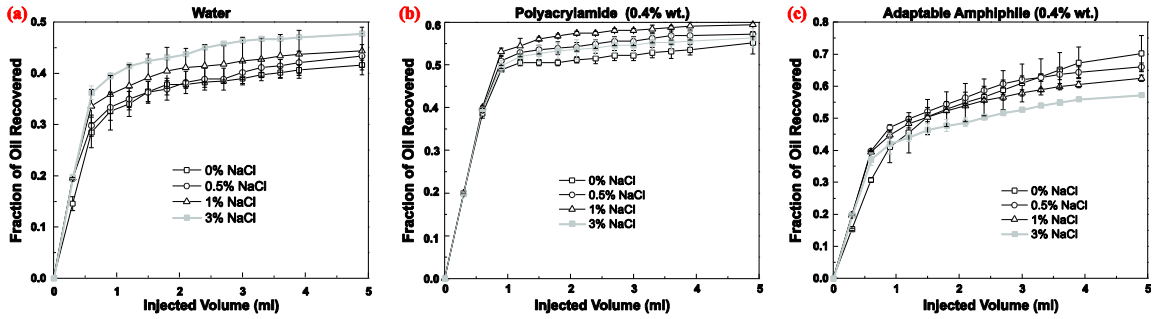

Figure 5.10 Fraction of displaced oil as a function of injected fluid volume at various NaCl concentrations for water, 0.4 wt% PAM solution, and 0.4 wt% adaptable amphiphile solution at 25˚C.

(a) water, **(b)** 0.4 wt% PAM solution, and **(c)** 0.4 wt% adaptable amphiphile solution. For all cases, pH was 8. Injected volume corresponds to 3.3 times PV. Note: For each NaCl concentration of three solutions, fraction of oil recovered from sand column was averaged with 4 repeats (error bar is 1 SD).

Table 5.3 IFT of three different fluids at oil interface as a function of NaCl concentration and the corresponding capillary numbers calculated by Darcy velocity, the measured viscosity, and interfacial tension.

The Darcy velocity was 0.34 mm/s for PAM and amphiphile and 0.48 mm/s for the water flooding Darcy velocity. PAM and adaptable amphiphile solutions were 0.4 wt%, 22˚C and pH was 8. Interfacial tension between each solution at different NaCl concentrations with paraffin oil was averaged with 4 repeats (1 SD).

NaCl (wt%)	Amphiphile σ (mJ/m^2)	PAM σ (mJ/m^2)	Water σ (mJ/m^2)	Ca (×10^{-2}) (Amphiphile)	Ca (×10^{-2}) (PAM)	Ca (×10^{-6}) (Water)
0	30.1±1.6	54.7±1.1	53.1±0.6	16.4±2.3	2.6±1.8	9.0±0.1
0.5	54.8±2.6	53.6±1.1	52.3±0.6	7.6±0.9	2.2±1.2	9.2±0.1
1.0	52.3±8.2	52.7±2.2	51.8±1.1	8.8±2.0	1.5±1.0	9.3±0.2
3.0	52.3±8.2	45.9±2.7	49.2±0.8	7.5±1.7	1.6±0.6	9.8±0.2

5.5 Mechanism for pH-switchable viscosity

To directly visualize the nanostructural changes responsible for pH-adjustable viscosity behavior at multiple length scales, we relied on optical microscopy and cryo-TEM. Figure 5.11 shows optical microscope and cryo-TEM micrographs of the complexation product of maleic acid and amino-amide in water under acidic and basic conditions. While small, plate-like structures were observed under acidic condition (pH of 4), large layered, tubular (cylindrical) structures were detected under basic condition (pH of 8). These structures having diameters of 300-800 nm, which were much larger than typical wormlike micelles (diameter of 5-10 nm i.e. about length of two surfactant monomers)[224].

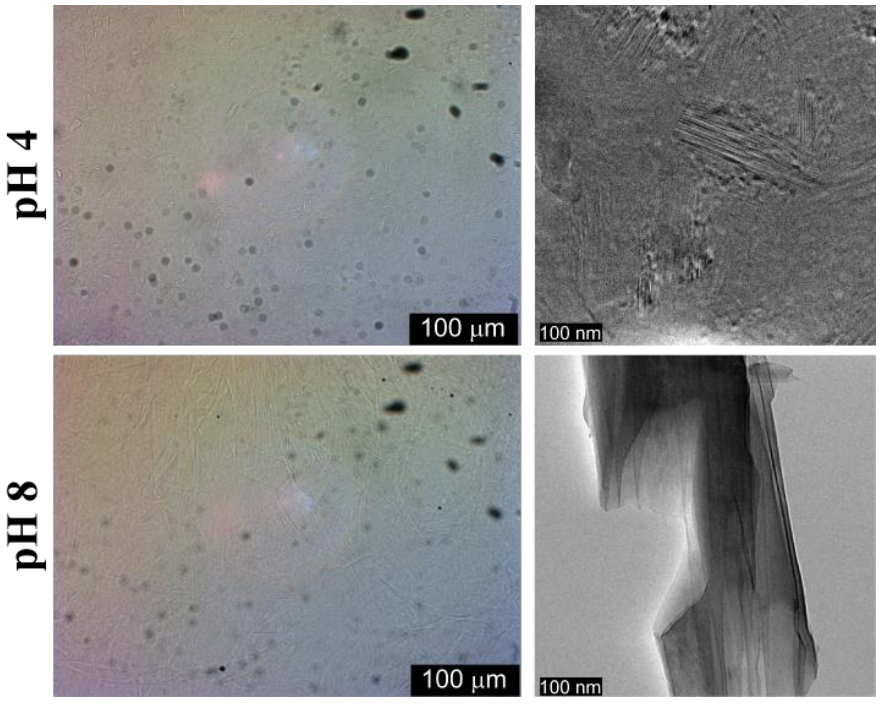

Figure 5.11 Optical microscopy and cryo-TEM micrographs of the complexation product of maleic acid and amino-amide in water.
(Left) optical microscope images, Right) Cryo-TEM images at acidic (pH=4)(top) and basic (pH=8)(bottom) conditions.

The switchable viscosity behavior is attributed to the complexation induced by the protonation of amino groups and deprotonation of carboxyl groups (Fig. 5.12). Below pH 4, while only one of the carboxyl groups of maleic acid is dissociated due to its pK_a values (pK_{a1}=1.9 and pK_{a2}=6.1), the amino-amide is positively charged at the amino group (pK_a=9.4). As the pH increases from 4 to 8, the degree of dissociation for the non-dissociated carboxyl group of maleic acid changes from almost none to almost all. On the other hand, amino amide is almost completely protonated below pH 7.4 because it has a pK_a of 9.4. As the pH increases from 7.4 to 11.4, the degree of protonation for the amino group changes from almost all to almost none. When maleic acid is completely dissociated, it can form intermolecular complexes with two amino-amides. On the other hand, it can only complex with one amino-amide when maleic acid only loses one proton through electrostatic interactions. We believe the transition from dimer to trimer type of complex is primarily responsible for the increased viscosity at basic pH values. It is important to note that when pH is above 7.4, then the amino-amide starts losing its charge and the electrostatic contribution of intermolecular interactions gradually disappear. This explanation is consistent with the decrease in viscosity upon increasing pH from 8 to 9.

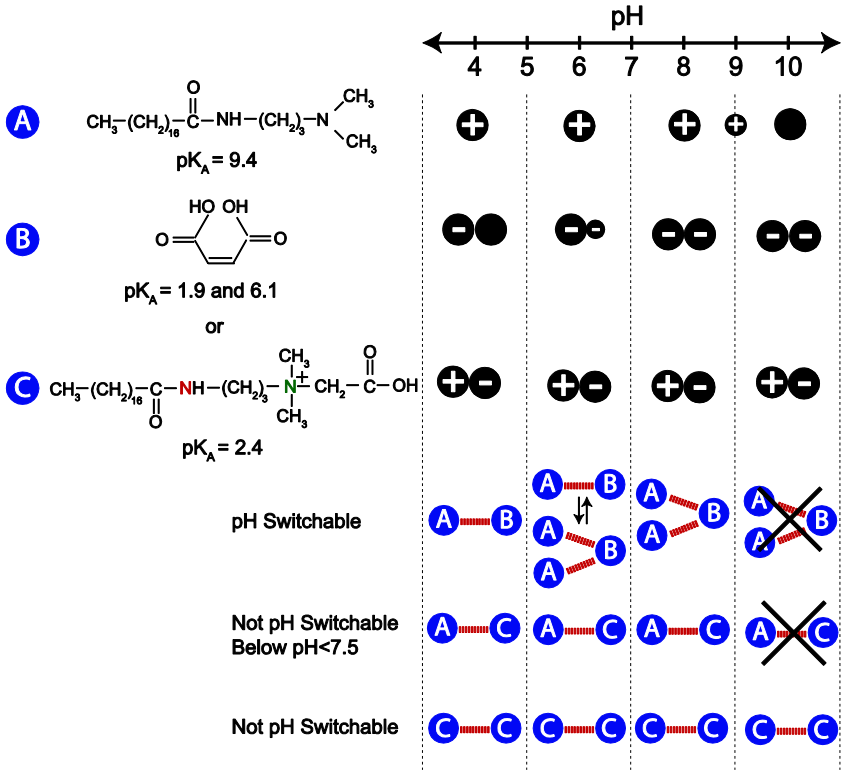

Figure 5.12 The effect of pH on the dissociation of the amino and carboxyl groups of the developed adaptable amphiphile.

It is also possible that quaternary amine (**C**) can also form complexation reactions with the amino-amide (**A**) or itself. Comparison of the relevant pK_a values suggest that neither **C**…**A** (794 Da) nor **C**…**C** (825 Da) complexes are expected to have a pH-switchable viscosity behavior. Furthermore, **C**…**C** complex is expected to be stable even at high pH values. Overall, we believe that while the zwitterionic quaternary amine does not directly provide the system with any pH responsiveness, it can still play a role in the supramolecular assembly of A…B complexes and enhance the effective viscosity of the system.

The formation of dimers and trimers cannot solely account for the enormous viscosities of the amphiphile solution because of their relatively small sizes. To explain this trend, the supramolecular assembly of dimers and trimers needs to be considered. As shown in Figure 5.11, the amphiphile system at basic conditions forms very large superstructures, which are much larger than typical wormlike micelles. The scaling theories suggest that the zero-shear viscosity of a Maxwell fluid is linearly depend upon the contour length[237]. While the contour length of the amphiphile system at pH 8 is roughly a few hundred micrometers (Fig. 5.11), that of high molecular weight water soluble polymers used in enhanced oil recovery is typically 0.1–10 μm (estimated from molecular weight information). Therefore, these amphiphile solutions display much larger viscosities than typical polymer solutions.

5.6 Conclusion

Our results indicate that the adaptable amphiphile with amino-amide groups display very intriguing pH-switchable physicochemical properties. For instance, the addition of just 2 wt% of adaptable amphiphile/maleic acid into water increased the viscosity of water by 4.5×10^5 times. Furthermore, the viscosity of the amphiphile solution can be increased 12 times by changing pH from 4 to 8 in a reversible manner. We also demonstrated the proof-of-concept for the use of adaptable amphiphile solutions in EOR as oil displacement fluids through column experiments. Such a tunable viscosity can be very beneficial for oil recovery applications when the injectivity becomes a limitation. We also showed that adaptable amphiphile solution has several advantages

over PAM solution, which is commonly used in mobility control. For instance, in comparison to PAM solution, adaptable amphiphile solution is less sensitive against temperature gradients and has reversible-viscosity dependence because of its ability to reversibly break and recombine. Tunable viscosity behavior can be beneficial to oil recovery appications when injectivity becomes a limitation. In addition, switchable viscosity can cut down the energy cost associated with pumping large volumes of viscous displacement fluid. Moreover, because oil reservoirs can show a rich variation in viscosity even within a given reservoir, the use of pH adjustable viscosity can alleviate the need for using different displacement fluids in different zones of reservoirs. Because of their increasing viscosity at basic pH values, we envision the use of the adaptable amphiphile system in carbonate reservoirs. It is important to note that the key raw material of the adaptable amphiphile system is stearic acid, which can sustainably be obtained from coconuts at high yield.

5.7 Appendix

5.7.1 Mass and nuclear-magnetic-resonance (NMR) spetroscopy

The chemical analysis of the long-chain amino-amide (first step) and adaptable amphiphile complex (second step) was performed by use of electrospray ionization mass spectroscopy (ESI-MS) and NMR spectroscopy. ESI-MS (MDS SCIEX API QStar Pulsar, Ontario, Canada) was used in the positive-ion mode. Sample was dissolved in methanol and electrosprayed by use of ion spray (needle) at 4.5 kV. Sheath gas and curtain gas flow were set to 40 and 20 psi, respectively. The sample flow rate was 7

μl/min. Proton NMR (H-NMR) was used to further confirm chemical reactions shown in Fig. 5.14. The products of the first step were dissolved in deuterated chloroform ($CDCl_3$), whereas the products of the second step were dissolved in deuterated water (D_2O). The solutions were analyzed by use of a Bruker 400 MHz NMR spectrotrometer (Bruker, Billerica, Masssachusets) at 298K.

5.7.2 Chemical characterization of adaptable amphiphile

Fig. 5.13a shows ESI-MS spectra of the product obtained at the end of first step in reaction of Fig. 5.2. The main peak that is responsible for 80.7% of the overall intensity is at 369 daltons, suggesting the formation of $C_{23}H_{49}N_2O^+$, which is a hydrogen adduct of amino-amide (A). The smaller peaks are ascribed to the isotopic distribution. ESI-MS was also utilized to determine the molecular weight of the complex forming upon the addition of maleic acid to amino-amide (Fig. 5.13b). In this case, the main peaks that are responsible for a total of 89.9% of the overall signal intensity are located at 794, 853, and 876 daltons. It is most likely that amino-amide…maleic acid…amino-amide (A…B…A) complex accounts for the peak at 853 daltons and the peak at 876 daltons is the sodium adduct of A…B…A complex. The peak at 794 daltons can be due to the formation of amino-amide…zwitterionic quaternary amine (A…C) (794 Da) complex. This scenario requires the formation of acetic acid which may form by the cleavage or decomposition of maleic acid[238] because of the extensive amount of sonication energy provided in the second step of the reaction. It is also possible that C…C complex can be responsible for the peak at 853 Da and the peak at 876 Da is its sodium adduct. Fig. 5.14

displays ^{1}H NMR spectrum of products obtained after first and second steps of synthesis in $CDCl_3$ and D_2O, respectively. For the first step of the reaction, the signals from two types of methyl groups (a and i) are observed at δ=2.4 and 0.9 ppm, respectively. Peak at δ=7.0 ppm is associated with the signals from the proton of amide (e). The other major peaks are shown on the molecular structure. In the second step of the reaction, if the quaternary amine with two carbonyl groups formed, the signal from amide peak disappears due to deuterium-hydrogen exchange[239]. The peak at δ=4.6 ppm is attributed to $–CH_2–$ (j) that is located between quaternary amine and carbonyl groups. The other $–CH_2–$attached to amino group (b) experiences a large shift because of the electron-withdrawing effect induced by the formation of quaternary amine after the completion of the reaction. In the second step of the reaction, the quaternary amine with one carbonyl group can also form by the deuteration of amino-amide. This quaternary amine can also explain observed NMR trends. Overall, the presence of relatively broad peaks compared to the peaks observed in the first step suggests that a mixture of these quaternary amines form.

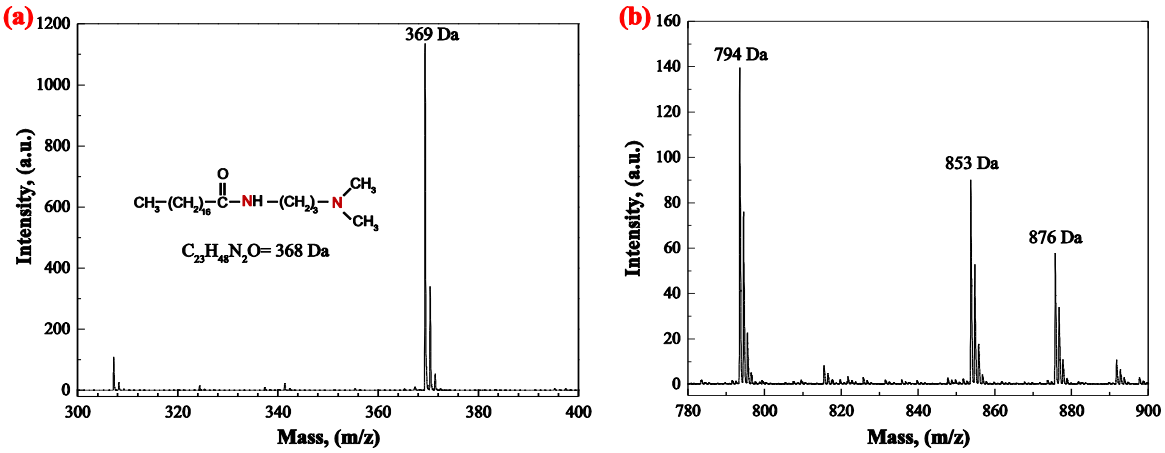

Figure 5.13 Mass spectrum of the adaptable amphiphile and the precursor. (a) the adaptable amino-amide amphiphile in $CDCl_3$ and **(b)** its condensation product with maleic acid in D_2O shown in Fig. 5.2

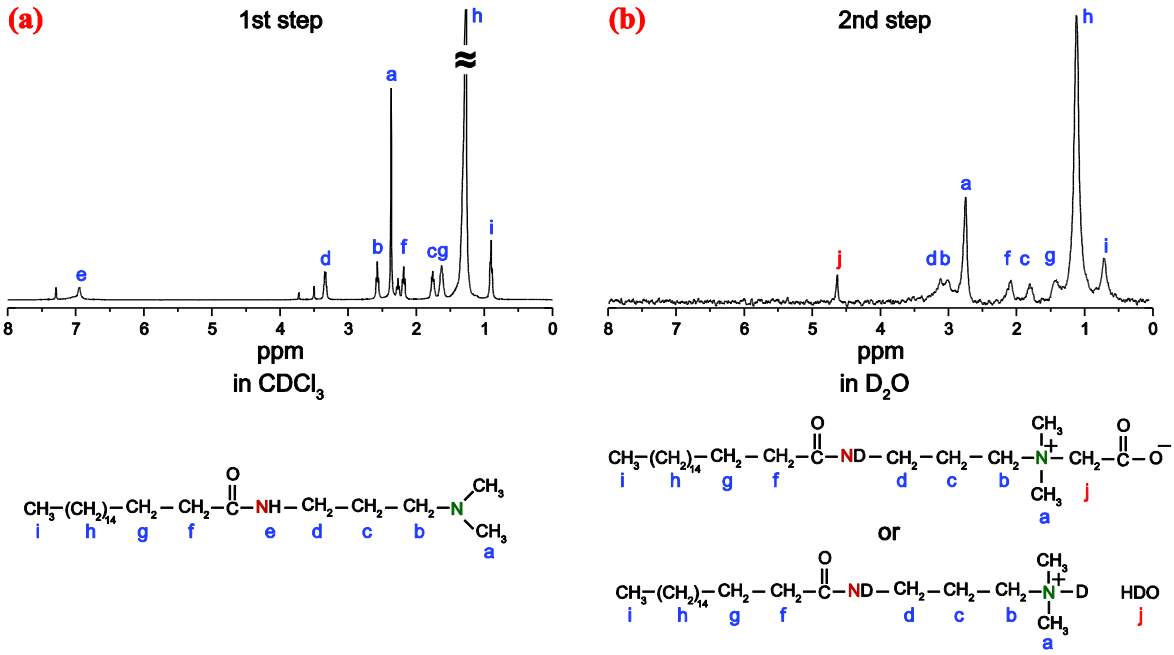

Figure 5.14 H-NMR spectra of the adaptable amphiphile and the precursor. (a) the adaptable amino-amide amphiphile in $CDCl_3$ and **(b)** its condensation product with maleic acid in D_2O shown in Fig. 5.2

5.7.3 Nomenclature

C_a = capillary number

E_a = the activation energy

k = Boltzmann constant

k_o = effective permeability of oil

k_w = effective permeability of water

pK_a = logarithmic acid-dissociation constant

R = universal gas constant

T = temperature

μ = viscosity

μ_0 = zero-shear viscosity

μ_o = oil viscosity

μ_w = water viscosity

CHAPTER VI

TRANSPORT OF POLYMERIC NANOPARTICULATE DRUG DELIVERY SYSTEM IN THE PROXIMITY OF SILICA AND SAND*

6.1 Introduction

Over the past few decades, significant developments in nanomedicine have occurred, particularly in cancer diagnosis and therapy[240], antibacterial therapeutics[241], and therapeutics for the central nervous system[242]. According to recent estimates, there are approximately 250 nanomedicines that have been approved for use, are under clinical trial, or on the verge of clinical study[243]. As research, production, and consumption of nanomedicine increases, there have been increasing concerns about the occurrence, transport behavior, and fate of nanomedicine in the environment and the potential consequences for human health[244].

The environmental concerns were exacerbated with studies indicating that some of the administered nanomedicines can be excreted from the kidney or the hepatobiliary system[245–247]. While the former route is capable of rapidly removing smaller particles from the vascular compartment relatively unaltered from their original form[248], the latter route typically leads to partial or full metabolization, which is eventually followed by biliary and fecal excretion[248,249].

*Reprinted with permission from " Transport of polymeric nanoparticulate drug delivery systems in the proximity of silica and sand" by I-Cheng Chen, Ming Zhang, Blake Teipel, Isa Silveira de Araujo, Yagmur Yegin and Mustafa Akbulut, 2015. *Environmental Science & Technology*, 49(6), pp.3575-3583. Copyright 2015 American Chemical Society.

After excretion, nanomedicine can reach the sewer system, and subsequently travel through a waste treatment facility before finding its way into receiving waters or land through the application of sewage sludge. However, prior studies have indicated that standard wastewater treatment does not capture nanomaterials, such as titanium dioxide nanoparticles, well[250,251]. While there are significant differences between physicochemical properties of titanium dioxide and nanomedicine, it is still an unknown and complimentary concern regarding how different types of nanomaterials interact with the standard wastewater treatment. In addition, therapeutic compounds tend to pose a challenge for waste water treatment plants[252,253]. According to the American Housing Survey for the United States: in 2009[254], the percentage of households connected to public sewage for waste water disposal is about 80%, and the remaining percentage mainly rely on septic tanks, which are primary treatment systems. It was reported that plumes from septic tanks can be tens of meters wide, several meters thick, and can extend tens to hundreds of meters downgradient of tile beds[255–257]. Furthermore, sewage systems can become defective and leaky[258], and such a leak can seep into a subsoil and transport through an unsaturated zone, capillary fringe, and saturated zone[259,260]. Likewise, polluted storm-water runoff can also contaminate waterbodies[261]. Because of these reasons, the possibility of groundwater contamination with therapeutic agents including nanomedicine is a valid concern.

Recently, environmental aspects of engineered nanoparticles are receiving increased attention as the consumption and production volumes of such nanoparticles increase. For instance, many field and laboratory investigations dealing with the

distribution, retention, and fate of nanomaterials such as TiO_2[35–37], SiO_2[38,39], CeO_2[40–42], ZnO[43,44], Fe_2O_3[45], Ag [46,47], Au[48,49], fullerenes[50–53] and carbon nanotubes [54,55] have been conducted. A general conclusion of these studies is that hydrodynamic parameters (such as flow velocity[40,43] as well as parameters that modulate the particle-surface and particle-particle interactions (such as surface potential of nanoparticles[36,41,46,56], the presence of organic species[55,57], particle aggregation[46,58], and concentration of NPs –i.e. interparticle distance– [38,40]) play a role on the retention and transport behavior of NPs. However, similar environmental studies on soft nanomaterials such as polymeric nanomedicine are rather limited. In particular, little is known about the adsorption dynamics, retention, and transport behavior of polymeric nanomedicine near and through environmental surfaces.

This work is concerned with the effect of surface chemistry on the adsorption dynamics and transport of polymeric nanoparticulate drug delivery systems on silica surfaces and through sand columns. Here, polymeric nanoparticulate drug delivery systems (PNDDS, Fig. 6.1) are of particular interest because PNDDS filled with therapeutic agents currently represent one of the most commonly used forms of nanomedicines due to their ability to solubilize hydrophobic molecules, as well as their higher payload capacity, prolonged blood circulation times, and enhanced thermodynamic solution stability[262–265]. Silica is of environmental significance as it is one of the most common minerals found on the surface of the earth[266]. The transport of PNDDS near flat surfaces and in saturated porous media was studied using quartz crystal microbalance with dissipation (QCM-D) and column transport experiments, respectively. In addition, the influence of ionic strength, salt type, and humic acid were

investigated for both of the flow geometries. The generated experimental data were described by DLVO theory, and Kramers' rate theory.

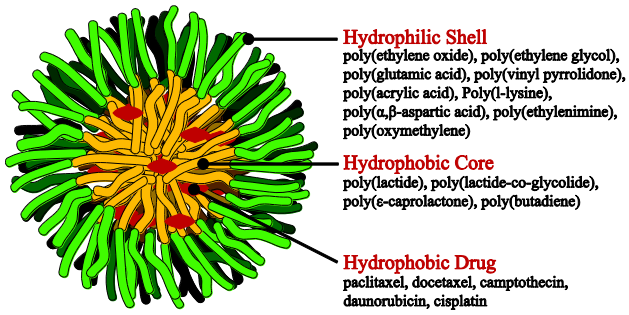

Figure 6.1 Illustration of PNDDS structure and typical building blocks used in current formulations.

6.2 Materials and methods

6.2.1 Materials

All PNDDSs were loaded with paclitaxel (Selleck Chemicals, Houston, TX), which is a commonly used therapeutic agent in formulations of various polymer nanomedicines[267]. The surface chemistry of PNDDS was systematically varied by selecting different hydrophilic polymer blocks that are typically used as steric stabilizers in contemporary polymeric nanomedicines. To be specific, five different diblock copolymers were used in this study: poly(caprolactone-b-ethyleneimine) (PCL-b-PEI, 2,500-b-2,500 g/mol, PolySciTech, West Lafayette, IN), poly(caprolactone-b-ethyleneoxide) (PCL-b-PEO, 6,500-b-5,000 g/mol, Polymer Source Inc., Dorval, QC, Canada), poly(lactide-b-n-vinylpyrrolidone) (PLA-b-PNVP, 6800-b-12,000 g/mol, Polymer Source Inc.), Poly(styrene-b-acrylic acid) (PS-b-PAA, 5200-b-4800 g/mol,

Polymer Source Inc.) and Pluronic F-127 (Sigma-Aldrich, St. Louis, MO). Tetrahydrofuran (THF, ≥99%, Sigma-Aldrich) was used for dissolving polymers and paclitaxel. Sodium chloride (NaCl, ≥99%), sodium sulfate (Na_2SO_4, ≥99%), calcium chloride dihydrate ($CaCl_2 \bullet 2H_2O$, ≥99%), calcium sulfate ($CaSO_4$, ≥99%) and humic acid (technical grade), which were purchased from Sigma-Aldrich, were used to mimic the conditions in environmental waters. Quartz sand (pure, 99.8%, 40-100 mesh, Acros Organics, Fair Lawn, NJ) was used for preparing a model environmental porous media.

6.2.2 Preparation of PNDDS loaded with paclitaxel

All PNDDSs were prepared using a generic precipitation method[268,269]. All polymeric nanomedicines were prepared using a rapid precipitation method[268,269]. Briefly, paclitaxel and one of the five amphiphilic diblock copolymers were molecularly dissolved in THF. Then, the THF solution was rapidly mixed with Milli-Q water (resistivity ≥18MΩ cm) with a tangential vortex mixer. The flow rates of THF and water streams were 5 ml min^{-1} and 50 ml min^{-1}, respectively. The resultant nanoparticle solutions were dialyzed overnight to remove THF. For all five polymeric nanomedicine, copolymer and paclitaxel concentration in THF was 0.1 wt% and 0.005 wt%, respectively (Table 6.1). All formulations also included a trace amount of Nile-red (0.001%) to enable the spectrofluorometric characterization. Nile-red, which is a hydrophobic agent, is imbibed into the core of the nanoparticle where its presence does not, therefore, affect the surface chemistry of the nanomedicine. The size distributions and zeta potential values of the PNDDS from different copolymers were measured using

dynamic light scattering (DLS, Zetasizer Nano ZS90, Malvern, Westborough, Massachusetts) to ensure same size of nanomedicine as in Table 6.1. The count rate from DLS measurement was used to determine the concentration of PNDDS using a pre-generated calibration curve. TEM micrographs of the resultant nanomedicine are shown in Figure 6.2.

Table 6.1 Five different copolymers used for producing nanomedicine loaded with paclitaxel. The concentration is in weight % (weight reagent/weight THF).
Size and zeta potential measurements of each nanoparticle were averaged with 6 repeats ± 1 SD.

Copolymer names	Copolymer concentration	Paclitaxel concentration	Particle size (diameter, nm)	Zeta potential in milli-Q H_2O
PCL-b-PEI	0.1%	0.005%	173.9±3.7	43.3±3.1
PS-b-PAA	0.1%	0.005%	181.8±1.8	-46.1±4.3
PCL-b-PEO	0.1%	0.005%	182.2±7.3	-27.7±6.4
PLA-b-PNVP	0.1%	0.005%	185.5±3.8	-32.0±5.4
Pluronic F127	0.1%	0.005%	180.9±4.5	-26.8±4.2

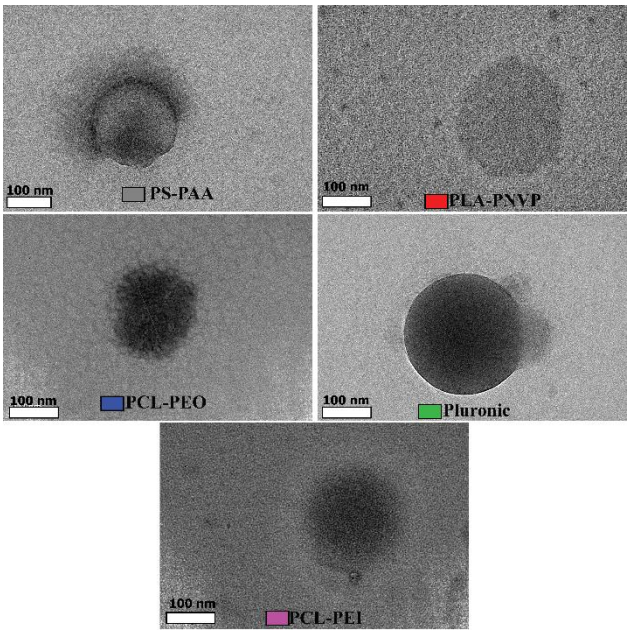

Figure 6.2 TEM micrographs of five different types of nanomedicine produced.

6.2.3 Quartz crystal microbalance with dissipation (QCM-D)

The adsorption dynamics of PNDDS onto the silica surface were studied using a QCM-D (E1, Q-sense, Biolin Scientific, Linthicum Heights, MD) and silica-coated sensors (QSX 303, Q-sense, Biolin Scientific). QCM experiments were conducted as described elsewhere[59,60]. In this study, for all types of PNDDS, the concentration was kept constant at 0.007 wt%, corresponding to an effective drug concentration of 3.5 ppm (~3.5 mg/L) in suspension and the flow velocity was 2.4×10^{-3} μm/s. The adsorption behavior was investigated as a function of ionic strength (i.e. with NaCl at ionic strengths of ~0 mM, 10 mM, and 100 mM), salt type (i.e. NaCl, Na_2SO_4, $CaCl_2$, and $CaSO_4$ at an ionic strength of 10 mM) and humic acid concentration (5 mg/L, 15 mg/L,

and 30 mg/L) for all PNDDS types. QCM experiments for each PNDDS surface chemistry were repeated at least four to five times to achieve statistical reliability.

6.2.4 Selection of ionic strengths and salts types

Our selection criterion is based on the data available on the ionic strength and salt types of various forms of waterbodies: The groundwater beneath Chihuahuan desert in Texas contains 190 mM Na^+, 23.5 mM Ca^{2+},48 mM Cl^-, 132 mM SO_4^{2-} in the unsaturated zones at a depth of 23.7 m[270]. For this groundwater, these four ions that we selected are the most abundant ones among all other ions. The western Murray Basin in Australia contains 170 mM Na^+, 75 mM Ca^{2+}, 287 mM Cl^-, 39 mM SO_4^{2-} in fresh groundwaters; 1964 mM Na^+, 157 mM Ca^{2+}, 2560 mM Cl^-, 654 mM SO_4^{2-} in brackish groundwaters[271]. In this case, these four ions are some of the most abundant ones among all other ions (Mg^{2+} concentrations are higher than Ca^{2+} concentrations). Aquifers near Sutherland in the Western Karoo, South Africa have 160 mM Na^+, 107 mM Ca^{2+}, 269 mM Cl^-, 148 mM SO_4^{2-}. For this groundwater, Na^+ and Ca^{2+} are the most common cations while Cl^- and SO_4^{2-} are two of the most common anions (HCO_3^- is the most abundant)[272]. Carbonate-rock aquifer at the Leetown Science Center of West Virginia, USA contains 1 mM Na^+, 0.5 mM Ca^{2+}, 0.37 mM Cl^-, 0.18 mM SO_4^{2-}. From this groundwater source, 70% of the cations are from $Ca^{2+}$and Na^+. Cl^- and SO_4^{2-} are two common anion ions (HCO_3^- is the most abundant)[273]. The groundwater from meadow complex in the Toquima Mountains of central Nevada, USA contains Na^+(19.5ppm, 0.8 mM), Ca^{2+}(113.6ppm, 2.8mM), Cl^-,(19.2ppm, 0.5 mM), SO_4^{2-}(37.2ppm, 0.4 mM). From

the springs and wells, these four ions are the most abundant ones among all other ions (NO_3^- concentration is similar to SO_4^{2-})[274]. The groundwater sources in Maryland Atlantic Coastal Plain, USA contains averaging Na^+(56ppm, 2.4 mM), Ca^{2+}(5.6ppm, 0.14mM), Cl^-,(7ppm, 0.2 mM), SO_4^{2-}(18.2ppm, 0.2 mM) in Upper Patapsco aquifer[275]. These are the four common ions from different wells. Na^+ is the most abundant cation (Ca^{2+} , Mg^{2+},and K^+ are at similar concentration). Cl^- and SO_4^{2-} two of the most common anions (HCO_3^- is the most abundant). The standard seawater contains Na^+ (0.486 mol/kg, ~ 486 mM), Ca^{2+} (0.011 mol/kg, ~ 11 mM), Cl^- (0.566 mol/kg, 566 mM), SO_4^{2-} (0.029 mol/kg, 29 mM)[276]. Cl^- and SO_4^{2-} are the most abundant anions in the seawater while Na^+ and Ca^{2+} are two of the most common 3 cations (Mg^{2+} is slightly more abundant than Ca^{2+}).

Considering the upper and lower limits of concentrations and most abundant types of salts of the abovementioned waterbodies, we selected to use NaCl, $CaCl_2$, Na_2SO_4, and $CaSO_4$ as model salts at concentrations of 10 mM and 100 mM. Conveniently, this set of salts also allowed us to investigate the effect of anion and cation valency on the transport behavior of PNNDS (We selected NaCl, $CaCl_2$, Na_2SO_4, and $CaSO_4$, corresponding to 1:1, 2:1, 1:2, and 2:2 type electrolytes).

6.2.5 PNDDS column transport experiments

For all experiments, columns were packed with pure quartz sand. The uniformity in size and shape of the sand grains and the variation in pore/channel geometry were characterized and confirmed using SEM (Fig. 6.3).

Polydimethylsiloxane (PDMS) of 5 PV was injected in a wet-packed sand column to fill the pores and channels of the column formed during packing. Then, the column was cured in oven at 110˚C for two hours to completely immobilize the sand grains in the polymer matrix. Then, the consolidated column was fractured into smaller pieces for SEM imaging.

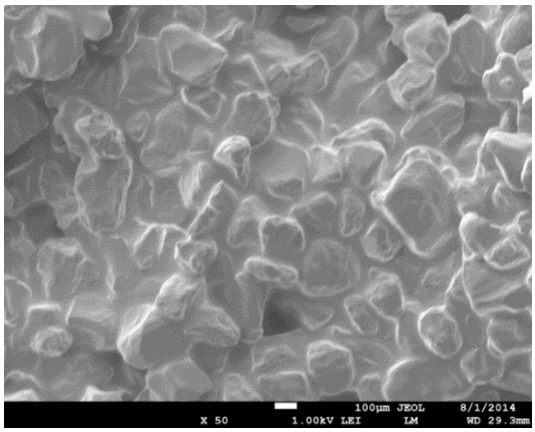

Figure 6.3 SEM micrographs of quartz sand consolidated with polydimethylsiloxane in the sand column.
The mean grain diameter was found to be 260 µm with a standard deviation of 50 µm. The zeta potential of quartz sand was measured using a Zetasizer Nano ZS90 in milli-q water, NaCl (ionic strength: 10 and 100 mM), Na_2SO_4 (ionic strength: 10 mM), $CaCl_2$ (ionic strength: 10 mM), $CaSO_4$ (ionic strength: 10 mM), and humic acid (5, 15, and 30 mg/L) after roller-milling the sand overnight to achieve particle sizes leading to Brownian motion (i.e. 500-700 nm).

Laboratory sand column transport experiments were conducted as described by Elimelech and co-workers[54,277]. The PNDDS transport experiments were performed in glass chromatography columns of 0.8 cm inner diameter packed with pure quartz sand. To minimize layering and air entrapment, sand columns were wet-packed by letting the quartz sand slowly sediment in milli-Q water while gently shaking and vibrating the column. The column height was approximately 8.0 cm for all experiments. Gravimetric analysis revealed that the porosity of the column was 0.44±0.01, which corresponded to a pore volume (PV) of 1.8 mL.

After preparing the column, first, 5 PV of milli-Q water was injected into the column to eliminate any potential mobile debris using a programmable syringe-pump (Nexus-6000, Chemyx Inc., Stafford, TX). Then, depending on the parameter of interest, the column was flushed with 5 PV of solution containing either NaCl, Na_2SO_4, or $CaCl_2$ at a concentration of 10 mM or humic acid at a concentration of 5 mg/L, 15 mg/L, or 30 mg/L to provide a uniform surface charge. Then, 3 PV of the various PNDDS suspensions with an effective drug concentration of 3.5 ppm (~3.5 mg/L) and a given concentration of salt or humic acid were injected. Finally, the column was rinsed with 2 PV of the appropriate solution (i.e. either of milli-Q water, NaCl, Na_2SO_4, $CaCl_2$, $CaSO_4$ or humic acid). The injection flow rate for all solutions was 0.3 mL/min. Once PNDDS began to inject into the sand column, the effluent was collected every 0.2 mL for a total volume of 8.8 mL, and subsequently diluted 10-fold with milli-Q water for analysis via spectrofluoremetry.

6.2.6 Selection of the drug concentration

The concentration of pharmaceuticals in the environment strongly depends upon how far they are from the contamination source. For common pharmaceuticals, the concentrations ranging from 1 ng/L to 100 μg/L in various types of groundwaters have previously been reported[278–280]. However, the drug concentrations can be orders of magnitude larger than these near their source. For instance, flows from some pharmaceutical formulation facilities in New York were reported to contain oxycodone up to concentrations of 1.7 mg/L and metaxalone up to concentrations of 3.8 mg/L[281]. A review article by Verlicchi et al.[282] has reported that hospital effluents can contain iodized contrast media (ICM) at an average concentration of ~1 mg/L, analgesics at an average concentration of 0.1 mg/L and a maximum concentration of 1 mg/L, antibiotics at an average concentration of 11 μg/L and a maximum concentration of 0.2 mg/L. There is no comparable data available for nanomedicine. In this study, we selected a concentration of 3.5 mg/L (~3.5 ppm), which is comparable with the drug concentrations in hospital and pharmaceutical manufacturing effluents. In some regions, where there are less strict regulations regarding the waste disposal and treatment, the concentration of drugs in the environment can be much larger as well: For instance, the effluent of a waste treatment plant serving bulk drug manufacturers near Hyderabad, India was reported to contain ciproflaxin in the range 28-31 mg/L, losartan in the range of 2.4-2.5 mg/L, and cetirizine in the range of 1.3-1.4 mg/L[283]. In addition, ciprofloxacin (up to 6.5 mg/L) and cetirizine (up to 1.2 mg/L) were detected in two lakes in India[284]. The list of

some other river systems with high drug concentration is also given in a review article by Hughes et al[285].

6.2.7 Spectrofluorometry

To determine the breakthrough concentration of the PNDDS, the core of PNDDS was pre-loaded with a trace amount of fluorescent Nile Red. The fluorescence intensity of the influent and effluent PNDDS solution was measured using a PTI QuantaMaster series spectrofluorometer (Photon Technology International, Inc,. NJ, USA) equipped with a PTI LPS-220B lamp, using 1 cm disposable cells. The excitation wavelength was 549 nm and the corresponding emission spectra were collected from 559 nm to 700nm. The concentration measurements were carried out after confirming that there are linear relationships between the fluorescence intensity and PNDDS concentration, following Beer-Lambert Law.

6.3 Results and discussion

6.3.1 Characterization of PNDDS and sand surface

To properly interpret the adsorption and transport behavior of PNDDS, the size and surface potential of PNDDS and surfaces interacting with these PNDDS need to be extensively investigated. Figure 6.4 displays the particle size distribution for PNDDS with five different surface chemistries. All of the size distributions were unimodal, relatively narrow, and peaked around 180±5 nm (in diameter) in milli-q water (Fig. 6.4). The ζ-potentials of PNDDS ranged from -46 mV to 43 mV in milli-Q water due to the

differences in the hydrophilic components of the diblock copolymers used for preparing PNDDS (Table 6.2). As expected, the presence of NaCl, Na_2SO_4, $CaCl_2$, and $CaSO_4$ tended to decrease the ζ-potentials for all types of PNDDS. The magnitude of the reduction depended on the salt and PNDDS type. For negatively charged PNDDS, multivalent Ca^{2+} ions in comparison to monovalent Na^+ ions led to more pronounced reductions. The presence of Ca^{2+} ions even caused aggregation and precipitation of PS-PAA type PNDDS (Fig. 6.5). The aggregation is presumably due to the formation of insoluble calcium complexes on polymer surfaces. In addition, the screening of divalent ions are stronger than that of monovalent ions. Hence, Ca^{2+} can cause a bigger reduction in electrostatic repulsive stabilization. For positively charged PNDDS, multivalent SO_4^{2-} ions in comparison to monovalent Cl^- ions gave rise to bigger reductions.

Table 6.2 The mean zeta potential of PNDDS and fine sand grains as a function of salt type and ionic strength.
Zeta potential result of each nanoparticle in different solutions was averaged with 6 repeats ± 1 SD.

Material	NaCl (0 mM) ζ (mV)	NaCl (10 mM) ζ (mV)	NaCl (100 mM) ζ (mV)	Na_2SO_4 (10 mM) ζ (mV)	$CaCl_2$ (10 mM) ζ (mV)	$CaSO_4$ (10 mM) ζ (mV)
PS-PAA	-46.1±4.3	-46.0±6.9	-26.5±1.4	-44.2±6.6	-13.2±3.6*	-14.3±3.0*
PLA-PNVP	-32.0±5.4	-25.4±10.1	-8.9±0.9	-23.0±9.5	-9.3±7.2	-10.8±5.6
PCL-PEO	-27.7±6.4	-4.2±6.6	-1.7±1.1	-3.1±8.0	-1.8±7.3	-3.7±4.6
Pluronic	-26.8±4.2	-2.6±7.3	-1.7±0.3	-1.7±6.5	-1.9±7.2	-2.9±4.4
PCL-PEI	+43.3±3.7	+38±8.1	+20.5±1.4	+14.6±5.4	+36.1±9.2	+15.8±5.9
Sand	-54.0±2.6	-53.7±2.5	-28.2±2.5	-60.5±2.2	-21.8±3.8	-21.4±3.8

* Aggregation and precipitation were observed.

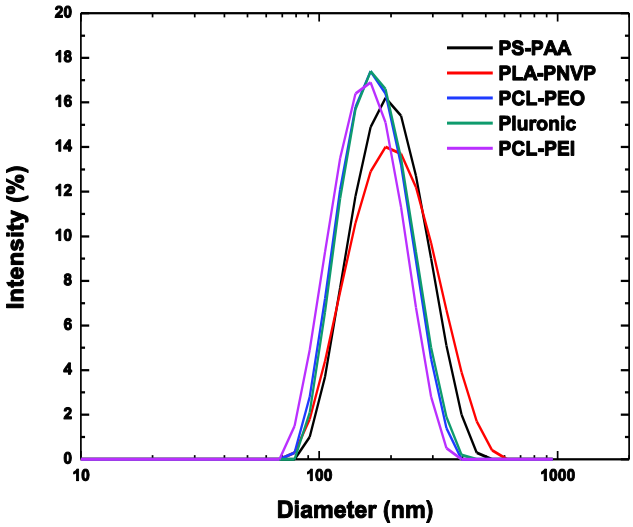

Figure 6.4 The intensity-weighted particle size distribution for five PNDDS.

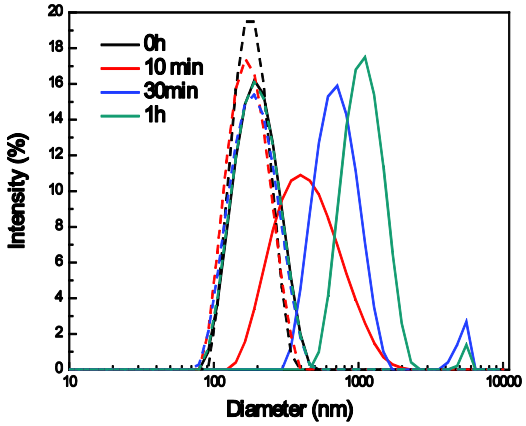

Figure 6.5 PS-PAA particle size distribution with time in a solution with different types of salt.
Dashed line: 10mM NaCl, Solid line: $CaCl_2$ solution (solid line)

For all PNDDS, there was no significant change in the particle size (hydrodynamic diameter) with respect to time in milli-q water during the time scales of transport studies. Likewise, the presence of salt did not change the size distribution for all PNDDS significantly except PS-PAA type PNDDS with $CaCl_2$ and $CaSO_4$. This prolonged stability was ascribed to the combination of steric and electrostatic effects due to the presence of long polymer chains and relatively large values of zeta potentials.

Regarding the characterization of the surfaces with which PNDDS interacted, the ζ-potential of the roller-milled sand grains was measured to be -54.0±2.6 mV in milli-Q water. The addition of Ca^{2+} ions (10 mM) significantly reduced ζ-potential to about -21 mV, probably due to the complexation of silanol groups and Ca^{2+} ions. While NaCl at a low ionic strength (10 mM) did not alter the ζ-potential significantly, NaCl at a high ionic strength (100 mM) reduced the ζ-potential to about -28 mV. Interestingly, the

presence of Na_2SO_4 slightly increased the magnitude of the ζ-potential. Similar trends with the sulfate ion were previously observed and attributed to the enhanced silica dissolution arising from the donation of electron from the adsorbed SO_4^{2-} ions[286]. Prior studies have shown that the ζ-potential of silica, which is the material coating the QCM-D sensors, is in the range of -70 to -90 mV in water[287–290]. These data will later be used to calculate the electrostatic interactions between PNDDS and silica/sand surfaces to explain the trends in QCM-D and column transport experiments.

6.3.2 Transport of PNDDS in the case of flow over a flat silica surface

The two most common flow conditions relevant to the environmental transport are flow over an external object (flat or curved) and flow through a porous media. In this study, we first focused on the transport of PNDDS suspension traveling on a flat silica surface as a function of time (Fig. 6.6). For PS-PAA (ζ≅–46mV), PLA-PNVP (ζ≅–32mV), PCL-PEO (ζ≅ –28mV), and Pluronic (ζ≅–27mV) in milli-Q water; there was no statistically significant adsorption observed on the silica surface. For PCL-PEI (ζ≅+43mV), initially, the adsorbed mass of the silica increased with time, indicating the rapid adsorption of the PCL-PEI on the silica surface. Later, the adsorbed mass reached a plateau, indicating that the silica surface was saturated with PCL-PEI (Fig. 6.7). The absence of adsorption for PS-PAA, PLA-PNVP, PCL-PEO, and Pluronic-type nanomedicine on silica was ascribed to high activation barriers (>200kT, Fig. 6.11). For PCL-PEI, there was no activation barrier: the adsorption could be described by the mass transfer coefficient described by the modified Leveque equation for QCM-D geometry.

Representative QCM-D frequency shifts of five PNDDS on the silica surface in different solutions are shown in Figure 6.8.

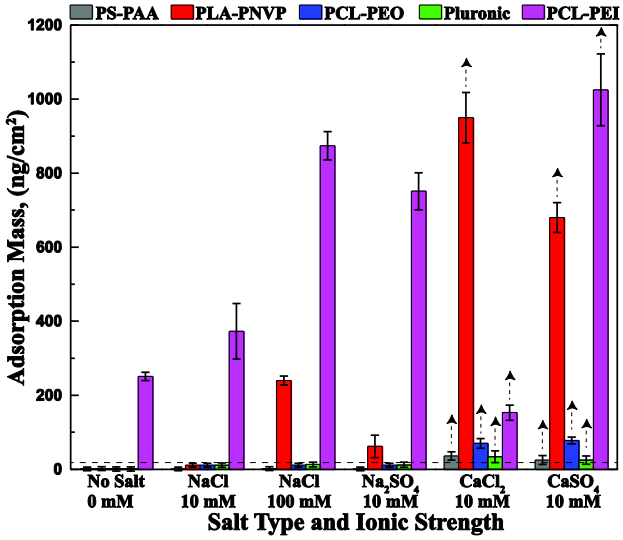

Figure 6.6 Steady-state mass adsorption of PNDDS on silica surface for five different surface chemistries as a function of salt type and ionic strength. For all types of PNDDS, the concentration was kept constant at 0.007 wt%. The flow rate was kept constant for all experiments and 2.5 μL/s to ensure a laminar flow behavior. The dashed arrows indicate that there is a continuous increase in the adsorption mass. For these cases, the adsorption mass was measured at 20 min. Note: Averaged Steady-state mass adsorption (1 SD) of all nanoparticles was repeated 3 times with no salt and 10mM NaCl solutions. 4 times repeats in 10mM Na_2SO_4, 10mM $CaCl_2$ and 10mM $CaSO_4$ solutions. 5 times repeats in 100mM NaCl solution.

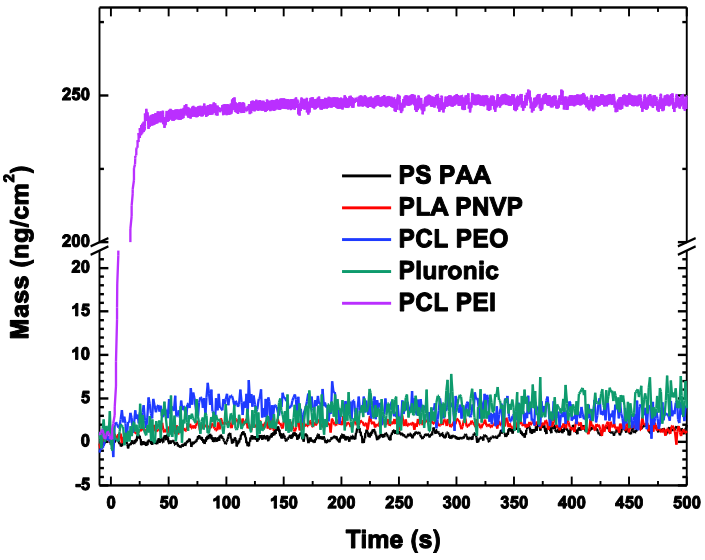

Figure 6.7 Mass adsorption of PNDDS on silica surface as a function of time for five different surface chemistries in Milli-Q water.
For all types of PNDDS, the concentration was kept constant at 0.007 wt%. The flow rate was and kept constant for all experiments and 2.5 μL/s to ensure a laminar flow behavior.

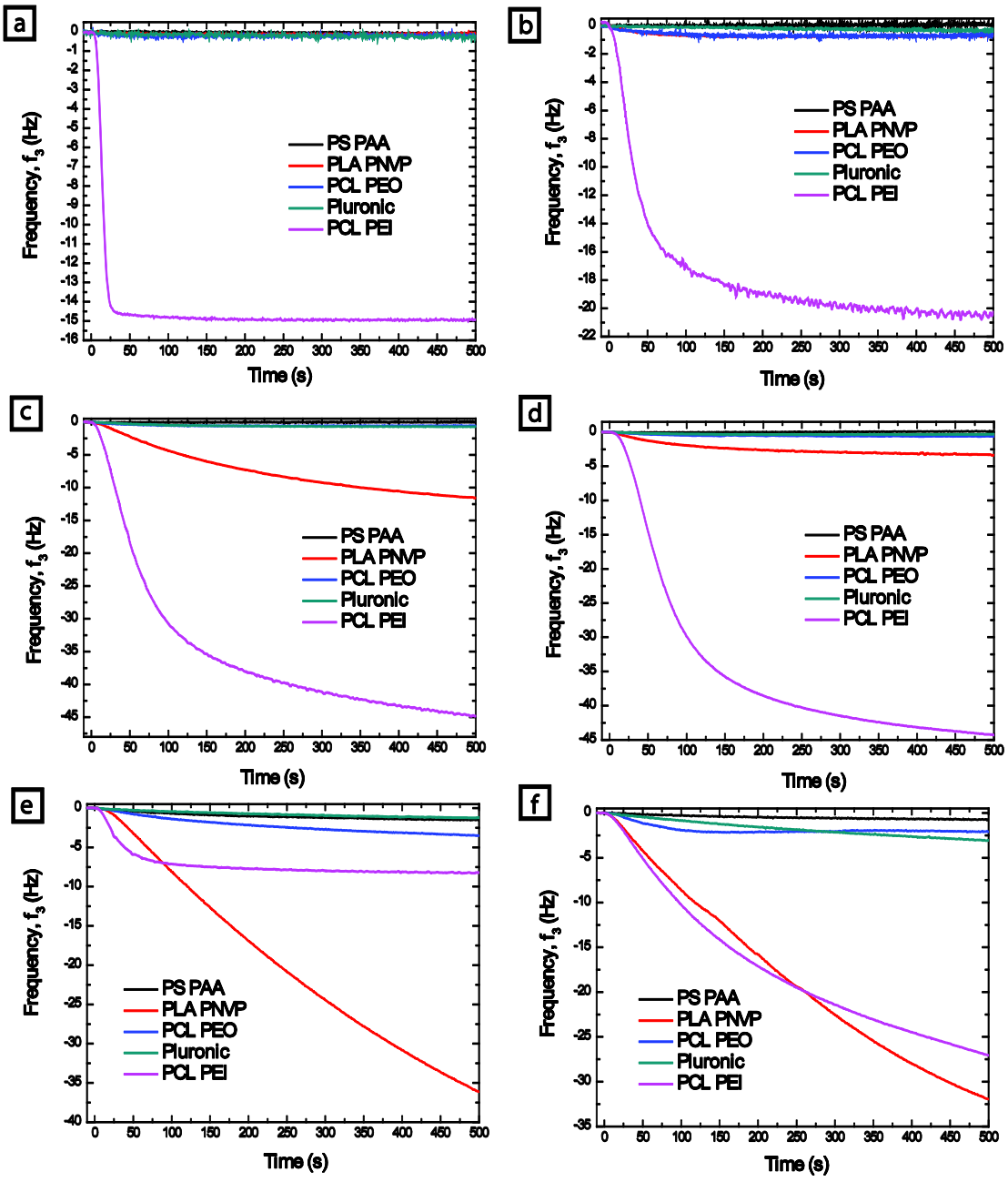

Figure 6.8 Representative QCM-D frequency shifts of PNDDS on silica surface as a function of time for five different surface chemistries in 6 different solutions.

a) Milli-Q water, b) 10mM NaCl, c) 100mM NaCl, d) 10mM Na_2SO_4, e) 10mM $CaCl_2$, and f) 10mM $CaSO_4$. For all types of PNDDS, the concentration was kept constant at 0.007 wt%. The flow rate was and kept constant for all experiments and 2.5 µL/s to ensure a laminar flow behavior.

When NaCl at a low ionic strength (10 mM) was added into the solution, there was no change in the adsorption behavior for PS-PAA ($\zeta \cong -46$mV), PLA-PNVP ($\zeta \cong -25$mV), PCL-PEO ($\zeta \cong -4$mV), and Pluronic($\zeta \cong -3$mV) (i.e., still no adsorption, $p<0.05$). Here, while the magnitude of the ζ-potential for negatively charged nanomedicine decreased, the steric repulsion due to polymeric nature of PNDDS was sufficient to prevent particulate adsorption. For PCL-PEI ($\zeta \cong +38$mV), the adsorption slightly increased ($p<0.05$). For this case, while the strong electrostatic attraction was probably more pronounced than the steric repulsion, the increased salinity yielded a decrease in the Debye length and range of electrostatic repulsion. Hence, a higher areal packing of positively charged nanomedicine on the substrate was possible.

When NaCl at a high ionic strength (100 mM) was introduced into the solution; PS-PAA, PCL-PEO, and Pluronic type nanomedicine were still non-adsorbent presumably since steric repulsion was enough to keep nanomedicine away from silica surface. For $NaSO_4$ (ionic strength of 10 mM), very similar trends were observed for these three types of nanomedicine. For PLA-PNVP type nanomedicine, the presence of SO_4^{2-} ions and high concentrations of Cl^- ions caused drastic changes in the adsorption behavior. This is most likely because even though PNVP in aqueous solution was found to carry a net negative charge, the existence of a partially positive charge on a nitrogen has previously been noted due to the tautomer formation[291,292]. It was shown that such nitrogen groups of PNVP strongly interact with SO_4^{2-} ions and many other anions, and may form zwitterionic complexes[292]. Hence, we believe the discrepancy between the adsorption behavior of PLA-PNVP and PS-PAA, PCL-PEO, and Pluronic type

nanomedicine can be explained by this phenomena. For PCL-PEI, the addition of NaCl at high ionic strength ($\zeta \cong +21$mV) or Na_2SO_4 ($\zeta \cong +15$mV) increased the adsorbed mass due to a higher areal packing as discussed above.

For $CaCl_2$ and $CaSO_4$ solutions, all types of PNDDS gave rise to non-equilibrium adsorption behavior (i.e. continuously increasing the adsorption mass with increasing time) as indicated by dashed arrows in Figure 6.6. These findings can be explained as follows: First, calcium salts often have a low water solubility[293] and can form complexes with silica and silicates[294], which is consistent with the observed significant reductions in the ζ-potentials of silica surfaces (from -54 mV to -21 mV). Second, for a similar reason, calcium ions can also complex with the negatively charged PNNDS surface, causing a decrease in the surface charge and even aggregation for PS-PAA (Table 6.2). To support this explanation, TEM imaging of PCL-PEO type nanomedicine in the presence of Ca^{2+} was carried out (Fig. 6.9). In comparison to the bare PCL-PEO (Fig. 6.2), there were noticeable dark (high contrast) regions indicating the presence of calcium atoms there.

Third, as the ζ-potential of nanomedicine gets close to zero, the formation of multilayers and higher areal packing densities are more likely to occur due to the decreased electrostatic repulsion.

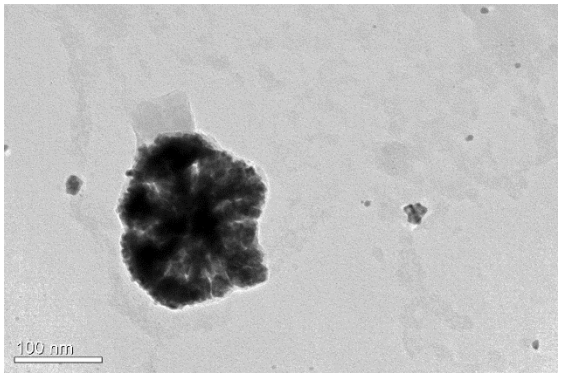

Figure 6.9 TEM micrographs of PCL-PEO in the presence of Ca^{2+} ions.

6.3.3 Theoretical considerations

To explain adsorption trends in QCM-D studies, we have relied on the potential energy profiles of adsorption for PNDDS. The interaction energy, *E*, between a charged nanoparticle and a charged substrate across an aqueous electrolyte solution is assumed to have two main contributions as described by Derjaguin and Landau, Verwey and Overbeek (DLVO) theory[295]. The first contribution is the attractive van der Waals interaction arising from dispersive interactions where the non-retarded van der Waals interaction energy between a spherical particle and a semi-infinite plate can be expressed as:

$$E_{vdw}(x) = -\frac{A}{6}\left[\frac{R}{x} + \frac{R}{x+2R} + ln\frac{x}{x+2R}\right] \quad [6.1]$$

where *A* is the Hamaker constant (Table 6.3), and R is the radius of particle. The second contribution is the electric double-layer interaction, which can be repulsive or attractive for a PNDDS/silica system. The double layer interaction energy between spherical particle and flat surfaces is given as follows[138]:

$$E_{DL}(x) = 64\pi\varepsilon_0\varepsilon\left(\frac{kT}{e}\right)^2 \tanh(\frac{e\psi_1}{4kT})\tanh(\frac{e\psi_2}{4kT})Re^{-\kappa x} \quad [6.2]$$

where ε is the dielectric constant of the medium; ε_0 is the permittivity of free space; e is the electron charge; k is Boltzmann constant; T is temperature; ψ_1 and ψ_2 are the surface potential of the PNDDS and silica surface, respectively; and κ^{-1} is the Debye length.

Because van der Waals interactions dominate over double-layer interactions at short distances, it is appropriate to introduce a short ranged repulsive term to avoid physically unrealistic situations where the particle approaches the substrate indefinitely. In this context, the Born repulsion, which is a short-range molecular interaction resulting from the overlap of electron orbitals, was considered. The Born repulsion between a spherical particle and a plate can be estimated by assuming that these molecular interactions are linearly superimposed[138]:

$$E_{Born}(d) = \frac{A\sigma^6}{7560}\left[\frac{x+8R}{(x+2R)^7} + \frac{6R-x}{d^7}\right] \quad [6.3]$$

where σ is the collision diameter (typically 0.3-0.5 nm). Summing the contribution from each effect leads to the total interaction energy between a particle and a plate:

$$E_{Tot} = E_{DL} + E_{vdw} + E_{Born} \quad [6.4]$$

Figure 6.10 displays the potential energy profiles of adsorption for all five PNDDS used in this study. A further analysis revealed that the activation energy was very large, and 455kT, 320kT, 285kT, and 200kT for PS-PAA, PLA-PNVP, PCL-PEO, and Pluronic; respectively. The corresponding rate constants of adsorption can be estimated using Kramers' rate theory[138,140]:

$$k_a = D(x^*)\sqrt{\frac{\left.\frac{d^2E(x)}{dx^2}\right|_{x=x^*}}{2\pi kT}}e^{-E_a/kT} \approx \frac{D(x^*)}{R}\sqrt{\frac{E_a}{2\pi kT}}e^{-E_a/kT} \quad [6.5]$$

where E(x) is the interaction potential between PNDDS and silica surface, E_a is the activation energy, x* is the distance at which the potential energy has a maximum, D(x*) is the diffusivity of PNDDS at the distance leading to the maximum in the potential energy profile. For all PNNDS, these large activations energies lead to infinitesimally small adsorption rates due to the exponential dependence. Hence, the absence of adsorption for PS-PAA, PLA-PNVP, PCL-PEO, and Pluronic on silica was ascribed to such high activation barriers.

Table 6.3 Hamaker constant of building blocks estimated from the Lifshitz theory.
The dielectric constant and refractive index of silica was taken to be 3.9 and 1.46, respectively. Black text indicates hydrophilic PNDDS shell while red text indicates hydrophobic core.

	Dielectric constant	Refractive index	Hamaker constant (J)
PEO	12.7	1.46	0.6E-20
PEI	3.4	1.67	1.4E-20
Pluoronic	12	1.47	0.7E-20
PAA	3.3	1.44	0.6E-20
PNVP	2.3	1.53	0.9E-20
PCL	3.2	1.48	0.8E-20
PLA	3.4	1.48	0.8E-20
PS	2.6	1.59	1.1E-20

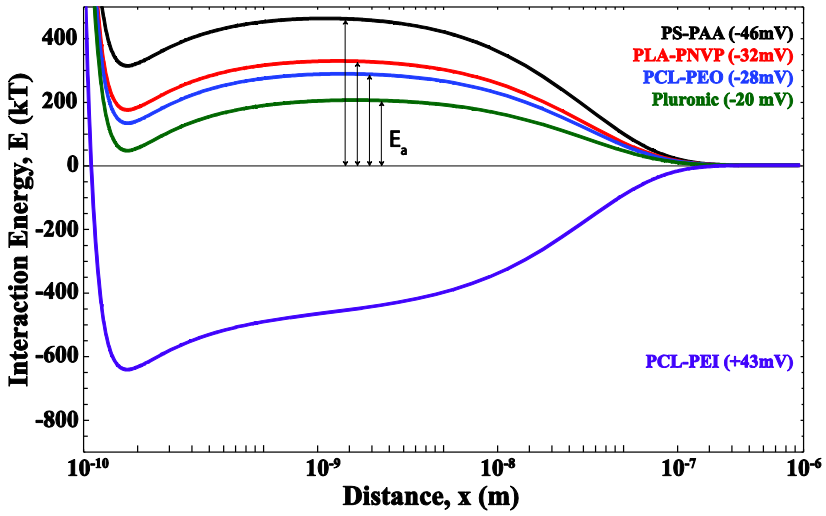

Figure 6.10 The interaction potential between a silica surface and polymeric nanomedicine in milli-Q water as a function of distance.
The following parameters were used to construct the graphs: silica surface potential of – 70 mV, cut-off distance of 0.3 nm, a Debye length of 65 nm (obtained by measuring the conductivity of aqueous solution in the column), and Hamaker constant of 1×10^{-20} J (obtained from the Lifshitz theory).

For PCL-PEI ($\zeta\cong$+43mV), there was no activation barrier, suggesting that the adsorption of PCL-PEI from the bulk to the interface is a transport-limited adsorption. In this case, for the QCM-D geometry, the adsorbate mass can be described by a modified Leveque solution[60]:

$$\frac{d\Gamma}{\partial t}\Big/_{C_{NP}} = k_a = \varrho D^{2/3} Q^{1/3} \qquad [6.6]$$

where C_{NP} is the concentration of nanoparticles in bulk; Q is the total volumetric flow rate; ϱ, is a geometrical constant and equal to 4.44×10^{3} $m^{-4/3}$ for the QCM-D chamber. This model assumes that at times long relative to the time required for the initial nanoparticle front to displace the pure water, a steady-state concentration boundary layer is established in the nanoparticle dispersion adjacent to the adsorbing surface. By fitting

the adsorbate mass versus time plot with Eqn. 6.6, we estimated the diffusivity of PCL-PEI nanomedicine to be 2.78±0.04 $\mu m^2/s$. Similarly, the diffusivity was also calculated using the particle size and the Stokes-Einstein equation, and found to be 2.84±0.22 $\mu m^2/s$. Overall, these two diffusivity values are very close, indicating that the modified Leveque equation describe the adsorption dynamics of PCL-PEI nanomedicine on silica surfaces sufficiently well.

In essence, since all PNDDS contain mostly organic copolymer and organic therapeutic agent, their Hamaker constants are similar, and in the order of $\sim 1\times10^{-20}$ J for PNDDS-water-silica system using Lifshitz mean field theory[295]. In addition, because they also have very similar sizes, the van der Waals energy is similar for all PNDDS. Therefore, the differences in the double-layer interactions are responsible for the differences in the adsorption behavior.

The absence of adsorption for PS-PAA, PLA-PNVP, PCL-PEO, and Pluronic-type nanomedicine on silica was ascribed to high activation barriers (>200kT, Fig. 6.10). For PCL-PEI, there was no activation barrier: the adsorption could be described by the mass transfer coefficient described by the modified Leveque equation for QCM-D geometry [60].

6.3.4 Transport of PNDDS in the case of flow through a porous media

For a flow through a porous media; the interplay among the particle size, Debye length, and characteristic length scales of pores and channels can lead to multiple scenarios differing from the particulate transport for the case of flow over an external object aside from hydrodynamical differences. For instance, size and charge exclusion effects have previously been observed [296–298]. Hence, it is essential to investigate the transport behavior of PNDDS in a porous media to better understand their environmental distribution and fate. In milli-Q water, PNDDS breakthrough curves displayed three different trends (Fig. 6.11a): PS-PAA ($\zeta \cong -46$mV), PLA-PNVP ($\zeta \cong -32$mV), and Pluronic ($\zeta \cong -27$mV) showed high mobility in the saturated columns packed with quartz sand (with no statistically significant difference among each other at a $p<0.05$ level). On the other hand, PCL-PEI ($\zeta \cong +43$mV) displayed no mobility and PCL-PEO ($\zeta \cong -28$mV) demonstrated limited mobility. Considering the sign of the ζ-potentials of nanomedicine and substrate, which is negative for PS-PAA, PLA-PNVP, Pluronic, and sand substrate and positive for PCL-PEI; these trends seem to be reasonable.

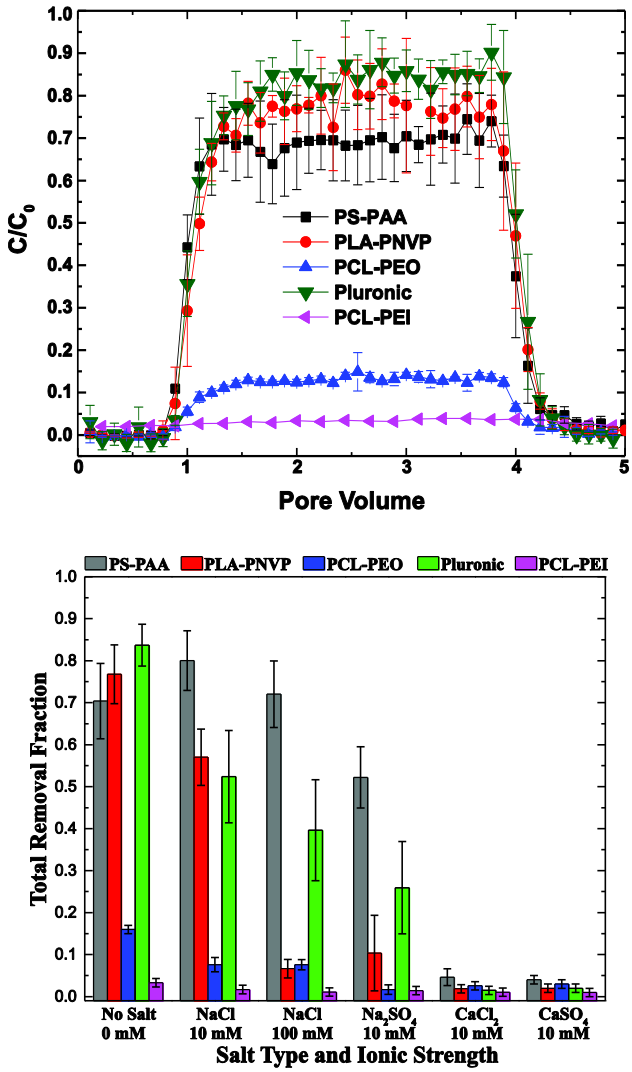

Figure 6.11 Breathrough curves of 5 PNDDS in sand column as a function of salt type and ionic strength.

(a) Breakthrough curves for five different types of PNDDS in milli-Q water-saturated columns packed with pure quartz sand, and (b) total recovery fractions as a function of ionic strength and salt type. Note: Averaged mass removal fraction (1 SD) of all nanoparticles with sand column experiments was repeated 3 times in 100mM NaCl, 10mM $CaCl_2$ and 10mM $CaSO_4$ solutions; 4 times repeats in no salt, 10mM NaCl and 10mM Na_2SO_4solutions.

The mobility of PCL-PEO type nanomedicine was much lower than that of PLA-PNVP and Pluronic ones while these three nanomedicine have similar ζ-potentials and sizes. This unusual behavior is attributed to the disintegration and degradation of PCL-PEO on the sand surface upon adsorption under high shear and in a confinement environment. In figure 6.11, AFM phase images of sand surfaces after breakthrough studies with PLA-PNVP, PCL-PEO, and PCL-PEI. For the case of bare sand, there was no detectable adsorbates on sand. For the case of PLA-PNVP, the presence of intact PLA-PNVP was detected, consistent with high glass transition temperature core. There was substantial rupture and disintegration of PCL-PEO and PCL-PEI observed after breakthrough studies in sand columns. The mechanical integrity of nanomedicine is related to the glass transition temperature of the core material[299]. PCL has a glass transition of T_g, –60 °C[300], while PS and PLA has a glass transition temperature of 60–70 °C and 40–50 °C, respectively[301,302]. Hence, at room temperature, PNDDS with PCL core is more vulnerable to the disintegration and rupture upon mechanical disturbances. We note that PCL-PEI, which has no mobility across sand columns, also tends to strongly deform and rupture on sand surfaces (Fig. 6.12), further supporting the abovementioned concepts.

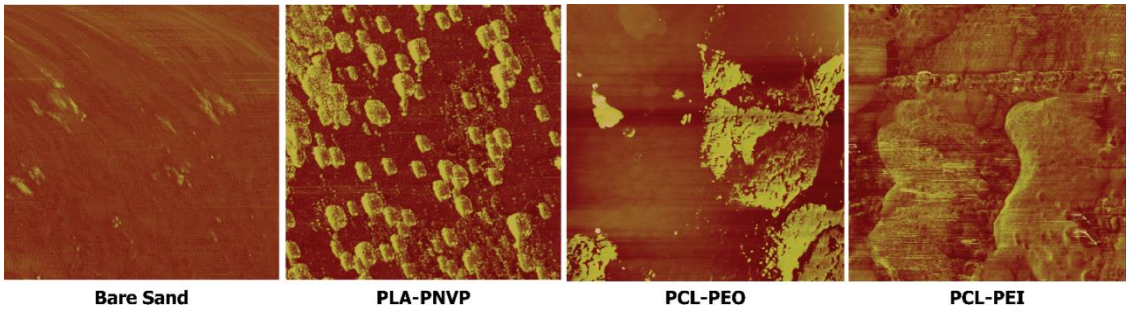

Figure 6.12 AFM micrographs of bare sand and sand after being exposed to PLA-PNVP, PCL-PEO, and PCL-PEI dispersions.

While studies involving nanomedicine in ultrapure water are useful for providing a mechanistic understanding of transport behavior, it is well-established that the environmental water bodies includes various types and concentrations of salts[303]. Hence, we have also investigated the influences of ionic strength and salt type on the PNDDS transport across sand columns (Fig. 6.11b). First, one can immediately notice the significant reductions in the PNDDS mobility in the presence of $CaCl_2$ and $CaSO_4$ solutions, in agreement with the increased adsorption of PNDDS onto flat silica surfaces with these salts. Second, PCL-PEI type nanomedicine showed no mobility under all conditions, consistent with its strong adsorption to the oppositely charged sand surfaces. Third, there was no change in the mobility of PS-PAA type nanomedicine with increasing the ionic strength ($p<0.05$). This is no surprise considering no major change in ζ-potentials and the lack of adsorption observed in QCM-D studies under these conditions. On the other hand, the mobility of PLA-PNVP and Pluronic-type nanomedicine mostly decreased with increasing the ionic strength. The reduced ζ-potentials may account for this trend (Table 6.2): It is well-documented that if the

electrostatic forces between ions and particles and porous media are repulsive, then the ions and particles can be excluded from locations near solid surfaces due to charge exclusion[297,298]. With charge exclusion, only a fraction of the pore space will be accessible to mobile ions and particles, thereby accelerating the transport of particles[297]. Hence, the decreased mobility of PLA-PNVP and Pluronic-type nanomedicine in the presence of electrolytes can be explained with the reduction in ζ-potentials and Debye length, and hence, charge exclusion. Enhanced PLA-PNVP and Pluronic-type nanomedicine retention may also be due to surface charge heterogeneity and roughness leading to locally reduced or eliminated energy barriers[304,305]. If ζ-potential of particles is small (as with PLA-PNVP and Pluronic-type nanomedicine under saline conditions), such heterogeneity and roughness may have a possibility to lead deposition. On the other hand, if ζ-potential is large (as with PS-PAA type nanomedicine), heterogeneity and roughness effect may not be enough to yield deposition.

6.3.5 Effect of humic acid on PNDDS transport

Natural organic matter in the environment, such as humic acid, can adsorb on nanoparticles, thereby causing changes in their surface chemistry and modulating their interactions through screening and/or depletion effects[306]. Humic acid gains a negative charge in aqueous media due to the dissociation of carboxylic acid groups[307]. Hence, we have studied the influence of humic acid on the PCL-PEI (positively charged) transport behavior. First, we focused on the transport behavior over a flat surface via QCM-D studies (Fig. 6.13). Control experiments with humic acid suspension revealed that there

was no detectable adsorption of humic acid on silica surfaces. When a small amount of humic acids (5 mg/L) was introduced into a PCL-PEI suspension, the total adsorbed mass on silica surfaces increased about 3-fold, which is most likely due to the larger areal packing that is stemming from the reduction in the interparticulate electrostatic repulsions on the plane of substrate. Also, the attachment of humic acid can increase the effective mass of PCL-PEI nanoparticles, thereby increasing the total adsorbed mass. When a larger amount of humic acid (15 mg/L) was present in the suspension, humic acid started to coat PCL-PEI type nanomedicine (TEM inset, Fig. 6.13) and hence, decreased the overall zeta-potential of PCL-PEI.

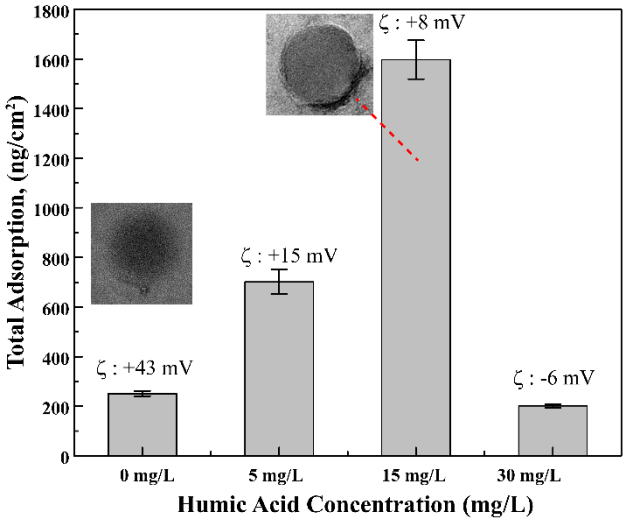

Figure 6.13 Total adsorption of PCL-PEI on silica surface as a function of amount of humic acid measured by QCM-D.
Inset TEM micrographs demonstrate the attachment of humic acid on PCL-PEI above certain concentrations. Note: At each humic acid concentration, steady-state mass adsorption of PCL-PEI PNDDS was repeated 4 times ± 1 SD. Zeta potential values were averaged with 6 repeats.

These changes corresponded to a much larger adsorption on silica surfaces. When there is excess amount of humic acid (30 mg/L) present with PCL-PEI suspension, the sign of the zeta-potential changed from positive to negative, suggesting an extensive coverage of humic acid on PCL-PEI surfaces. In this case, the adsorbed mass was lower than that without any humic acid. Although the mean zeta-potential value was negative, there was still adsorption on negatively charged silica surfaces. The existence of a broad distribution of zeta-potential, reaching to positive zeta potential values around the tail of distribution, can account for this trend (Fig. 6.14).

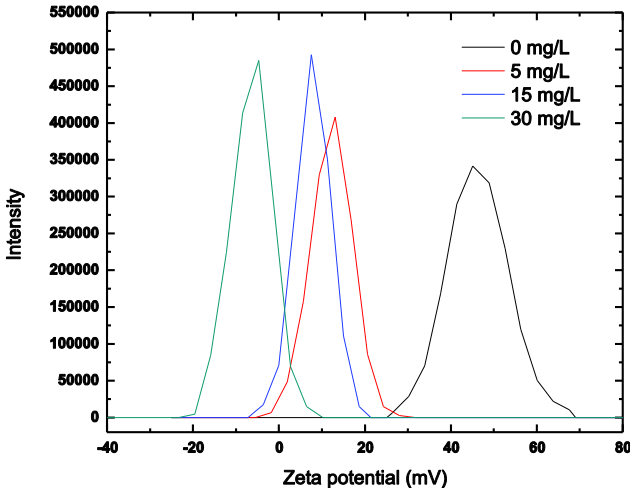

Figure 6.14 Zeta-potential distribution of PCL-PEI as a function of amount of humic acid.

Regarding the influence of humic acid in sand column experiments, there was no measurable breakthrough for PCL-PEI type nanomedicine. In other words, the presence of humic acid did not facilitate the transport of positively charged nanomedicine in porous media containing negatively charged packing materials.

6.4 Conclusion

In summary, this laboratory study showed that nanomedicine with positive surface charge displayed strong adsorption towards silica surfaces and no mobility in porous media composed of quartz sand even in the presence of humic acid. The mobility of negatively charged nanomedicine strongly depended on the amount and type of salt present in the aqueous media: In the absence of any salt, negatively charged nanomedicine demonstrated high levels of mobility in porous media of quartz sand and over flat silica surfaces. The presence of $CaCl_2$ and $CaSO_4$, even at low ionic strengths, strongly limited the mobility of nanomedicine in sand columns and initiated adsorption on flat silica surfaces. Considering the majority of polymeric nanomedicine tend to possess a negative surface charge, it may be possible to effectively block environmental transport of nanomedicine via salts such as $CaCl_2$ and $CaSO_4$. This study has focused on one class of nanomedicine: polymeric nanoparticulate drug delivery systems. Considering that production and consumption of nanomedicine increases day by day, there is an increasing need to conduct more studies focusing on the environmental transport behavior of other types nanomedicine to obtain a holistic understanding of their fate and distribution in the environment. We also noted that the nanoparticles can display different colloidal stability and aggregation behavior in porous media and under nanoconfinement.

6.5 Appendix

6.5.1 Relative importance of steric and electrostatic contribution in colloidal stability

According to extended-DLVO theory, the steric stabilization effect including osmotic and elastic contributions need to be taken into account due to the presence of polymer chains of PNDDS[308]. The osmotic effect will appear when two particles are closer than a distance equal to 2δ, twice of the effective average thickness of polymeric shell, δ, of PNDDS[309]. However, if the two particles are closer than a distance δ, some of the polymer molecules will experience elastic compression, leading to a net loss in configurational entropy. In terms of steric stabilization, we expect that all PNDDS studied here would have orders of magnitude steric repulsions because these have similarly hydrophilic surface characteristics (contact angle is less than 30° for all polymeric shell materials) and similar molecular weights in their shell (hydrophilic) polymers. Overall, while the steric contribution exists for all PNDDS, the differences in their colloidal stability should be due the differences in their electostatic contributions.

6.5.2 Statistical analysis of QCM and sand column transport data

One-way analysis of variance (ANOVA) with Tukey's post hoc test were used to determine significant differences between QCM adsorption and sand column mobility data with respect to the salt type/concentration and with respect to polymer type. All analyses were performed by using Microsoft Office Excel® (Microsoft Corp., Redmond, WA, USA) statistical software packages.

Table 6.4 The effect of salt type and ionic strength on the QCM adsorption behavior for each PNDDS.
Different letters in each column indicate statistically significant difference ($p<0.05$).

	PS-PAA	PLA-PNVP	PCL-PEO	Pluronic	PCL-PEI
No salt	B	E	B	B	D
NaCl 10 mM	B	E	B	B	C
NaCl 100 mM	B	C	B	B	A
Na_2SO_4 10mM	B	D	B	B	B
$CaCl_2$ 10mM	A	A	A	A	E
$CaSO_4$ 10mM	A	B	A	A	A

Table 6.5 The effect of PNDDS surface chemistry on the QCM adsorption behavior for each salinity condition.
Different letters in each row indicate statistically significant difference ($p<0.05$).

	PS-PAA	PLA-PNVP	PCL-PEO	Pluronic	PCL-PEI
No salt	B	B	B	B	A
NaCl 10 mM	B	B	B	B	A
NaCl 100 mM	C	B	C	C	A
Na_2SO_4 10 mM	C	B	C	C	A
$CaCl_2$ 10 mM	D	A	C	D	B
$CaSO_4$ 10mM	D	B	C	D	A

Table 6.6 The effect of salt type and ionic strength on the sand column transport behavior for each PNDDS.
Different letters in each column indicate statistically significant difference ($p<0.05$).

	PS-PAA	PLA-PNVP	PCL-PEO	Pluronic	PCL-PEI
No salt	AB	A	A	A	A
NaCl 10 mM	A	B	B	B	AB
NaCl 100 mM	A	C	B	BC	AB
Na_2SO_4 10mM	B	CD	C	C	AB
$CaCl_2$ 10mM	C	D	C	D	AB
$CaSO_4$ 10mM	C	D	C	D	B

Table 6.7 The effect of PNDDS surface chemistry on the sand column transport behavior for each salinity condition.
Different letters in each row indicate statistically significant difference ($p<0.05$).

	PS-PAA	PLA-PNVP	PCL-PEO	Pluronic	PCL-PEI
No salt	A	A	B	A	C
NaCl 10 mM	A	B	C	B	D
NaCl 100 mM	A	C	C	B	D
Na_2SO_4 10 mM	A	BC	C	B	C
$CaCl_2$ 10 mM	A	AB	AB	AB	B
$CaSO_4$ 10mM	A	AB	AB	AB	B

CHAPTER VII

SUMMARY

In this dissertation, dynamics of asphalt recovery by surfactant flooding, a new amphiphilic material with supramolecular assembling structures for chemical EOR and the transport behaviors of polymeric nanomedicines in the porous media were presented in three chapters. In chapter IV, we investigated desorption dynamics of asphalts happened at liquid-liquid-solid interfaces. Removal of asphalts from silica surfaces using a commercial nonionic surfactant floods as a function of surfactant concentrations and exposure time was studied at nanoscale using characterization techniques including quartz crystal microbalance with dissipation (QCM-D), atomic force microscopy (AFM), ellipsometry, and dynamic light scattering (DLS). It was found that the asphalt recovery was inefficient below the CMC of the surfactant solution, recovery efficiency increased with increasing surfactant concentration until the surfactant concentration of 2-3×CMC, then reached a plateau. The removal dynamics could be well described by a two-term exponential decay model with one fast desorption process forming large microemulsions and one slow desorption process forming small micelles. To obtain a more general model of surfactant flooding to apply in heavy oil recovery, future work could be done on changing different parameters like the rock surfaces to $CaCO_3$, the heavy oil sources, and injecting solution chemistries.

In chapter V, the proof of concept for the use of adaptable amphiphile solutions in chemical EOR as oil displacement fluids through sand column experiments at various

reservoir conditions. One commercial PAM polymer was chosen as the competitor among all conditions like pH, salinities, and temperatures in rheology measurements and sand column experiments. pH-adaptable amphiphiles, unlike the PAM polymer, will be able to maintain the viscous property even after high shear rates. The reversible supramolecular structures in the fluid will remain after flowing through small pores. For future work, different rock surfaces like carbonate need to be tested, since this is the reservoir type that can apply first in economical aspect. With similar concept in synthesis, temperature adaptable amphiphiles can be synthesized for investigation. The other direction is to apply this high viscous material in conformance control instead of flooding. This can be compared with the candidate hydrolyzed PAM polymer. Moreover, due to the adaptable viscosity, this material can be applied to shale reservoirs. Low viscosity above ground will be able to save costs of pumping injecting fluid, and higher viscosity underground will be able to carry sands to the desired positions with less settling amount during transportation.

In chapter VII, the laboratory study showed the transport of different surface chemistries of PNDDS towards silica surfaces and saturated porous media of quartz sands at various solution conditions. Their transport behaviors were characterized via QCM-D, sand column, spectrofluorometry, and DLS techniques. For PNDDS having positive zeta-potential displayed strong adsorption onto silica surfaces and no mobility in porous media of quartz sands, even in the presence of humic acid. The mobility of negatively charged nanomedicine strongly depended on the amount and types of salt in the aqueous media: In the absence of any salt, negatively charged PNDDS demonstrated

high mobility in porous media of quartz sand and over flat silica surfaces. With the bridging effect of Ca^{2+}, PNDDS tended to adsorb to the silica surfaces and decreased the mobility. In the future, besides the different environmental related media we can try such as soils, we shall also focus on the nanoconfinement effect of PNDDS when flowing through porous structures. The other issue is due to the soft layer of polymers, drugs in the hydrophobic core may release when passing through small pore regions. More researches can be done to make this PNDDS transportation model complete.

REFERENCES

1. Donaldson, E. C.; Chilingar, G. V.; Yen, T. F. *Enhanced Oil Recovery*. (Elsevier, 1985).

2. Taber, J. J. Research on Enhanced Oil Recovery: Past, Present and Future. *Pure Appl. Chem.* **52,** 1323–1347 (1980).

3. Lake, L. W., Schmidt, R. L. and Venuto, P. B. A Niche for Enhanced Oil Recovery in The 1990s. *Oilf. Rev.* **17,** 62–67 (1992).

4. Ehrlich, R. and Wygal Jr., R. J. Interrelation of Crude-Oil and Rock Properties with Recovery of Oil by Caustic Waterflooding. *Soc. Pet. Eng. J.* **17,** 263–270 (1977).

5. Morrow, N. R. Wettability and Its Effect on Oil Recovery. *J. Pet. Technol.* **42,** 1476–1484 (1990).

6. Dandekar, A. Y. *Petroleum Reservoir Rock and Fluid Properties*. (Taylor & Francis, 2006).

7. Lake, L. W. *Enhanced Oil Recovery*. (Prentice Hall, 1989).

8. Islam, M. R. Emerging Technologies in Enhanced Oil Recovery. *Energy Sources* **21,** 97–111 (1999).

9. Thomas, S. Enhanced Oil Recovery – An Overview. *Sci. Technol.* **63,** 9–19 (2008).

10. Sheng, J. *Modern Chemical Enhanced Oil Recovery: Theory and Practice*. (Gulf Professional Publishers, 2011).

11. Green, D. W. and Willhite, G. P. *Enhanced Oil Recovery- SPE Text-book Series Vol 6* (Society of Petroleum Engineers, 1998).

12. Austad, T., Matre, B., Milter, J., Sævareid, A. and Øyno, L. Chemical Flooding of Oil Reservoirs 8. Spontaneous Oil Expulsion from Oil- and Water-Wet Low Permeable Chalk Material by Imbibition of Aqueous Surfactant Solutions. *Colloids Surfaces A Physicochem. Eng. Asp.* **137,** 117–129 (1998).

13. Seethepalli, A., Adibhatla, B. and Mohanty, K. K. Physicochemical Interactions During Surfactant Flooding of Fractured. *SPE J.* **9,** 411–418 (2004).

14. Schramm, L. L. *Surfactants : Fundamentals and Applications in The Petroleum Industry*. (Cambridge University Press, 2000).

15. Salager, J. L., Morgan, J. C., Schechter, R. S., Wade, W. H. and Vasquez, E. Optimum Formulation of Surfactant-Water-Oil Systems for Minimum Interfacial-Tension or Phase-Behavior. *Soc. Pet. Eng. J.* **19,** 107–115 (1979).

16. Heredia, K. L., Bontempo, D., Ly, T., Byers, J. T., Halstenberg, S. and Maynard, H. D. In situ Preparation of Protein - 'Smart' Polymer Conjugates with Retention of Bioactivity. *J. Am. Chem. Soc.* **127,** 16955–16960 (2005).

17. Vemula, P. K. and John, G. Smart Amphiphiles: Hydro/Organogelators for in situ Reduction of Gold. *Chem. Commun.*, 2218–2220 (2006).

18. Fairman, R. and Åkerfeldt, K. S. Peptides as Novel Smart Materials. *Curr. Opin. Struct. Biol.* **15,** 453–463 (2005).

19. Etheridge, M. L., Campbell, S. A., Erdman, A. G., Haynes, C. L., Wolf, S. M. and McCullough, J. The Big Picture on Nanomedicine: The State of Investigational and Approved Nanomedicine Products. *Nanomedicine Nanotechnology, Biol. Med.* **9,** 1–14 (2013).

20. Borm, P. J. A. and Müller-Schulte, D. Nanoparticles in Drug Delivery and Environmental Exposure: Same Size, Same Risks? *Nanomedicine* **1,** 235–249 (2006).

21. Chan, V. S. W. Nanomedicine: An Unresolved Regulatory Issue. *Regul. Toxicol. Pharmacol.* **46,** 218–224 (2006).

22. Oberdörster, G., Oberdörster, E. and Oberdörster, J. Nanotoxicology: An Emerging Discipline Evolving from Studies of Ultrafine Particles. *Environ. Health Perspect.* **113,** 823–839 (2005).

23. Mundargi, R. C., Babu, V. R., Rangaswamy, V., Patel, P. and Aminabhavi, T. M. Nano/micro Technologies for Delivering Macromolecular Therapeutics Using Poly(d,l-lactide-co-glycolide) and Its Derivatives. *J. Control. Release* **125,** 193–209 (2008).

24. Sahoo, S. K. and Labhasetwar, V. Nanotech Approaches to Drug Delivery and Imaging. *Drug Discov. Today* **8,** 1112–1120 (2003).

25. Soppimath, K. S., Aminabhavi, T. M., Kulkarni, A. R. and Rudzinski, W. E. Biodegradable Polymeric Nanoparticles as Drug Delivery Devices. *J. Control. Release* **70,** 1–20 (2001).

26. Allen, T. M. and Cullis, P. R. Drug Delivery Systems: Entering The Mainstream. *Science* **303,** 1818–1822 (2004).

27. Otsuka, H., Nagasaki, Y. and Kataoka, K. PEGylated Nanoparticles for Biological and Pharmaceutical Applications. *Adv. Drug Deliv. Rev.* **64,** 246–255 (2012).

28. Chen, I.-C., Zhang, M., Teipel, B., Araujo, I. S. D., Yegin, Y. and Akbulut, M. Transport of Polymeric Nanoparticulate Drug Delivery Systems in The Proximity of Silica and Sand. *Environ. Sci. Technol.* **49,** 3575–83 (2015).

29. Thomas, S. and Farouq ali, S. M. Status and Assessment of Chemical Oil Recovery Methods. *Energy Sources* **21,** 177–189 (1999).

30. Wang, B. Y., Xu, H. and Zhang, X. Tuning The Amphiphilicity of Building Blocks: Controlled Self-Assembly and Disassembly for Functional Supramolecular Materials. *Adv. Mater.* **21,** 2849–2864 (2009).

31. Gil, E. S. and Hudson, S. M. Stimuli-Reponsive Polymers and Their Bioconjugates. *Prog. Polym. Sci.* **29,** 1173–1222 (2004).

32. Ju, X.-J., Xie, R., Yang, L. and Chu, L.-Y. Biodegradable 'Intelligent' Materials in Response to Chemical Stimuli for Biomedical Applications. *Expert Opin. Ther. Pat.* **19,** 683–696 (2009).

33. Zhang, H. X., Meng, X. and Li, P. Light and Thermal-Stimuli Responsive Materials. *Prog. Chem.* **20,** 657–672 (2008).

34. Chen, I.-C., Yegin, C., Zhang, M., Akbulut, M. Use of pH-Responsive Amphiphilic Systems as Displacement Fluids in Enhanced Oil Recovery. *SPE J.* **19,** 1035–1046 (2014).

35. French, R. A., Jacobson, A. R., Kim, B., Isley, S. L., Penn, R. L. and Baveye, P. C. Influence of Ionic Strength, pH, and Cation Valence on Aggregation Kinetics of Titanium Dioxide Nanoparticles. *Environ. Sci. Technol.* **43,** 1354–1359 (2009).

36. Solovitch, N., Labille, J., Rose, J., Chaurand, P., Borschneck, D., Wiesner, M. R. and Bottero, J.-Y. Concurrent Aggregation and Deposition of TiO_2 Nanoparticles in A Sandy Porous Media. *Environ. Sci. Technol.* **44,** 4897–4902 (2010).

37. Praetorius, A., Scheringer, M. and Hungerbühler, K. Development of Environmental Fate Models for Engineered Nanoparticles: A Case Study of TiO_2 Nanoparticles in The Rhine River. *Environ. Sci. Technol.* **46,** 6705–6713 (2012).

38. Wang, C., Bobba, A. D., Attinti, R., Shen, C., Lazouskaya, V., Wang, L.-P. and Jin, Y. Retention and Transport of Silica Nanoparticles in Saturated Porous Media: Effect of Concentration and Particle Size. *Environ. Sci. Technol.* **46,** 7151–7158 (2012).

39. Brunner, T. J., Wick, P., Manser, P., Spohn, P., Grass, R. N., Limback, L. K., Bruinink, A. and Stark, W. J. In Vitro Cytotoxicity of Oxide Nanoparticles: Comparison to Asbestos, Silica, and The Effect of Particle Solubility. *Environ. Sci. Technol.* **40,** 4374–4381 (2006).

40. Cornelis, G., Ryan, B., McLaughlin, M. J., Kirby, J. K., Beak, D. and Chittleborough, D. Solubility and Batch Retention of CeO_2 Nanoparticles in Soils. *Environ. Sci. Technol.* **45,** 2777–2782 (2011).

41. Thill, A., Zeyons, O., Spalla, O., Chauvat, F., Rose, J., Auffan, M. and Flank, A. M. Cytotoxicity of CeO_2 Nanoparticles for Escherichia Coli. Physico-Chemical Insight of The Cytotoxicity Mechanism. *Environ. Sci. Technol.* **40,** 6151–6156 (2006).

42. Barton, L. E., Auffan, M., Bertrand, M., Barakat, M., Catherine, S., Masion, A. Borschneck, D., Olivi, L., Roche, N., Wiesner, M. R. and Bottero, J.-Y. Transformation of Pristine and Citrate-Functionalized CeO_2 Nanoparticles in A Laboratory-Scale Activated Sludge Reactor. *Environ. Sci. Technol.* **48,** 7289–7296 (2014).

43. Jiang, X., Wang, X., Tong, M. and Kim, H. Initial Transport and Retention Behaviors of ZnO Nanoparticles in Quartz and Porous Media Coated with Escherichia Coli Biofilm. *Environ. Pollut.* **174,** 38–49 (2013).

44. Lombi, E., Donner, E., Tavakkoli, E., Turney, T. W., Naidu, R., Miller, B. W. and Scheckel, K. G. Fate of Zinc Oxide Nanoparticles during Anaerobic Digestion of Wastewater and Post-Treatment Processing of Sewage Sludge. *Environ. Sci. Technol.* **46,** 9089–9096 (2012).

45. Hong, Y., Honda, R. J., Myung, N. V. and Walker, S. L. Transport of Iron-Based Nanoparticles: Role of Magnetic Properties. *Environ. Sci. Technol.* **43,** 8834–8839 (2009).

46. El Badawy, A. M., Hassan, A. A., Scheckel, K. G., Suidan, M. T. and Tolaymat, T. M. Key Factors Controlling The Transport of Silver Nanoparticles in Porous Media. *Environ. Sci. Technol.* **47,** 4039–45 (2013).

47. Levard, C., Hotze, E. M., Lowry, G. V and Brown Jr, G. E. Environmental Transformations of Silver Nanoparticles: Impact on Stability and Toxicity. *Environ. Sci. Technol.* **46,** 6900–6914 (2012).

48. Darlington, T. K., Neigh, A. M., Spencer, M. T., Nguyen, O. T. and Oldenburg, S. J. Nanoparticle Characteristics Affecting Environmental Fate and Transport through Soil. *Environ. Toxicol. Chem.* **28,** 1191–1199 (2009).

49. Gardea-Torresdey, J. L., Parsons, J. G., Gomez, E., Peralta-Videa, J., Troiani, H. E., Santiago, P. and Yacaman, M. J. Formation and Growth of Au Nanoparticles inside Live Alfalfa Plants. *Nano Lett.* **2,** 397–401 (2002).

50. Cai, L., Tong, M., Ma, H. and Kim, H. Cotransport of Titanium Dioxide and Fullerene Nanoparticles in Saturated Porous Media. *Environ. Sci. Technol.* **47,** 5703–5710 (2013).

51. Tong, Z., Bischoff, M., Nies, L., Applegate, B. and Turco, R. F. Impact of Fullerene (C_{60}) on A Soil Microbial Community. *Environ. Sci. Technol.* **41,** 2985–2991 (2007).

52. Chang, X. and Vikesland, P. J. Effects of Dilution on The Properties of C_{60}. *Environ. Pollut.* **181,** 51–59 (2013).

53. Zhang, L., Hou, L., Wang, L., Kan, A. T., Chen, W. and Tomson, M.B. Transport of Fullerene Nanoparticles (nC_{60}) in Saturated Sand and Sandy Soil: Controlling Factors and Modeling. *Environ. Sci. Technol.* **46,** 7230–7238 (2012).

54. Jaisi, D. P. and Elimelech, M. Single-Walled Carbon Nanotubes Exhibit Limited Transport in Soil Columns. *Environ. Sci. Technol.* **43,** 9161–9166 (2009).

55. Petersen, E. J., Zhang, L. Mattison, N. T., O'Carroll, D. M., Whelton, A. J., Uddin, N., Nguyen, T., Huang, Q., Henry, T. B., Holbrook, R. D. and Chen, K. L. Potential Release Pathways, Environmental Fate, and Ecological Risks of Carbon Nanotubes. *Environ. Sci. Technol.* **45,** 9837–9856 (2011).

56. Fang, J., Shan, X. quan, Wen, B., Lin, J. ming and Owens, G. Stability of Titania Nanoparticles in Soil Suspensions and Transport in Saturated Homogeneous Soil Columns. *Environ. Pollut.* **157,** 1101–1109 (2009).

57. Wang, P., Shi, Q., Liang, H., Steuerman, D. W., Studky, G. D. and Keller, A. A. Enhanced Environmental Mobility of Carbon Nanotubes in The Presence of Humic Acid and Their Removal from Aqueous Solution. *Small* **4,** 2166–2170 (2008).

58. Dunphy Guzman, K. A., Finnegan, M. P. and Banfield, J. F. Influence of Surface Potential on Aggregation and Transport of Titania Nanoparticles. *Environ. Sci. Technol.* **40,** 7688–7693 (2006).

59. Zhang, M. and Akbulut, M. Adsorption, Desorption, and Removal of Polymeric Nanomedicine on and from Cellulose Surfaces: Effect of Size. *Langmuir* **27,** 12550–12559 (2011).

60. Zhang, M., Soto-Rodríguez, J., Chen, I-C., Akbulut, M. Adsorption and Removal Dynamics of Polymeric Micellar Nanocarriers Loaded with A Therapeutic Agent on Silica Surfaces. *Soft Matter* **9,** 10155–10164 (2013).

61. Zhang, M., Ellis, E. A., Cisneros-Zevallos, L. and Akbulut, M. Uptake and Translocation of Polymeric Nanoparticulate Drug Delivery Systems into Ryegrass. *Rsc Adv.* **2,** 9679–9686 (2012).

62. Nelson, R.C., Lawson, J. B., Thigpen, D. R. and Stegemeier, G. L. Cosurfactant-Enhanced Alkaline Flooding. *SPE/DOE Enhanced Oil Recovey Symp.,* 413 – 423 (1984).

63. Clark, S. R., Pitts, M. J. and Smith, S. M. Design and Application of An Alkaline-Surfactant-Polymer Recovery System to The West Kiehl Field. *Soc. Pet. Eng.* **1,** 172 – 179 (1993).

64. Anderson, W. G. Wettability Literature Survey-Part 6: The Effects of Wettability on Waterflooding. *J. Pet. Technol.* **39,** 1605–1622 (1987).

65. Strand, S. *Wettability Alteration in Chalk: A Study of Surface Chemistry*. (University of Stavanger, 2005).

66. Morrow, N. R. Wettability and Its Effect on Oil-Recovery. **42,** 1476–1484 (1990).

67. Falls, A. H., Thigpen, D. R., Nelson, R. C., Ciaston, J. W., Lawson, J. B., Good, P. A., Ueber, R.C. and Shahin, G. T. Field Test of Cosurfactant-Enhanced Alkaline Flooding. *SPE Reserv. Eng.* **9,** 217–223 (1994).

68. Bragg, J. R., Gale, W. W., Mcelhannon, W. A. J. R., Davenport, O. W. and Petrichuk, M. D. Loudon Surfactant Flood Pilot Test. *3rd Jt. SPE/DOE Enhanced Oil Recovey Symp.Proc.*, 933–952 (1982).

69. Jay, V., Turner, J., Bob, V., Pitts, M. J., Wyatt, K., Surkalo, H. and Patterson, D. Alkaline-Surfactant-Polymer Flooding of the Cambridge Minnelusa Field. *SPE Reserv. Eval. Eng.* **3,** 552–558 (2000).

70. Shutang, G., Li, H., Yang, Z., Pitts, M. J., Surkalo, H. and Wyatt, K. Alkaline/Surfactant/Polymer Pilot Performance of The West Central Saertu, Daqing Oil Field. *SPE Reserv. Eng.* **11,** 181–188 (1996).

71. Wang, D., Zhang, Z., Cheng, J., Yang, J., Gao S. and Lin, L. Pilot Test of Alkaline Surfactant Polymer Flooding in Daqing Oil Field. *SPE Reserv. Eng.* **12,** 229–233 (1997).

72. Wassmuth, F. R., Arnold, W., Green, K. and Cameron, N. Polymer Flood Application to Improve Heavy Oil Recovery at East Bodo. *J. Can. Pet. Technol.* **48,** 55–61 (2009).

73. Teeuw, D., Rond, D. and Martin, J. H. Design of A Pilot Polymer Flooding in The Marmul Field, Oman. *SPE/AIME Middle East Oil Show Conf. Proc.*, 513–524 (1983).

74. Koning, E. J. L., Mentzer, E., Heemskerk, J., Oman, P. D. and BV, S. R. Evalutation of A Pilot Polymer Flood in The Marmul Field, Oman. *SPE Tech. Conf. Proc.*, 385–393 (1988).

75. Mungan, N. Interfacial Effects in Immiscible Liquid-Liquid Displacement in Porous Media. *Soc. Pet. Eng. J.* **6,** 247–253 (1966).

76. W.W. Owens and Archer, D. L. The Effect of Rock Wettability on Oil-Water Relative Permeability Relationships. *J. Pet. Technol.* **23,** 873–878 (1971).

77. Shah, D. O. *Improved Oil Recovery by Surfactant and Polymer Flooding*. (Academic Press, 2012).

78. Gogarty, W. B. and Surkalo, H. Field Test of Micellar Solution Flooding. *J. Pet. Technol.* **24,** 1161–1169 (1972).

79. R.C. Earlougher Jr., J.E. ONeal and Surkalo, H. Micellar Solution Flooding - Field Test Results and Process Improvements. *J. Can. Pet. Technol.* **15,** 52–59 (1976).

80. Hill, H. J., Reisberg, J. and Stegemeier, G. L. Aqueous Surfactant Systems for Oil Recovery. *SPE/AIME Mid-Continent Improved Oil Recovery Symp. Prepr., 3798* (1972).

81. French, M. S., Keys, G. W., Stegemeier, G. L., Ueber, R. C., Abrams, A. and Hill, H. J. Field Test of An Aqueous Surfactant System for Oil Recovery, Benton Field, Illinois. *J. Pet. Technol.* **25,** 195–204 (1973).

82. Pursley, S. A. and Graham, H. L. Borregos Field Surfactant Pilot Test. *J. Pet. Technol.* **27,** 695–700 (1975).

83. Pursley, S. A., Healy, R. N. and Sandvik, E. I. A Field Test of Surfactant Flooding. *J. Pet. Technol.* **25,** 793–802 (1973).

84. Lake, L. W. and Pope, G. A. Status of Micellar-Polymer Field Tests. *Pet. Eng. Int.* 38–60 (1979).

85. Sheng, J. J. Optimum Phase Type and Optimum Salinity Profile in Surfactant Flooding. *J. Pet. Sci. Eng.* **75,** 143–153 (2010).

86. Mohan, K., Gupta, R. and Mohanty, K. K. Wettability Altering Secondary Oil Recovery in Carbonate Rocks. *Energy & Fuels* **25,** 3966–3973 (2011).

87. Ravari, R. R., Strand, S. and Austad, T. Combined Surfactant-Enhanced Gravity Drainage (SEGD) of Oil and The Wettability Alteration in Carbonates: The Effect of Rock Permeability and Interfacial Tension (IFT). *Energy & Fuels* **25,** 2083–2088 (2011).

88. Shen, P., Zhu, B., Li, X.-B. and Wu, Y.-S. An Experimental Study of The Influence of Interfacial Tension on Water–Oil Two-Phase Relative Permeability. *Transp. Porous Media* **85,** 505–520 (2010).

89. Zhang, H., Dong, M. and Zhao, S. Which One Is More Important in Chemical Flooding for Enhanced Court Heavy Oil Recovery, Lowering Interfacial Tension or Reducing Water Mobility? *Energy & Fuels* **24,** 1829–1836 (2010).

90. Yu, Q., Jiang, H. and Zhao, C. Study of Interfacial Tension between Oil and Surfactant Polymer Flooding. *Pet. Sci. Technol.* **28,** 1846–1854 (2010).

91. Babadagli, T. Evaluation of The Critical Parameters in Oil Recovery from Fractured Chalks by Surfactant Injection. *J. Pet. Sci. Eng.* **54,** 43–54 (2006).

92. Wu, W., Pan, J. and Guo, M. Mechanisms of Oil Displacement by ASP-Foam and Its Influencing Factors. *Pet. Sci.* **7,** 100–105 (2010).

93. Pope, G. A. The Application of Fractional Flow Theory to Enhanced Oil Recovery. *SPE J.* **20,** 191–205 (1980).

94. Hirasaki, G. and Zhang, D. Surface Chemistry of Oil Recovery from Fractured, Oil-Wet, Carbonate Formations. *SPE J.* **9,** 151–162 (2004).

95. Liu, Q., Dong, M., Ma, S. and Tu, Y. Surfactant Enhanced Alkaline Flooding for Western Canadian Heavy Oil Recovery. *Colloids Surfaces A Physicochem. Eng. Asp.* **293,** 63–71 (2007).

96. Hirasaki, G., Miller, C. and Puerto, M. Recent Advances in Surfactant EOR. *SPE J.* **16,** 889–907 (2011).

97. Liu, S. *Alkaline Surfactant Polymer Enhanced Oil Recovery Process*. (Rice University, 2008).

98. Standnes, D. C., Nogaret, L. A. D., Chen, H. L. and Austad, T. An Evaluation of Spontaneous Imbibition of Water into Oil-Wet Carbonate Reservoir Cores Using A Nonionic and A Cationic Surfactant. *Energy & Fuels* **16,** 1557–1564 (2002).

99. Standnes, D. C. and Austad, T. Wettability Alteration in Carbonates: Low-Cost Ammonium Surfactants Based on Bio-Derivatives from The Coconut Palm as Active Chemicals to Change The Wettability form Oil-Wet to Water-Wet Conditions. *Colloids Surfaces A Physicochem. Eng. Asp.* **218,** 161–173 (2003).

100. Guo, S., Wang, H., Shi, J., Pan, B. and Cheng, Y. Synthesis and Properties of A Novel Alkyl-Hydroxyl-Sulfobetaine Zwitterionic Surfactant for Enhanced Oil Recovery. *J. Pet. Explor. Prod. Technol.* **5,** 321–326 (2015).

101. Sanz, C. A. and Pope, G. A. Alcohol-Free Chemical Flooding: From Surfactant Screening to Coreflood Design. *SPE Symp. on Oilfield Chem.,* 117–128 (1995).

102. Svein M. and Skjaeveland, J. K. *Recent Advances in Improved Oil Recovery Methods for North Sea Sandstone Reservoirs*. (Norwegian Petrolum Directorate, 1992).

103. Willhite, D. W. G. and Pope, G. A. *Enhanced Oil Recovery (SPE Textbook Series) Volume 6*. (Society of Petroleum Engineers, 1998).

104. Pope, G. A. Recent Developments and Remaining Challenges of Enhanced Oil Recovery. *J. Pet. Technol.* **63,** 65–68 (2011).

105. Pye, D. J. Improved Secondary Recovery by Control of Water Mobility. *J. Pet. Technol.* 1**6,** 911–916 (1964).

106. Needham, R. B., Threlkeld, C. B. and Gall, J. W. Control of Water Mobility Using Polymers and Multivalent Cations. *SPE Improved Oil Recovey Symp.Proc.*, 139–148 (1974).

107. Wang, D., Li, Q., Gong, X., Wang, Y. and Co, D. O. I. L. The Engineering and Technical Aspects of Polymer Flooding in Daqing Oil Field. *SPE Oil Gas Int. Conf. Proc.*, 1–8 (2000).

108. Maitin, B. K. Performance Analysis of Several Polyacrylamide Floods in North German Oil Fields. *SPE/DOE Enhanced Oil Recovery Symp. Proc.*, 159–165 (1992).

109. Putz, A. G. and Rivenq, R. C. Commercial Polymer Injection in The Courtenay Field. *J. Pet. Sci. Eng.* **7,** 15–23 (1992).

110. Wang, D., Seright, R., Shao, Z. and Wang, J. Key Aspects of Project Design for Polymer Flooding at The Daqing Oilfield. *SPE Reserv. Eval. Eng.* **11,** 1117–1124 (2008).

111. De Melo, M. A., Holleven, C. R., Silva, I. G., Correia, A.D. B., Silva, G. A., Rosa, A. J., Lins Jr., A. G. and Lima, J. C. D. Evaluation of Polymer Injection Projects in Brazil. *SPE Lat. Am. Caribb. Pet. Eng. Conf.*, 20–23 (2005).

112. Norman, C., Turner, B. O., Romero, J. L., Centeno, G. A. and Muruaga, E. A Review of Over 100 Polymer Gel Injection Well Conformance Treatments in Argentina and Venezuela: Design, Field Implementation, and Evaluation. *Int. Oil Conf. Exhib. Mex.*, 1–8 (2006).

113. Tiwari, D., Marathe, R. V., Patel, N. K., Ramachandran, K. P., Maurya, C. R. and Tewari, P. K. Performance Of Polymer Flood In Sanand Field, India-A Case Study. *SPE Asia Pacific Oil and Gas Conf. Exhib.*, 1–9 (2008).

114. Chelaru, C., Diaconu, I. and Simionescu, I. Polyacrylamide Obtained by Plasma-Induced Polymerization for A Possible Application in Enhanced Oil Recovery. *Polym. Bull.* **40,** 757–764 (1998).

115. Taylor, K. C. and Nasr-El-Din, H. A. The Effect of Synthetic Surfactants on The Interfacial Behaviour of Crude Oil/Alkali/Polymer Systems. *Colloids Surfaces A Physicochem. Eng. Asp.* **108,** 49–72 (1996).

116. Zhao, Y., Zhou, J., Xu, X., Liu, W., Zhang, J., Fan, M. and Wang, J. Synthesis and Characterization of A Series of Modified Polyacrylamide. *Colloid Polym. Sci.* **287,** 237–241 (2009).

117. Kjøniksen, A. L., Beheshti, N., Kotlar, H. K., Zhu, K. and Nyström, B. Modified Polysaccharides for Use in Enhanced Oil Recovery Applications. *Eur. Polym. J.* **44,** 959–967 (2008).

118. Yahya, G. O., Ali, S. A., Al-Naafa, M. A. and Hamad, E. Z. Preparation and Viscosity Behavior of Hydrophobically Modified Poly(vinyl alcohol)(PVA). *J. Appl. Polym. Sci.* **57,** 343–352 (1995).

119. Zhang, S., She, Y. and Gu, Y. Evaluation of Polymers as Direct Thickeners for CO_2 Enhanced Oil Recovery. *J. Chem. Eng. Data* **56,** 1069–1079 (2011).

120. Wever, D. A. Z., Picchioni, F. and Broekhuis, A. A. Polymers for Enhanced Oil Recovery: A Paradigm for Structure-Property Relationship in Aqueous Solution. *Prog. Polym. Sci.* **36,** 1558–1628 (2011).

121. Shupe, R. Chemical Stability of Polyacrylamide Polymers. *J. Pet. Technol.* **33,** 1513–1529 (1981).

122. Selle, O. *An Experimental Study of Viscous Surfactant Flooding for Enhance Oil Recovery.* (Norwegian University of Science and Technology, 2006).

123. Frampton, H., Morgan, J. C., Cheung, S. K., Munson, L. and Chang, K. T. Development of A Novel Waterflood Conformance Control System. *SPE Symp.on Improved Oil Recovery*, 1–9 (2004).

124. Pritchett, J., Frampton, H., Brinkman, J., Cheung, S., Morgan, J., Chang, K. T., Williams, D. and Goodgame, J. Field Application of A New In-Depth Waterflood Conformance Improvement Tool. *SPE International Improved Oil Recovery Conf.*, 1–8 (2003).

125. Elimelech, M., Gregory, J., Jia, X. and Williams, R. A. *Particle Deposition and Aggregation: Measurement, Modelling and Simulation.* (Butterworth-Heinemann, 1995).

126. Yao, K., Habibian, M. T. and O'Melia, C. R. Water and Waste Water Filtration: Concepts and Applications. *Environ. Sci. Technol.* **5,** 1105–1112 (1971).

127. Rajagopalan, R. and Tien, C. Trajectory Analysis of Deep-Bed Filtration with The Sphere-In-Cell Porous Media Model. *AIChE J.* **22,** 523–533 (1976).

128. Grolimund, D., Elimelech, M., Borkovec, M., Barmettler, K., Kretzschmar, R. and Sticher, H.Transport of in situ Mobilized Colloidal Particles in Packed Soil Columns. *Environ. Sci. Technol.* **32,** 3562–3569 (1998).

129. Derjaguin, B. and Landau, L. Theory of The Stability of Strongly Charged Lyophobic Sols and The Adhesion of StronglyCharged Particles in Solutions of Electrolytes. *Prog. Surf. Sci.* **43,** 30–59 (1993).

130. Tufenkji, N. and Elimelech, M. Breakdown of Colloid Filtration Theory: Role of The Secondary Energy Minimum and Surface Charge Heterogeneities. *Langmuir* **21,** 841–852 (2005).

131. Tufenkji, N. and Elimelech, M. Deviation from The Classical Colloid Filtration Theory in The Presence of Repulsive DLVO Interactions. *Langmuir* **20,** 10818–10828 (2004).

132. Nel, A. E., Madler, L., Velegol, D., Xia, T., Hoek, E. M. V., Somasundaran, P., Klaessig, F., Castranova, V. and Thompson, M. Understanding Biophysicochemical Interactions at The Nano-Bio Interface. *Nat. Mater.* **8,** 543–557 (2009).

133. Min, Y., Akbulut, M., Kristiansen, K., Golan, Y. and Israelachvili, J. The Role of Interparticle and External Forces in Nanoparticle Assembly. *Nat. Mater.* **7,** 527–538 (2008).

134. Nel, A., Xia, T., Mädler, L. and Li, N. Toxic Potential of Materials at The Nanolevel. *Science* **311,** 622–627 (2006).

135. Oberdörster, G., Maynard, A., Donaldson, K., Castranova, V., Fitzpatrick, J., Ausman, K., Carter, J., Karn, B., Kreyling W., Lai, D., Olin, S., Monteiro-Riviere, N., Warheit, D. and Yang, H. Principles for Characterizing The Potential Human Health Effects from Exposure to Nanomaterials: Elements of A Screening Strategy. *Part. Fibre Toxicol.* **2,** 8 (2005).

136. Zhang, M. *Transports of Polymer Nanomedicine in The Environment*. (Texas A&M University, 2013).

137. Tadmor, R. The London-van der Waals Interaction Energy Between Objects of Various Geometries. *J. Phys. Condens. Matter* **13,** L195–L202 (2001).

138. Prieve, D. C. and Ruckenstein, E. The Surface Potential of Double-Layer Interaction Force between Surfaces Characterized by Multiple Ionizable Groups. *J. Theor. Biol.* **56,** 205–228 (1976).

139. Ruckenstein, E. and Prieve, D. C. Rate of Deposition of Brownian Particles under The Action of London and Double-Layer Forces. *J. Chem. Soc. Faraday Trans. 2* **69,** 1522 (1973).

140. Kramers, H. A. Brownian Motion in A Field of Force and The Diffusion Model of Chemical Reactions. *Physica* **7,** 284–304 (1940).

141. Happel, J. Viscous Flow in Multiparticle Systems: Slow Motion of Fluids Relative to Beds of Spherical Particles. *AIChE J.* **4,** 197–201 (1958).

142. Tufenkji, N. and Elimelech, M. Correlation Equation for Predicting Single-Collector Efficiency in Physicochemical Filtration in Saturated Porous Media. *Environ. Sci. Technol.* **38,** 529–536 (2004).

143. Chilingarian, G. V. and Yen, T. F. *Asphaltenes and Asphalt.* (Elsevier, 1994).

144. Buckley, J. S. and Liu, Y. Some Mechanisms of Crude Oil/Brine/Solid Interactions. *J. Pet. Sci. Eng.* **20,** 155–160 (1998).

145. Pernyeszi, T., Patzkó, Á., Berkesi, O. and Dékány, I. Asphaltene Adsorption on Clays and Crude Oil Reservoir Rocks. *Colloids Surfaces A Physicochem. Eng. Asp.* **137,** 373–384 (1998).

146. Wu, Y., Shuler, P. J., Blanco, M., Tang, Y. and Goddard, W. A. I. An Experimental Study of Wetting Behavior and Surfactant EOR in Carbonates with Model Compounds. *SPE J.* **13,** 26–34 (2008).

147. Marx, K. A. Quartz Crystal Microbalance: A Useful Tool for Studying Thin Polymer Films and Complex Biomolecular Systems at The Solution - Surface Interface. *Biomacromolecules* **4,** 1099–1120 (2003).

148. O'Sullivan, C. K. and Guilbault, G. G. Commercial Quartz Crystal Microbalances - Theory and Applications. *Biosens. Bioelectron.* **14,** 663–670 (1999).

149. Fowkes, F. M. Attractive Forces at Interfaces. *Ind. Eng. Chem.* **56,** 40–52 (1964).

150. Ardebrant, H. and Pugh, R. J. Wetting Studies on Silicate Minerals and Rocks Used in Bituminous Highways. *Colloids and Surfaces* **58,** 111–130 (1991).

151. Jada, A. and Salou, M. Effects of The Asphaltene and Resin Contents of The Bitumens on The Water-Bitumen Interface Properties. *J. Pet. Sci. Eng.* **33,** 185–193 (2002).

152. Lin, M.-S., Chaffin, J. M., Liu, M., Glover, C. J., Davison, R. R. and Bullin J. A. The Effect of Asphalt Composition on The Formation of Asphaltenes and Their Contribution to Asphalt Viscosity. *Fuel Sci. Technol. Int.* **14,** 139–162 (1996).

153. Corbett, L. W. Composition of Asphalt Based on Generic Fractionation, Using Solvent Deasphaltening, Elution-Adsorption Chromatography, and Densimetric Characterization. *Anal. Chem.* **41,** 576–579 (1969).

154. Farooq, U., Asif, N., Tweheyo, M. T., Sjöblom, J. and Øye, G. Effect of Low-Saline Aqueous Solutions and pH on The Desorption of Crude Oil Fractions from Silica Surfaces. *Energy & Fuels* **25,** 2058–2064 (2011).

155. Farooq, U., Sjoeblom, J. and Øye, G. Desorption of Asphaltenes from Silica-Coated Quartz Crystal Surfaces in Low Saline Aqueous Solutions. *J. Dispers. Sci. Technol.* **32,** 1388–1395 (2011).

156. Richards, R. *Surface and Nanomolecular Catalysis*. (CRC Press, 2006).

157. Liu, Y. and Buckley, J. S. Evolution of Wetting Alteration by Adsorption from Crude Oil. *SPE Form. Eval.* **12,** 5–14 (1997).

158. Dong, J., Chowdhry, B. and Leharne, S. Investigation of The Wetting Behavior of Coal Tar in Three Phase Systems and Its Modification by Poloxamine Block Copolymeric Surfactants. *Environ. Sci. Technol.* **38,** 594–602 (2004).

159. Denekas, M. O., Mattax, C. C. and Davis, G. T. Effects of Crude Oil Components on Rock Wettability. *Trans. Am. Inst. Min. Metall. Eng.* **216,** 330–333 (1959).

160. Al-Blehed, M. S., Sayyouh, M. H. and Desouky, S. M. An Engineering-Economic Evaluation of Enhanced Recovery of Saudi Crudes by Chemical Flooding. *Eng. Costs Prod. Econ.* **21,** 105–109 (1991).

161. Tong, Z. X., Morrow, N. R. and Xie, X. Spontaneous Imbibition for Mixed-Wettability States in Sandstones Induced by Adsorption from Crude Oil. *J. Pet. Sci. Eng.* **39,** 351–361 (2003).

162. Wang, J., Opedal, N. V. D. T., Lu, Q., Xu, Z., Zeng, H. and Sjoblom, J. Probing Molecular Interactions of An Asphaltene Model Compound in Organic Solvents Using A Surface Forces Apparatus (SFA). *Energy & Fuels* **26,** 2591–2599 (2012).

163. Liu, J., Zhang, L., Xu, Z. and Masliyah, J. Colloidal Interactions between Asphaltene Surfaces in Aqueous Solutions. *Langmuir* **22,** 1485–1492 (2006).

164. Notley, S. M., Eriksson, M. and Wågberg, L. Visco-Elastic and Adhesive Properties of Adsorbed Polyelectrolyte Multilayers Determined in situ with QCM-D and AFM Measurements. *J. Colloid Interface Sci.* **292,** 29–37 (2005).

165. Rodahl, M. and Kasemo, B. On The Measurement of Thin Liquid Overlayers with The Quartz-Crystal Microbalance. *Sensors and Actuators A: Phys.* **54,** 448–456 (1996).

166. Rodahl, M., Rodahl, M., Kasemo, B. and Kasemo, B. A Simple Setup to Simultaneously Measure The Resonant Frequency and The Absolute Dissipation Factor of A Quartz Crystal Microbalance. *Rev. Sci. Instrum.* **67,** 3238–3241 (1996).

167. Rodahl, M., Hook, F., Fredriksson, C., Keller, C. A., Krozer, A., Brzezinski, P., Voinova, M. and Kasemo, B. Simultaneous Frequency and Dissipation Factor QCM Measurements of Biomolecular Adsorption and Cell Adhesion. *Faraday Discuss.* **107,** 229–246 (1997).

168. Kaufman, J. H., Kanazawa, K. K. and Street, G. B. Gravimetric Electrochemical Voltage Spectroscopy: in situ Mass Measurements during Electrochemical Doping of The Conducting Polymer Polypyrrole. *Phys. Rev. Lett.* **53,** 2461–2464 (1984).

169. Martin, S. J., Frye, G. C., Ricco, A. J. and Senturia, S. D. Effect of Surface Roughness on The Response of Thickness-Shear Mode Resonators in Liquids. *Anal. Chem.* **65,** 2910–2922 (1993).

170. Butt, H.-J. and Graf, K. . K. *Physics and Chemistry of Interfaces, 2nd ed*. (Wiley-VCH, 2006).

171. Cerofolini, G. F. Adsorption and Surface Heterogeneity. *Surf. Sci.* **24,** 391–403 (1971).

172. Johnson, R. D. and Arnold, F. H. Multipoint Binding and Heterogeneity in Immobilized Metal Affinity Chromatography. *Biotechnol. Bioeng.* **48,** 437–443 (1995).

173. Krumrine, P., Falcone Jr., J. and Campbell, T. Surfactant Flooding: The Effect of Alkaline Additives on IFT, Surfactant Adsorption, and Recovery Efficiency. *Soc. Pet. Eng. J.* **22,** 503–513 (1982).

174. Kao, R. L., Wasan, D. T., Nikolov, A. D. and Edwards, D. A. Mechanisms of Oil Removal from A Solid Surface in The Presence of Anionic Micellar Solutions. *Colloids and Surfaces* **34,** 389–398 (1988).

175. Liu, Q., Yuan, S., Yan, H. and Zhao, X. Mechanism of Oil Detachment from A Silica Surface in Aqueous Surfactant Solutions: Molecular Dynamics Simulations. *J. Phys. Chem. B* **116,** 2867–2875 (2012).

176. Dong, M., Ma, S. and Liu, Q. Enhanced Heavy Oil Recovery through Interfacial Instability: A Study of Chemical Flooding for Brintnell Heavy Oil. *Fuel* **88,** 1049–1056 (2009).

177. Luning Prak, D. J., Abriola, L. M., Weber, W. J., Bocskay, K. A. and Pennell, K. D. Solubilization Rates of n-Alkanes in Micellar Solutions of Nonionic Surfactants. *Environ. Sci. Technol.* **34,** 476–482 (2000).

178. Vinatieri, J. E. Correlation of Emulsion Stability with Phase Behavior in Surfactant Systems for Tertiary Oil Recovery. *SPE J.* **20,** 402–406 (1980).

179. Rudin, J. and Wasan, D. T. Mechanisms for Lowering of Interfacial Tension in Alkali/Acidic Oil Systems: Effect of Added Surfactant. *Ind. Eng. Chem. Res.* **31,** 1899–1906 (1992).

180. Wade, W. H., Morgan, J. C., Schechter, R. S., Jacobson, J. K. and Salager, J. L. Interfacial Tension and Phase Behavior of Surfactant Systems. *SPE J.* **18,** 242–252 (1978)

181. Bryant, E. M., Bowman, R. S. and Buckley, J. S. Wetting Alteration of Mica Surfaces with Polyethoxylated Amine Surfactants. *J. Pet. Sci. Eng.* **52,** 244–252 (2006).

182. Salehi, M., Johnson, S. J. and Liang, J. T. Mechanistic Study of Wettability Alteration Using Surfactants with Applications in Naturally Fractured Reservoirs. *Langmuir* **24,** 14099–14107 (2008).

183. Hammond, P. S. and Unsal, E. Spontaneous Imbibition of Surfactant Solution into An Oil-Wet Capillary: Wettability Restoration by Surfactant-Contaminant Complexation. *Langmuir* **27,** 4412–4429 (2011).

184. Qiao, W., Li, J., Zhu, Y. and Cai, H. Interfacial Tension Behavior of Double Long-Chain 1,3,5-triazine Surfactants for Enhanced Oil Recovery. *Fuel* **96,** 220–225 (2012).

185. Geffroy, C., Cohen Stuart, M. A., Wong, K., Cabane, B. and Bergeron, V. Adsorption of Nonionic Surfactants onto Polystyrene: Kinetics and Reversibility. *Langmuir* **16,** 6422–6430 (2000).

186. Colegate, D. and Bain, C. Adsorption Kinetics in Micellar Solutions of Nonionic Surfactants. *Phys. Rev. Lett.* **95,** 198302–198305 (2005).

187. Miller, R. and Lunkenheimer, K. Adsorption Kinetics Measurements of Some Nonionic Surfactants. *Colloid Polym. Sci.* **264,** 357–361 (1986).

188. Douglas, J. F., Johnson, H. E. and Granick, S. A Simple Kinetic Model of Polymer Adsorption and Desorption. *Science* **262,** 2010–2012 (1993).

189. Wang, Y., Rajagopalan, R. and Mattice, W. L. Kinetics of Detachment of Homopolymers from A Solid Surface. *Phys. Rev. Lett.* **74,** 2503–2506 (1995).

190. Connors, K. A. *Chemical Kinetics: The Study of Reaction Rates in Solution*. (Wiley-VCH, 1990).

191. Chanda, J. and Bandyopadhyay, S. Molecular Dynamics Study of Surfactant Monolayers Adsorbed at The Oil/Water and Air/Water Interfaces. *J. Phys. Chem. B* **110,** 23482–23488 (2006).

192. Sternling, C. V. and Scriven, L. E. Interfacial Turbulence: Hydrodynamic Instability and The Marangoni Effect. *AIChE J.* **5,** 514–523 (1959).

193. Hu, H. and Larson, R. G. Analysis of The Effects of Marangoni Stresses on The Microflow in An Evaporating Sessile Droplet. *Langmuir* **21,** 3972–3980 (2005).

194. Wang, S., Liu, J., Zhang, L., Xu, Z. and Masliyah, J. Colloidal Interactions between Asphaltene Surfaces in Toluene. *Energy & Fuels* **23,** 862–869 (2009).

195. Pei, H., Zhang, G., Ge, J., Jin, L. and Liu, X. Analysis of Microscopic Displacement Mechanisms of Alkaline Flooding for Enhanced Heavy-Oil Recovery. *Energy & Fuels* **25,** 4423–4429 (2011).

196. Buchgraber, M., Clemens, T., Castanier, L. and Kovscek, A. A Microvisual Study of The Displacement of Viscous Oil by Polymer Solutions. *SPE Reserv. Eval. Eng.* **14,** 269–280 (2011).

197. Seright, R. Potential for Polymer Flooding Reservoirs with Viscous Oils. *SPE Reserv. Eval. Eng.* **13,** 730–740 (2010).

198. Babadagli, T. Selection of Proper Enhanced Oil Recovery Fluid for Efficient Matrix Recovery in Fractured Oil Reservoirs. *Colloids Surfaces A Physicochem. Eng. Asp.* **223,** 157–175 (2003).

199. Kjøniksen, A.-L., Beheshti, N., Kotlar, H. K., Zhu, K. and Nyström, B. Modified Polysaccharides for Use in Enhanced Oil Recovery Applications. *Eur. Polym. J.* **44,** 959–967 (2008).

200. Mothé, C. G., Correia, D. Z., De Franca, F. P. and Riga, A. T. Thermal and Rheological Study of Polysaccharides for Enhanced Oil Recovery. *J. Therm. Anal. Calorim.* **85,** 31–36 (2006).

201. Babadagli, T. Development of Mature Oil Fields - A Review. *J. Pet. Sci. Eng.* **57,** 221–246 (2007).

202. Huang, S. and Dong, M. Alkaline/Surfactant/Polymer (ASP) Flood Potential in Southwest Saskatchewan Oil Reservoirs. *J. Can. Pet. Technol.* **43,** 56–61 (2004).

203. Li, X. P., Ji, Y. Q., Wu, B., Li, G. Z. and Zheng, L. Q. New Type Flooding Systems in Enhanced Oil Recovery. *Chinese Chem. Lett.* **20,** 1251–1254 (2009).

204. Panmai, S., Prud'homme, R. K. and Peiffer, D. G. Rheology of Hydrophobically Modified Polymers with Spherical and Rod-Like Surfactant Micelles. *Colloids Surfaces A Physicochem. Eng. Asp.* **147,** 3–15 (1999).

205. Ericsson, C. A., Söderman, O., Garamus, V. M., Bergström, M. and Ulvenlund, S. Effects of Temperature, Salt, and Deuterium Oxide on The Self-Aggregation of Alkylglycosides in Dilute Solution. *Langmuir* **20,** 1401–1408 (2004).

206. Davies, T. S., Ketner, A. M. and Raghavan, S. R. Self-Assembly of Surfactant Vesicles that Transform into Viscoelastic Wormlike Micelles upon Heating. *J. Am. Chem. Soc.* **128,** 6669–6675 (2006).

207. Kumars, R., Kalur, G. C., Ziserman, L., Danino, D. and Raghavan, S. R. Wormlike Micelles of a C_{22}-Tailed Zwitterionic Betaine Surfactant: From Viscoelastic Solutions to Elastic Gels. *Langmuir* **23,** 12849–12856 (2007).

208. Kusano, T., Iwase, H., Yoshimura, T. and Shibayama, M. Structural and Rheological Studies on Growth of Salt-Free Wormlike Micelles Formed by Star-Type Trimeric Surfactants. *Langmuir* **28,** 16798–16806 (2012).

209. Wang, X., Wang, R., Zheng, Y., Sun, L., Yu, L., Jiao, J. and Wang, R. Interaction between Zwitterionic Surface Activity Ionic Liquid and Anionic Surfactant: Na^+-Driven Wormlike Micelles. *J. Phys. Chem. B* **117,** 1886–1895 (2013).

210. Taber, J. J., Martin, F. D. and Seright, R. S. EOR Screening Criteria Revisited—Part 2: Applications and Impact of Oil Prices. *SPE Reserv. Eval. Eng.* **12,** 199–206 (1997).

211. Taber, J. J., Martin, F. D. and Seright, R. S. EOR Screening Criteria Revisited - Part 1: Introduction to Screening Criteria and Enhanced Recovery Field Projects. *SPE Reserv. Eng.* **12,** 189–198 (1997).

212. Lichaa, P. M., Alpustun, H., Abdul, J. H., Nofal, W. A. and Fuseni, A. B. Wettability Evaluation of A Carbonate Reservoir Rock. *Advanced in Core Evaluation III, Reserv. Manag.* 327–358 (1993).

213. Chu, Z. and Feng, Y. A Facile Route towards The Preparation of Ultra-Long-Chain Amidosulfobetaine Surfactants. *Synlett* **20,** 2655–2658 (2009).

214. Kim, T. W. AND Kovscek, A. R. Wettability Alteration of A Heavy Oil/Brine/Carbonate System with Temperature. *Energy & Fuels* **27,** 2984–2998 (2013).

215. Stauffer, C. E. The Measurement of Surface Tension by The Pendant Drop Technique. *J. Phys. Chem.* **69,** 1933–1938 (1965).

216. Girault, H. H., Schiffrin, D. J. and Smith, B. D. V. Drop Image Processing for Surface and Interfacial Tension Measurements. *J. Electroanal. Chem. Interfacial Electrochem.* **137,** 207–217 (1982).

217. Nativ-Roth, E., Yerushalmi-Rozen, R. and Regev, O. Phase Behavior and Shear Alignment in SWNT-Surfactant Dispersions. *Small* **4,** 1459–1467 (2008).

218. Maia, A. M. S., Borsali, R. and Balaban, R. C. Comparison between A Polyacrylamide and A Hydrophobically Modified Polyacrylamide Flood in A Sandstone Core. *Mater. Sci. Eng. C* **29,** 505–509 (2009).

219. Wever, D. A. Z., Polgar, L. M., Stuart, M. C. A., Picchioni, F. and Broekhuis, A. A. Polymer Molecular Architecture as A Tool for Controlling The Rheological Properties of Aqueous Polyacrylamide Solutions for Enhanced Oil Recovery. *Ind. Eng. Chem. Res.* **52,** 16993–17005 (2013).

220. Hieber, C. A. and Chiang, H. H. Shear-Rate-Dependence Modeling of Polymer Melt Viscosity. *Polym. Eng. Sci.* **32,** 931–938 (1992).

221. Mungan, N. Rheology and Adsorption of Aqueous Polymer Solutions. *J.Can. Pet. Technol.* **8,** 45–50 (1969).

222. Dreiss, C. A. Wormlike Micelles: Where Do We Stand? Recent Developments, Linear Rheology and Scattering Techniques. *Soft Matter* **3,** 956 (2007).

223. Tirtaatmadja, V., Tam, K. C. and Jenkins, R. D. Effects of Temperature on The Flow Dynamics of A Model HASE Associative Polymer in Nonionic Surfactant Solutions. *Langmuir* **15,** 7537–7545 (1999).

224. Yang, J. Viscoelastic Wormlike Micelles and Their Applications. *Curr. Opin. Colloid Interface Sci.* **7,** 276–281 (2002).

225. Cates, M. E. and Candau, S. J. Statics and Dynamics of Worm-Like Surfactant Micelles. *J. Phys. Condens. Matter* **2,** 6869–6892 (1990).

226. Colby, R. H., Fetters, L. J., Funk, W. G. and Graessley W. W. Effects of Concentration and Thermodynamic Interaction on The Viscoelastic Properties of Polymer Solutions. *Macromolecules* **24,** 3873–3882 (1991).

227. Onogi, S., Masuda, T., Miyanaga, N. and Kimura, Y. Dependence of Viscosity of Concentrated Polymer Solutions upon Molecular Weight and Concentration. *J. Polym. Sci. Part A-2 Polym. Phys.* **5,** 899–913 (1967).

228. Arrhenius, S. The Viscosity of Solutions. *Biochem. J.* **11,** 112–134 (1917).

229. Shrestha, R. G., Shrestha, L. K. and Aramaki, K. Wormlike Micelles in Mixed Amino Acid-Based Anionic/Nonionic Surfactant Systems. *J. Colloid Interface Sci.* **322,** 596–604 (2008).

230. Song, A. and Hao, J. Highly Viscous Wormlike Micellar Phases Formed from The Mixed AOT/C_{14}DMAO/H_2O system. *J. Colloid Interface Sci.* **353,** 231–236 (2011).

231. Kuryashov, D. A., Philippova, O. E., Molchanov, V. S., Bashkirtseva, N. Y. and Diyarov, I. N. Temperature Effect on The Viscoelastic Properties of Solutions of Cylindrical Mixed Micelles of Zwitterionic and Anionic Surfactants. *Colloid J.* **72,** 230–235 (2010).

232. Beaumont, J., Louvet, N., Divoux, T., Fardin, M.-A., Bodiguel, H., Lerouge, S., Manneville, S. and Colin A. Turbulent Flows in Highly Elastic Wormlike Micelles. *Soft Matter* **9,** 735–749 (2013).

233. Taylor, K. C. and Nasr-El-Din, H. A. Water-Soluble Hydrophobically Associating Polymers for Improved Oil Recovery: A Literature Review. *J. Pet. Sci. Eng.* **19,** 265–280 (1998).

234. Yadali Jamaloei, B. and Kharrat, R. Analysis of Microscopic Displacement Mechanisms of Dilute Surfactant Flooding in Oil-Wet and Water-Wet Porous Media. *Transp. Porous Media* **81,** 1–19 (2010).

235. Trabelsi, S., Hutin, A., Argillier, J.-F., Dalmazzone, C., Bazin, B. and Langevin, D. Effect of Added Surfactants in An Enhanced Alkaline/Heavy Oil System. *Energy & Fuels* **25,** 1681–1685 (2011).

236. Chen, I-C. and Akbulut, M. Nanoscale Dynamics of Heavy Oil Recovery Using Surfactant Floods. *Energy & Fuels* **26,** 7176–7182 (2012).

237. Liberatore, M. W., Nettesheim, F., Vasquez, P. A., Helgeson, M. E., Wagner, N. J., Kaler, E. W., Cook, L. P., Porcar, L. and Hu, Y. T. Microstructure and Shear Rheology of Entangled Wormlike Micelles in Solution. *J. Rheol.***53,** 441 (2009).

238. Daniel, L. and Katima, J. H. Y. Factors Influencing Catalytic Wet Peroxide Oxidation of Maleic Acid in Aqueous Phase over Copper/Micelle Templated Silica-3-Aminopropyltrimethoxysilane Catalyst. *Water Sci. Technol.* **60,** 2621–2627 (2009).

239. Klotz, I. M. and Feidelseit, P. L. Deuterium-Hydrogen Exchange in A cis-Lactam Amide Group. *J. Am. Chem. Soc.* **88,** 5103–5105 (1966).

240. Misra, R., Acharya, S. and Sahoo, S. K. Cancer Nanotechnology: Application of Nanotechnology in Cancer Therapy. *Drug Discov. Today* **15,** 842–50 (2010).

241. Huh, A. J. and Kwon, Y. J. 'Nanoantibiotics': A New Paradigm for Treating Infectious Diseases Using Nanomaterials in The Antibiotics Resistant Era. *J. Control. Release* **156,** 128–145 (2011).

242. Muldoon, L. L., Tratnyek, P. G., Jacobs, P. M., Doolittle, N. D., Christoforidis, G. A., Frank, J. A., Lindau, M., Lockman, P. R., Manninger, S. P., Qiang, Y., Spence, A. M., Stupp, S. I., Zhang, M. and Neuwelt, E. A. Imaging and Nanomedicine for Diagnosis and Therapy in The Central Nervous System: Report of The Eleventh Annual Blood-Brain Barrier Disruption Consortium meeting. *Am. J. Neuroradiol.* **27,** 715–721 (2006).

243. Etheridge, M. L., Campbell, S. A., Erdman, A. G., Haynes, C. L., Wolf, S. M. and McCullough, J.The Big Picture on Nanomedicine: The State of Investigational and Approved Nanomedicine Products. *Nanomedicine Nanotechnology, Biol. Med.* **9,** 1–14 (2013).

244. Mahapatra, I., Clark, J., Dobson, P. J., Owen, R. and Lead, J. R. Potential Environmental Implications of Nano-Enabled Mmedical Applications: Critical Review. *Environ. Sci. Process. Impacts* **15,** 123–144 (2013).

245. Choi, H. S., Liu, W., Misra, P., Tanaka, E., Zimmer, J. P., Ipe, B. I., Bawendi, M. G. and Frangioni, J. V. Renal Clearance of Quantum Dots. *Nat. Biotechnol.* **25,** 1165–1170 (2007).

246. Minchin, R. Nanomedicine: Sizing Up Targets with Nanoparticles. *Nat. Nanotechnol.* **3,** 12–13 (2008).

247. He, X., Nie, H., Wang, K., Tan, W., Wu, X. and Zhang, P. In Vivo Study of Biodistribution and Urinary Excretion of Surface-Modified Silica Nanoparticles. *Anal. Chem.* **80,** 9597–9603 (2008).

248. Longmire, M., Choyke, P. L. and Kobayashi, H. Clearance Properties of Nano-sized Particles and Molecules as Imaging Agents: Considerations and Caveats. *Nanomedicine* **3,** 703–717 (2008).

249. Ghibellini, G., Vasist, L. S., Leslie, E. M., Heizer, W. D., Kowalsky, R. J., Calvo, B. F. and Brouwer, K. L. In Vitro-in Vivo Correlation of Hepatobiliary Drug Clearance in Humans. *Clin. Pharmacol. Ther.* **81,** 406–413 (2007).

250. Kiser, M. A., Westerhoff, P., Benn, T., Wang, Y., Perez-Rivera, J. and Hristovski, K. Titanium Nanomaterial Removal and Release from Wastewater Treatment Plants. *Environ. Sci. Technol.* **43,** 6757–6763 (2009).

251. Reijnders, L. Cleaner Nanotechnology and Hazard Reduction of Manufactured Nanoparticles. *J. Clean. Prod.* **14,** 124–133 (2006).

252. Gros, M., Petrović, M., Ginebreda, A. and Barceló, D. Removal of Pharmaceuticals during Wastewater Treatment and Environmental Risk Assessment Using Hazard Indexes. *Environ. Int.* **36,** 15–26 (2010).

253. Joss, A., Keller, E., Alder, A. C., Gobel, A., McArdell, C. S., Ternes, T. and Siegrist, H. Removal of Pharmaceuticals and Fragrances in Biological Wastewater Treatment. *Water Res.* **39,** 3139–3152 (2005).

254. U.S. Census Bureau American Housing Survey for The United States : 2009. *Curr. Hous. Reports*, 175 (2011).

255. Carrara, C., Ptacke, C. J., Robertson, W. D., Blowes, D. W., Moncur, M. C. Sverko, E.and Backus, S. Fate of Pharmaceutical and Trace Organic Compounds in Three Septic System Plumes, Ontario, Canada. *Environ. Sci. Technol.* **42,** 2805–2811 (2008).

256. Ptacek, C. J. Geochemistry of A Septic-System Plume in A Coastal Barrier Bar, Point Pelee, Ontario, Canada. *J. Contam. Hydrol.* **33,** 293–312 (1998).

257. Swartz, C. H., Reddy, S., Benotti, M. J., Yin, H., Barber, L. B., Brwonawell, B. J. and Rudel R. A. Steroid Estrogens, Nonylphenol Ethoxylate Metabolites, and Other Wastewater Contaminants in Groundwater Affected by A Residential Septic System on Cape Cod, MA. *Environ. Sci. Technol.* **40,** 4894–4902 (2006).

258. Wolf, L., Zwiener, C. and Zemann, M. Tracking Artificial Sweeteners and Pharmaceuticals Introduced into Urban Groundwater by Leaking Sewer Networks. *Sci. Total Environ.* **430,** 8–19 (2012).

259. Buerge, I. J., Keller, M., Buser, H.-R., Müller, M. D. and Poiger, T. Saccharin and Other Artificial Sweeteners in Soils: Estimated Inputs from Agriculture and Households, Degradation, and Leaching to Groundwater. *Environ. Sci. Technol.* **45,** 615–621 (2010).

260. Rutsch, M., Rieckermann, J., Cullmann, J., Elllis, J. B., Vollertsen, J. and Krebs, P. Towards A Better Understanding of Sewer Exfiltration. *Water Res.* **42,** 2385–2394 (2008).

261. Bay, S., Jones, B. H., Schiff, K. and Washburn, L. Water Quality Impacts of Stormwater Discharges to Santa Monica Bay. *Mar. Environ. Res.* **56,** 205–223 (2003).

262. Kumari, A., Yadav, S. K. and Yadav, S. C. Biodegradable Polymeric Nanoparticles Based Drug Delivery Systems. *Colloids Surfaces B: Biointerfaces* **75,** 1–18 (2010).

263. Soppimath, K. S., Aminabhavi, T. M., Kulkarni, A. R. and Rudzinski, W. E. Biodegradable Polymeric Nanoparticles as Drug Delivery Devices. *J. Control. Release* **70,** 1–20 (2001).

264. Brannon-Peppas, L. and Blanchette, J. O. Nanoparticle and Targeted Systems for Cancer Therapy. *Adv. Drug Deliv. Rev.* **64,** 206–212 (2012).

265. Tong, R., Gabrielson, N. P., Fan, T. M. and Cheng, J. Polymeric Nanomedicines Based on Poly(lactide) and Poly(lactide-co-glycolide). *Curr. Opin. Solid State Mater. Sci.* **16,** 323–332 (2012).

266. Skinner, B. J. Earth Resources. *Proc. Natl. Acad. Sci.* **76,** 4212–4217 (1979).

267. Ma, P. and Mumper, R. J. Paclitaxel Nano-Delivery Systems: A Comprehensive Review. *J. Nanomed. Nanotechnol.* **4,** 1000164–1000199 (2013).

268. Akbulut, M., Ginart, P., Gindy, M. E., Theriault, C., Chin, K. H., Soboyejo, W. and Prud'homme, R. K. Generic Method of Preparing Multifunctional Fluorescent Nanoparticles Using Flash Nanoprecipitation. *Adv. Funct. Mater.* **19,** 718–725 (2009).

269. Liu, Y., Cheng, C., Prud'homme, R. K. and Fox, R. O. Mixing in a Multi-Inlet Vortex Mixer (MIVM) for Flash Nano-Precipitation. *Chem. Eng. Sci.* **63,** 2829–2842 (2008).

270. Fisher, R. S. and Mullican III, W. F. Hydrochemical Evolution of Sodium-Sulfate and Sodium-Chloride Groundwater Beneath The Northern Chihuahuan Desert, Trans-Pecos, Texas, USA. *Hydrogeol. J.* **5,** 4–16 (1997).

271. Herczeg, A. L., Dogramaci, S. S. and Leaney, F. W. J. Origin of Dissolved Salts in A Large, Semi-Arid Groundwater System: Murray Basin, Australia. *Mar. Freshw. Res.* **52,** 41–52 (2001).

272. Adams, S., Titus, R., Pietersen, K., Tredoux, G. and Harris, C. Hydrochemical Characteristics of Aquifers Near Sutherland in The Western Karoo, South Africa. *J. Hydrol.* **241,** 91–103 (2001).

273. Niel Plummer, L., Sibrell, P. L., Casile, G. C., Busenberg, E., Hunt, A. G. and Schlosser, P. Tracing Groundwater with Low-Level Detections of Halogenated VOCs in A Fractured Carbonate-Rock Aquifer, Leetown Science Center, West Virginia, USA. *Appl. Geochemistry* **33,** 260–280 (2013).

274. Atekwana, E. A. and Richardson, D. S. Geochemical and Isotopic Evidence of A Groundwater Source in The Corral Canyon Meadow Complex, Central Nevada, USA. *Hydrol. Process.* **18,** 2801–2815 (2004).

275. Plummer, L. N., Eggleston, J. R., Andreasen, D. C., Raffensperger, J. P., Hunt, A. G. and Casile G. C. Old Groundwater in Parts of The Upper Patapsco Aquifer, Atlantic Coastal Plain, Maryland, USA: Evidence from Radiocarbon, Chlorine-36 and Helium-4. *Hydrogeol. J.* **20,** 1269–1294 (2012).

276. Millero, F. J., Feistel, R., Wright, D. G. and McDougall, T. J. The Composition of Standard Seawater and The Definition of The Reference-Composition Salinity Scale. *Deep Sea Res. Part I Oceanogr. Res. Pap.* **55,** 50–72 (2008).

277. Jaisi, D. P., Saleh, N. B., Blake, R. E. and Elimelech, M. Transport of Single-Walled Carbon Nanotubes in Porous Media: Filtration Mechanisms and Reversibility. *Environ. Sci. Technol.* **42,** 8317–8323 (2008).

278. Rabiet, M., Togola, A., Brissaud, F., Seidel, J.-L., Budzinski, H. and Elbaz-Poulichet, F. Consequences of Treated Water Recycling as Regards Pharmaceuticals and Drugs in Surface and Ground Waters of A Medium-sized Mediterranean Catchment. *Environ. Sci. Technol.* **40,** 5282–5288 (2006).

279. Vieno, N. M., Tuhkanen, T. and Kronberg, L. Seasonal Variation in The Occurrence of Pharmaceuticals in Effluents from A Sewage Treatment Plant and in The Recipient Water. *Environ. Sci. Technol.* **39,** 8220–8226 (2005).

280. Kümmerer, K. Drugs in The Environment: Emission of Drugs, Diagnostic Aids and Disinfectants into Wastewater by Hospitals in Relation to Other Sources - A Review. *Chemosphere* **45,** 957–969 (2001).

281. Phillips, P. J., Smith, S. G., Kolpin, D. W., Zaugg, S. D., Buxton, H. T., Furlong, E. T., Esposito, K. and Stinson, B. Pharmaceutical Formulation Facilities as Sources of Opioids and Other Pharmaceuticals to Wastewater Treatment Plant Effluents. *Environ. Sci. Technol.* **44,** 4910–4916 (2010).

282. Verlicchi, P., Galletti, A., Petrovic, M. and Barceló, D. Hospital Effluents as A Source of Emerging Pollutants: An Overview of Micropollutants and Sustainable Treatment Options. *J. Hydrol.* **389,** 416–428 (2010).

283. Larsson, D. G. J., de Pedro, C. and Paxeus, N. Effluent from Drug Manufactures Contains Extremely High Levels of Pharmaceuticals. *J. Hazard. Mater.* **148,** 751–755 (2007).

284. Fick, J., Soderstrom, H., Lindberg, R. H., Phan, C., Tysklind, M. and Larsson D. G. J. Contamination of Surface, Ground, and Drinking Water from Pharmaceutical Production. *Environ. Toxicol. Chem.* **28,** 2522–2527 (2009).

285. Hughes, S. R., Kay, P. and Brown, L. E. Global Synthesis and Critical Evaluation of Pharmaceutical Data Sets Collected from River Systems. *Environ. Sci. Technol.* **47,** 661–677 (2013).

286. Bai, S., Urabe, S., Okaue, Y. and Yokoyama, T. Acceleration Effect of Sulfate Ion on The Dissolution of Amorphous Silica. *J. Colloid Interface Sci.* **331,** 551–554 (2009).

287. Scales, P. J., Grieser, F., Healy, T. W., White, L. R. and Chan, D. Y. C. Electrokinetics of The Silica-Solution Interface: A Flat Plate Streaming Potential Study. *Langmuir* **8,** 965–974 (1992).

288. Xu, G., Zhang, J. and Song, G. Effect of Complexation on The Zeta Potential of Silica Powder. *Powder Technol.* **134,** 218–222 (2003).

289. Bousse, L., Mostarshed, S., Shoot, B. V. D., Rooij, N. F. D., Gimmel, P. and Gopel, W. Zeta Potential Measurements of Ta_2O_5 and SiO_2 Thin Films. *J. Colloid Interface Sci.* **147,** 22–32 (1991).

290. Revil, A., Pezard, P. A. and Glover, P. W. J. Streaming Potential in Porous Media: 1. Theory of The Zeta Potential. *J. Geophys. Res. Solid Earth* **104,** 20021–20031 (1999).

291. Takagishi, T. and Kuroki, N. Interaction of Polyvinylpyrrolidone with Methyl Orange and Its Homologs in Aqueous Solution: Thermodynamics of The Binding Equilibria and Their Temperature Dependences. *J. Polym. Sci. Polym. Chem. Ed.* **11,** 1889–1901 (1973).

292. Güner, A. Properties of Aqueous Salt Solutions of Polyvinylpyrrolidone. I. Viscosity Characteristics. *J. Appl. Polym. Sci.* **62,** 785–788 (1996).

293. Reemtsma, T., Bredow, A. and Gehring, M. The Nature and Kinetics of Organic Matter Release from Soil by Salt Solutions. *Eur. J. Soil Sci.* **50,** 53–64 (1999).

294. Greenberg, S. A., Chang, T. N. and Anderson, E. Investigation of Colloidal Hydrated Calcium Silicates. I. Solubility Products. *J. Phys. Chem.* **64,** 1151–1157 (1960).

295. Israelachvili, J. N. *Intermolecular and Surface Forces: Revised 3rd Edition*. (Academic Press, 2011).

296. Lenhart, J. J. and Saiers, J. E. Transport of Silica Colloids through Unsaturated Porous Media: Experimental Results and Model Comparisons. *Environ. Sci. Technol.* **36,** 769–777 (2002).

297. Bradford, S. A., Simunek, J., Bettahar, M., van Genuchten, M. T. and Yates, S. R. Modeling Colloid Attachment, Straining, and Exclusion in Saturated Porous Media. *Environ. Sci. Technol.* **37,** 2242–2250 (2003).

298. Gvirtzman, H. and Gorelick, S. M. Dispersion and Advection in Unsaturated Porous Media Enhanced by Anion Exclusion. *Nature* **352,** 793–795 (1991).

299. Nakayama, M., Okano, T., Miyazaki, T., Kohori, F., Sakai, K. and Yokoyama, M. Molecular Design of Biodegradable Polymeric Micelles for Temperature-Responsive Drug Release. *J. Control. Release* **115,** 46–56 (2006).

300. Wu, C.-S. A Comparison of The Structure, Thermal Properties, and Biodegradability of Polycaprolactone/Chitosan and Acrylic Acid Grafted Polycaprolactone/Chitosan. *Polymer* **46,** 147–155 (2005).

301. Satomi, N., Takahara, A. and Kajiyama, T. Determination of Surface Glass Transition Temperature of Monodisperse Polystyrene Based on Temperature-Dependent Scanning Viscoelasticity Microscopy. *Macromolecules* **32,** 4474–4476 (1999).

302. Passerini, N. and Craig, D. Q. M. An Investigation into The Effects of Residual Water on The Glass Transition Temperature of Polylactide Microspheres Using Modulated Temperature DSC. *J. Control. Release* **73,** 111–115 (2001).

303. Ottofuelling, S., Von Der Kammer, F. and Hofmann, T. Commercial Titanium Dioxide Nanoparticles in Both Natural and Synthetic Water: Comprehensive Multidimensional Testing and Prediction of Aggregation Behavior. *Environ. Sci. Technol.* **45,** 10045–10052 (2011).

304. Bhattacharjee, S., Ko, C.-H. and Elimelech, M. DLVO Interaction between Rough Surfaces. *Langmuir* **14,** 3365–3375 (1998).

305. Bhattacharjee, S., Ryan, J. N. and Elimelech, M. Virus Transport in Physically and Geochemically Heterogeneous Subsurface Porous Media. *J. Contam. Hydrol.* **57,** 161–187 (2002).

306. Xie, B., Xu, Z., Guo, W. and Li, Q. Impact of Natural Organic Matter on The Physicochemical Properties of Aqueous C_{60} Nanoparticles. *Environ. Sci. Technol.* **42,** 2853–2859 (2008).

307. Tan, X. L., Wang, X. K., Geckeis, H. and Rabung, T. H. Sorption of Eu(III) on Humic Acid or Fulvic Acid Bound to Hydrous Alumina Studied by SEM-EDS, XPS, TRLFS, and Batch Techniques. *Environ. Sci. Technol.* **42,** 6532–6537 (2008).

308. Vincent, B., Edwards, J., Emmett, S. and Jones, A. Depletion Flocculation in Dispersions of Sterically-Stabilised Particles ('Soft Spheres'). *Colloids and Surfaces* **18,** 261–281 (1986).

309. Romero-Cano, M. S., Martín-Rodríguez, A. and De las Nieves, F. J. Electrosteric Stabilization of Polymer Colloids with Different Functionality. *Langmuir* **17,** 3505–3511 (2001).